UNIVERSITY OF ALBERTA

MICROSTUCTURE CHARACTERIZATION OF TRIBLOCK COPOLYMER/HOMOPOLYMER BLENDS USING TEM AND DSC

BY

NILESH N. OAK ©

A THESIS SUBMITTED TO

THE FACULTY OF GRADUATE STUDIES AND RESEARCH
IN PARTIAL FULFILLMENT OF THE REQUIREMENTS FOR THE DEGREE
OF MASTER OF SCIENCE

DEPARTMENT OF CHEMICAL ENGINEERING

EDMONTON, ALBERTA

FALL 1995

National Library
of Canada

Acquisitions and
Bibliographic Services Branch

395 Wellington Street
Ottawa, Ontario
K1A 0N4

Bibliothèque nationale
du Canada

Direction des acquisitions et
des services bibliographiques

395, rue Wellington
Ottawa (Ontario)
K1A 0N4

Your file Votre référence

Our file Notre référence

THE AUTHOR HAS GRANTED AN IRREVOCABLE NON-EXCLUSIVE LICENCE ALLOWING THE NATIONAL LIBRARY OF CANADA TO REPRODUCE, LOAN, DISTRIBUTE OR SELL COPIES OF HIS/HER THESIS BY ANY MEANS AND IN ANY FORM OR FORMAT, MAKING THIS THESIS AVAILABLE TO INTERESTED PERSONS.

L'AUTEUR A ACCORDE UNE LICENCE IRREVOCABLE ET NON EXCLUSIVE PERMETTANT A LA BIBLIOTHEQUE NATIONALE DU CANADA DE REPRODUIRE, PRETER, DISTRIBUER OU VENDRE DES COPIES DE SA THESE DE QUELQUE MANIERE ET SOUS QUELQUE FORME QUE CE SOIT POUR METTRE DES EXEMPLAIRES DE CETTE THESE A LA DISPOSITION DES PERSONNE INTERESSEES.

THE AUTHOR RETAINS OWNERSHIP OF THE COPYRIGHT IN HIS/HER THESIS. NEITHER THE THESIS NOR SUBSTANTIAL EXTRACTS FROM IT MAY BE PRINTED OR OTHERWISE REPRODUCED WITHOUT HIS/HER PERMISSION.

L'AUTEUR CONSERVE LA PROPRIETE DU DROIT D'AUTEUR QUI PROTEGE SA THESE. NI LA THESE NI DES EXTRAITS SUBSTANTIELS DE CELLE-CI NE DOIVENT ETRE IMPRIMES OU AUTREMENT REPRODUITS SANS SON AUTORISATION.

ISBN 0-612-06513-8

Canada

UNIVERSITY OF ALBERTA

RELEASE FORM

NAME OF AUTHOR: **NILESH N. OAK**

TITLE OF THE THESIS: **MICROSTUCTURE CHARACTERIZATION OF TRIBLOCK COPOLYMER/HOMOPOLYMER BLENDS USING TEM AND DSC**

DEGREE: **MASTER OF SCIENCE**

YEAR THIS DEGREE GRANTED: **1995**

Permission is hereby granted to the University of Alberta Library to reproduce single copies of this thesis and to lend or sell such copies for private, scholarly or scientific research purpose only.

The author reserves all other publication and other rights in association with the copyright in the thesis, and except as hereinbefore provided neither the thesis nor any substantial portion thereof may be printed or otherwise reproduced in any material form whatever without the author's prior written permission.

Nilesh Oak

C/O Prof. M.C. Williams
Department of Chemical Engineering
536-Chemical Mineral Engg. Bldg.
University of Alberta, Edmonton
Alberta T6G 2G6

DATED: October 1995

THE UNIVERSITY OF ALBERTA

FACULTY OF GRADUATE STUDIES AND RESEARCH

The undersigned certify that they have read, and recommend to the Faculty of Graduate Studies and Research, for acceptance, a thesis entitled MICROSTRUCTURE CHARACTERIZATION OF TRIBLOCK COPOLYMER/HOMOPOLYMER BLENDS USING TRANSMISSION ELECTRON MICROSCOPY AND DIFFERENTIAL SCANNING CALORIMETRY submitted by NILESH N. OAK in partial fulfillment of the requirements for the degree of MASTER OF SCIENCE.

M. C. Williams

M.C. Williams (Supervisor)

U. Sundararaj

R. F. Egerton

R. Egerton (External Examiner)

Dated: June, 1995

To Archarya Vinoba Bhave, My SadGuru

ABSTRACT

The microstructures in the blends of a triblock copolymer (SBS) and two polystyrenes were characterized by transmission electron microscopy. The polymer materials were: Dow vector 4461-D - an poly [b-styrene-b-butadiene-b-styrene] SBS copolymer having a weight average molecular weight M_w = 61,290 and 44% styrene (i.e, M_S = 13,483 and M_B = 34,322), and Pressure Chemical Company Polystyrene (PS13 having M_w= 13,000, and PS65 having M_w= 65,000). All the samples had polydispersity of less than 1.06. Blends were prepared by dissolving a mixture of copolymer and homopolystyrene in dipentene (a neutral solvent for the system of styrene and butadiene) and solvent was slowly evaporated in vacuum at 60^0C for 8 weeks followed by annealing at higher temperatures for 2 weeks.

In the first series of blends, polystyrene (PS13) having molecular weight equal to that of the S-block molecular weight of copolymer was blended (4%, 8%, 18%, 37% 44% and 60%hPS) in SBS. In the second series, polystyrene (PS65) having molecular weight equal to that of copolymer molecular weight was blended to give mixtures (4%, 8%, 16% and 32% SBS) in hPS. Cryo-ultramicrotomy was employed (-90 to -135^0C) to get ultrathin sections (~ 50-90 nm) of the polymer film and the sections were stained in vapors of OsO_4.

TEM micrographs verified for the first series of blends, that the microphase separated SBS host accomodated small fractions of hPS within its lamellar S-block domains as these domains experienced swelling. At 37%hPS a new 'soda-straw' morphology was discovered and at 60%hPS, complete destruction of lamellar morphology of copolymer was seen. In the second blend series, small SBS concentrations produced no visible macrophase separation and SBS was apparently solubilized (perhaps as micelles). Then, at 32%SBS, macrophase separation was seen wherein the copolymer-rich phase adopted a morphology identical to that of pure copolymer, apparently rejecting hPS from its PS lamellar domains.

Differential scanning calorimetry (DSC) experiments provided evidence for the neutral nature of the solvent (dipentene). In the first blend series, a glass transition for the interphase was observed in all blends. A model for predicting T_g^I from the simultaneously measured T_g^S and T_g^B, in terms of the average interphase composition, was most successful when that composition was assumed equal to the overall copolymer composition. The interphase transition was not observed when, instead of dipentene, toluene (preferential solvent for polystyrene) was used. The variations in glass transitions of styrene and butadiene phases in blends were interpreted in terms of morphological features of the system. In the second blend series, two polystyrene glass transitions were observed, corresponding to S-block and hPS.

ACKNOWLEDGMENTS

I would like to express my sincere thanks to the following:

Professor M.C. Williams for providing me the opportunity to work on this thesis, and for his support and guidance, both intellectually and emotionally.

Mr. Rakesh Bhatnagar for his immense help with TEM and Cryo-ultramicrotomy, without whose help this project would not have been possible.

Dr. Andy Guo for molecular weight characterization of polystyrenes.

Dr. U. Sundararaj, Dr. R. Egerton and Dr. J. Ryan for their participation and valuable input as committee members.

Cindy and Bev for administrative help and conversation.

Bob and Walter for technical support.

All the members of Polymer and Rheology Laboratory.

Natural Sciences and Engineering Research Council for financial support.

Rupa, my best friend and wife, for her love and patience and for her active participation (more than me!) in completion of this thesis.

TABLE OF CONTENTS

Page

CHAPTER 1 INTRODUCTION: BLOCK COPOLYMER 1

1.1 PHYSICAL BLENDING 1
1.2 INTRAMOLECULAR BLENDING 3
  1.2.1 Alternating and Random Copolymers 3
  1.2.2 Block Copolymers 4
1.3 BLOCK COPOLYMER ARCHITECTURE 4
1.4 MICROSTRUCTURE 5
1.5 BLOCK COPOLYMERS AND BLENDS 14
1.6 ROLE OF SOLVENT IN BLOCK COPOLYMER STUDIES 15
  1.6.1 Selective Solvent and Block Copolymer 16
  1.6.2 Neutral Solvent and Block Copolymer 16
  1.6.3 Selective Solvent in Blends of Block Copolymer/Homopolymer 16
  1.6.4 Neutral Solvent in Blends of Block Copolymer/Homopolymer 17

CHAPTER 2 INTRODUCTION TO ELECTRON MICROSCOPY 18

2.1 SCANNING ELECTRON MICROSCOPY 20
  2.1.1 Image Formation in SEM 20
  2.1.2 Magnification and Resolution in SEM 22
  2.1.3 Advantages and Limitations of SEM 23
  2.1.4 Sample Preparation for SEM 23
2.2 TRANSMISSION ELECTRON MICROSCOPY 23
  2.2.1 Image Formation in TEM 24
  2.2.2 Magnification and Resolution in TEM 26
  2.2.3 Advantages and Limitations of TEM 26
  2.2.4 Sample Preparation for TEM 27

CHAPTER 3 REVIEW OF LITERATURE 29

3.1 THEORY OF MICROPHASE SEPARATION IN PURE BLOCK COPOLYMERS 29
3.2 GENERAL FEATURES OF BLOCK COPOLYMERS/ HOMOPOLYMERS BLENDS 30
3.3 WHEN THE COPOLYMER IS DILUTE: THE MICELLE CONCEPT 31

3.4 WHEN THE HOMOPOLYMER IS DILUTE: SWELLING OF MICROSTRUCTURE 33
3.5 EXPERIMENTS 35
    3.5.1 Disorder and Micelle Formation in Block Copolymer/Homopolymers Blends 35
    3.5.2 Block Copolymer/Homopolymer Blends: Effect of Molecular Weight on Solubility 38
    3.5.3 Blends of AB and Homopolymer 40
    3.5.4 ABA (Triblock) and Homopolymer (A or B) Type of Blends 43

CHAPTER 4 MATERIALS AND METHODS 49

4.1 BLEND PREPARATION 49
    4.1.1 Mechanical Blending (Melt Blending) 49
    4.1.2 Solution Blending 51
    4.1.3 Blend Protocol (SBS + PS) Using Neutral Solvent 54
4.2 PREPARATION OF SPECIMENS FOR ELECTRON MICROSCOPY 57
    4.2.2 Specimens for TEM 57
4.3 CRYO-ULTRAMICROTOMY 60
    4.3.1 Preparation of the Specimen 60
    4.3.2 Knives 62
    4.3.3 Temperature Selection for Cryo-ultramicrotomy 64
    4.3.4 Collection of Sections 64
    4.3.5 Osmium Staining 65
    4.3.6 Cryo-ultramicrotome Equipment 65
4.4 DIFFERENTIAL SCANNING CALORIMETRY 65
4.5 ELECTRON MICROSCOPES 66
4.6 BRABENDER DO-CORDER 66
4.7 MATERIALS 67

CHAPTER 5 TRANSMISSION ELECTRON MICROSCOPY 68

5.1 MORPHOLOGY IN SBS BLOCK COPOLYMERS 68
5.2 SOLUTION BLENDING: MORPHOLOGY IN BLENDS OF BLOCK COPOLYMER AND hPS 72
    5.2.1 Solution blends with $M_S \approx M_{hPS}$ 75
    5.2.2 Solution blends with $M_{SBS} \approx M_{hPS}$ 95
5.3 Microdomain Spacings in Copolymer/Homopolymer Blends 99

CHAPTER 6 DIFFERENTIAL SCANNING CALORIMETRY 101

6.1 INTRODUCTION 101

6.2 DSC SCANS FOR PURE SBS TRIBLOCK COPLOYMER (S29) AND HOMOPOLYMERS 101
6.3 DSC SCANS (FOR SOLUTION BLENDS WITH $M_S = M_{PS} = 13,000$) 105
  6.3.1 Results of Three Heating Cycles 105
  6.3.2 Scanning to 270^{0}C at the Rate of 10^{0}C/min. 114
  6.3.3 Scanning to 270^{0}C at the Rate of 5^{0}C/min. 117
  6.3.4 60% hPS Blend with Trace Amount of Solvent (Dipentene) 119
6.4 DSC SCANS (FOR SOLUTION BLENDS WITH $M_{SBS} = M_{PS} \cong 62,000$) 121
6.5 DSC RESULTS: Effects of Scanning Rate and Solvent of Blending 125

CHAPTER 7 DISCUSSIONS **129**

7.1 IS DIPENTENE A TRUE SOLVENT? 129
  7.1.1 Solubility Parameter Consideration 129
  7.1.2 Turbidity Analysis of Solution 131
  7.1.3 Molecular Structural Similarities 131
  7.1.4 Microstructures 131
7.2 TEM MICROGRAPHS 133
  7.2.1 Microphase and Macrophase Separation in Homopolymer/Copolymer Blends 133
  7.2.2 A Priori Predictions of Miscibility and Comparison with Results 137
  7.2.3 Compositions of Phases in Homopolymer/Copolymer Blends 138
  7.2.4 Observations of New Morphologies 139
7.3 DIFFERENTIAL SCANNING CALORIMETRY 141
  7.3.1 Pure Copolymer and Homopolymer 141
  7.3.2 Thermal Cyclic Tests on Blends of Block Copolymer and Homopolymer 142
  7.3.3 Equilibrium or Non-Equilibrium Morphologies? 144
  7.3.4 Intermediate Glass Transition in Blends of SBS & hPS 145
  7.3.5 Interphase Glass Transition: Comparison with Previous Data 148
  7.3.6 Effect of Solvent on Interphase Composition 151
  7.3.7 Glass Transitions in Copolymer/Homopolymer Blends $M_{SBS} = M_{hPS} \cong 62,000$ 151
7.4 TEM AND DSC RESULTS: A COMPARISON 152

REFERENCES **154**

APPENDICES

LIST OF TABLES

Table **Page**

Table 3.1. Review of block copolymer/homopolymer blends 46

Table 4.2 Solvent removal and annealing procedure 57

Table 5.1 Solution blends of polystyrenes (PS13 and PS65) with SBS (S129) 74

Table 6.1 Tabulation of DSC data of Figures 6.1-2 105

Table 6.2 Tabulation of DSC data of Figures 6.3-5 110

Table 6.3 Tabulation of DSC data of Figure 6.6 115

Table 6.4 Tabulation of DSC data of Figure 6.7 117

Table 6.5 Tabulation of DSC data of Figure 6.8 121

Table 6.6 Tabulation of DSC data of Figure 6.9 123

Table 6.7 Tabulation of DSC data of Figure 6.11 128

Table 7.1 Comparison of predicted intermediate glass transitions with the data 146

Table 7.2 Comparison of predicted intermediate glass transitions with the data 147

Table 7.3 Comparison of data on intermediate glass transitions 150

LIST OF FIGURES

Figure		Pages
Figure 1.1	Schematic representation of triblock copolymer	2
Figure 1.2	Schematic representation of alternating and random copolymers	6
Figure 1.3	Schematic representation of block copolymer architecture	7
Figure 1.4	Schematic representation of microphase separation in block copolymer	8
Figure 1.5	Morphologies observed in block copolymers	10
Figure 1.6	Schematic representation of microstructural dimensions (spherical, cylindrical and lamellar morphologies)	13
Figure 2.1	Various modes of beam-specimen interactions in Electron microscopy	21
Figure 2.2	Comparison of TEM with OM	25
Figure 3.1	Schematic representation of microphase and macrophase separation in SB/hPS blends	32
Figure 4.1	Chemical structures of dipentene, styrene and butadiene	56
Figure 5.1	TEM micrograph of SBS 129 (direct casting)	69
Figure 5.2	TEM micrograph of SBS 127 (direct casting)	70
Figure 5.3	TEM micrograph of SBS 129 (cryomicrotomy)	71
Figure 5.4	TEM micrograph of SBS 127 (as received)	73
Figure 5.5	TEM micrograph of 4% hPS blend	76
Figure 5.6	TEM micrograph of 4% hPS blend	77
Figure 5.7	TEM micrograph of 4% hPS blend	78

LIST OF FIGURES (CONTINUED)

Figure	Pages
Figure 5.8 TEM micrograph of 8% hPS blend	79
Figure 5.9 TEM micrograph of 8% hPS blend	80
Figure 5.10 TEM micrograph of 8% hPS blend	81
Figure 5.11 TEM micrograph of 18% hPS blend	82
Figure 5.12 TEM micrograph of 18% hPS blend	83
Figure 5.13 TEM micrograph of 37% hPS blend	85
Figure 5.14 TEM micrograph of 37% hPS blend	86
Figure 5.15 TEM micrograph of 37% hPS blend	87
Figure 5.16-a TEM micrograph of 37% hPS blend	88
Figure 5.16-b TEM micrograph of 37% hPS blend	89
Figure 5.17 TEM micrograph of 44% hPS blend	90
Figure 5.18 TEM micrograph of 60% hPS blend	92
Figure 5.19 TEM micrograph of 60% hPS blend	93
Figure 5.20 TEM micrograph of 60% hPS blend	94
Figure 5.21 TEM micrograph of 16% SBS blend	96
Figure 5.22 TEM micrograph of 32% SBS blend	97
Figure 5.23 TEM micrograph of 32% SBS blend	98
Figure 6.1 DSC scans of as-received and as-cast SBS	103

LIST OF FIGURES (CONTINUED)

Figure **Pages**

Figure 6.2 DSC scans of PS13, PS65, PB165 104

Figure 6.3 DSC scans of first blend series (first heating cycle) 107

Figure 6.4 DSC scans of first blend series (second heating cycle) 108

Figure 6.5 DSC scans of first blend series (third heating cycle) 109

Figure 6.5-a,b Variation of glass transition temperatures in cyclic thermal tests 111

Figure 6.6 DSC scans of first blend series @ 10^0C/min. 112

Figure 6.7 DSC scans of first blend series @ 5^0C/min. 116

Figure 6.7-a Effect of PS addition on glass transition temperatures in SBS-PS blends 118

Figure 6.8 DSC scan of 60% hPS blend @ 10^0C/min. 120

Figure 6.9 DSC scans of second blend series . 122

Figure 6.9-a Perturbations in glass transitions of hPS and block-S upon SBS addition 124

Figure 6.10 DSC scans of SBS 129 at various scanning rates 126

Figure 6.11 DSC scans of SBS 129 cast from dipentene & toluene 127

CHAPTER 1

INTRODUCTION: BLOCK COPOLYMER

The field of polymer science and technology has developed over the last several decades primarily through chemical diversity. To begin with, there was the development of new polymers from a seemingly endless variety of monomers. Next, came the concept of random copolymerization which was used as an effective technique for tailoring or modifying polymers. The concept of physically blending two or more homopolymers emerged to obtain new products with desired properties. Later, more controlled copolymerization (block and graft) was introduced.

One specific area that has held and continues to hold the attention of investigators is the area of "complex polymeric composites". These composites, representing polymers composed of two or more components, offer properties either (a) intermediate of component homopolymers or (b) substantially different from either homopolymer. This work is primarily concerned with one such member of the latter type of composites: block copolymer.

Block copolymers are polymeric chains having two or more monomer constituents grouped in large segments or blocks which are covalently bonded to other segments to form a single linear chain (Figure 1.1).

1.1 Physical Blending

Consider the case of simply mixing two homopolymers. If these are compatible and form a homogeneous mixture, the latter possesses material properties intermediate between those of its components; in fact, these properties -- e.g., the glass transition temperature (T_g) of the blend -- may often be calculated by weighting the properties of the homopolymers to match the bulk composition [85] (e.g., for components 1 and 2, $T_{g\text{-blend}} = w_1 T_{g(1)} + w_2 T_{g(2)}$). If the homopolymers are chemically dissimilar, large scale separation

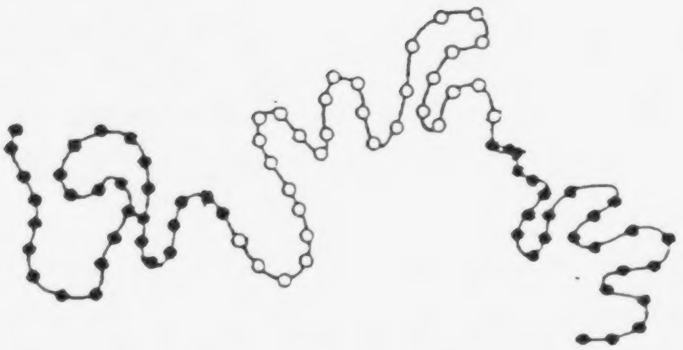

Figure 1.1 Triblock copolymer of the ABA type; end blocks are of the same chemical structure

normally occurs at phase separating conditions as the system seeks a minimum in its free energy to determine its state of equilibrium [59, 60]. An important point here concerning macrophase separation is that the resultant phases are much larger than the size scale of polymer coils (in fact, these macrophases are often visible either with the unaided eye or with a low-magnification optical microscope).

1.2 Intramolecular Blending

Designing polymeric composites with a greater diversity of bulk properties has led to the development of "microcomposites" in which the "mixing" is accomplished on a molecular level within a polymer molecule. That is, rather than simply blending two homopolymers and obtaining a macrocomposite, one could perform a copolymerization and intersperse or sequences of one component amidst sequences of the other component. Similar to the macroscopic blend described above, phase separation may again be the thermodynamically-favored equilibrium state. However, due to the fact that the unlike components are covalently bonded together in the case of the microcomposite, the size scales of the resulting phases are dependent on sequence length or block length in the copolymer, the chemical characteristics of the components, and the degree of copolymerization [70, 49].

1.2.1 Alternating and Random Copolymers

For the sake of consistency, the classes of copolymers to be discussed further here exhibit an equal molar composition of A-monomers and B-monomers. In one limit of the copolymerization process, the resulting copolymer exhibits an arrangement in which the sequence length is one monomer unit and the monomers alternate (Figure 1.2, top). Logically, this copolymer is referred to as an *alternating* copolymer. A random copolymer is exemplified by the larger, variable length sequences of A and B (Figure 1.2, bottom). To retain its "random" nature, this class of copolymer possesses "like" sequences that are generally short; consequently, microphases cannot form in a random copolymer even if the components are thermodynamically incompatible.

1.2.2 Block Copolymers

In the case that the architecture of the copolymer consists of rather long sequences of each component, the copolymer is said to possess "blockiness" and is often referred to as a "block" (or "blocked") copolymer. If the block copolymer molecule is comprised of more than three alternating sequences, the block copolymer is categorized as a multiblock copolymer. Other forms are discussed below.

Currently, the major commercial use of block copolymers in their bulk state is for high quality synthetic rubbers described as 'thermoplastic elastomers' [31]. They can be melt-processed or solution-cast like thermoplastics at high temperatures and yet display rubberlike elasticity at low temperature, in the absence of chemical crosslinks. This requires that the copolymer contain three or more blocks, that the S-block is rigid and B-block rubbery at room temperature, that phase separation occurs at the molecular size scale, and that the S-phase is not so extensive as to prevent B-phase continuity. The explanation as to how this can occur will be given shortly.

The availability of these macromolecules prompted further studies of their solution and bulk properties. These findings, in turn, have led to a much better understanding of the structure-property relationships of block copolymers in general. In particular, one can now relate molecular weight and composition to morphology, rheology, viscoelastic behavior, solution properties, and solid-state mechanical properties.

1.3 Block Copolymer Architecture

The sequence arrangement is so important that it is recognized as a primary engineering variable: the molecular architecture.

There are several architectural variations of the block copolymer component segments. The sequential architecture in block copolymers is the prime consideration in defining the synthetic technique to be used in preparing a particular block copolymer structure. Most importantly, architecture plays a dominant role in determining the inherent properties that are attained by a copolymer produced from a pair of component monomers.

Three basic architectures of block copolymers are shown in Figure 1.3. The diblock architecture is the simplest. The diblocks are commonly known as A-B block copolymers, and are composed of one block of "A" monomer repeat units and another block of "B" monomer repeat units. Triblock copolymers made from A and B monomers (A-B-A or BAB block copolymer) consist of a single block of "B" monomer repeat units sandwiched between two blocks of "A" monomer repeat units, or vice versa. A generalization of this sequencing leads to the multiblock copolymers cited earlier. Other, less common architectural forms involve star-shaped macromolecules in which three or more diblock sequences radiate from a central hub, comb block copolymers (A-blocks affixed by one end at intervals along a long B-chain), and 'tapered' block copolymers. Tapered block copolymers have a gradually changing composition between pure A and pure B blocks.

The focus of this work will be exclusively on triblock copolymers composed of polystyrene (S) end blocks and a polybutadiene (B) middle block and on their blends with polystyrene. For these components, the A-B-A sequence is written as S-B-S, and the molecule is commonly referred to as an SBS triblock copolymer. In the work to be reported here, the SBS polymers will be commercial samples for which the two S-blocks have the same length.

1.4 Microstructure

If blocks A and B used in the formation of block copolymers are thermodynamically incompatible, then phase separation occurs below a characteristic "separation temperature" - T_s. This phase separation results in microstructures. The general term describing the geometrical relationship of these microstructures is the 'morphology'. The morphology will consist of either dispersed domains of one component embedded in a continuous matrix of the other component, or co-continuous lamellar structures. The transition from well-mixed segments to the dispersed-domain morphology is shown in Figure 1.4 for a monodisperse block copolymer possessing a diblock architecture. For $T > T_s$ (where T_s depends on composition and molecular weight), the

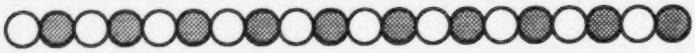

Alternating Copolymer

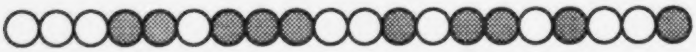

Random Copolymer

Figure 1.2 Schematic representation of alternating and random copolymers.

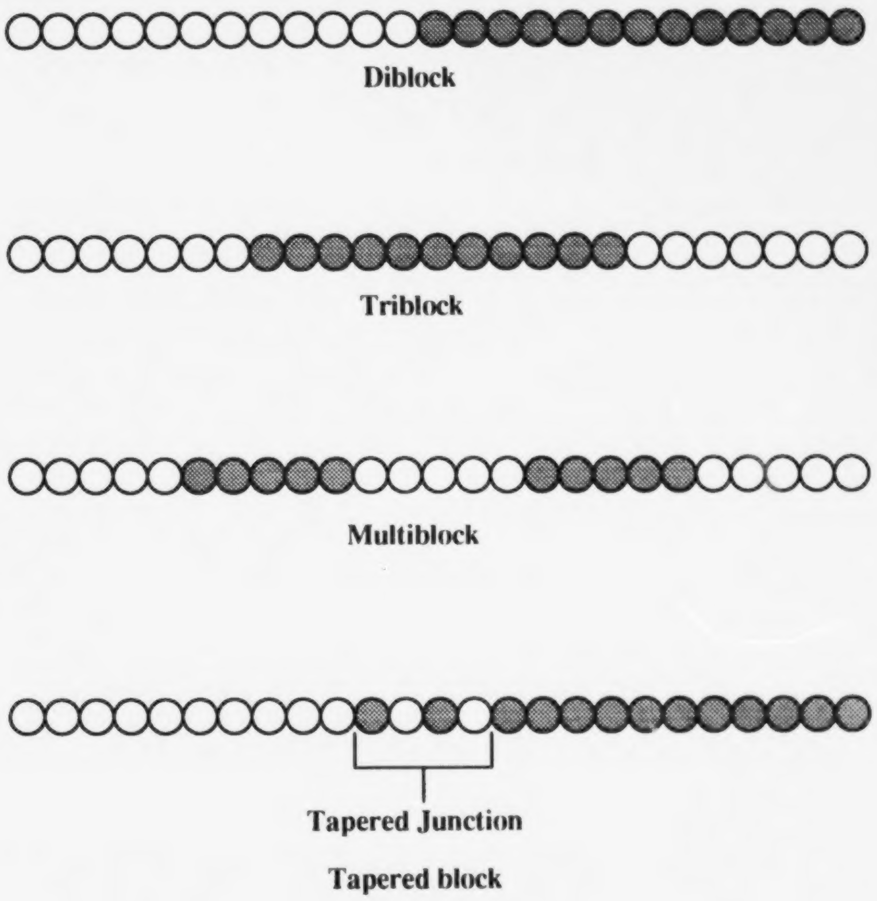
Diblock
Triblock
Multiblock
Tapered Junction
Tapered block

Figure 1.3 Schematic representation of diblock/triblock/multiblock and Tapered block copolymer architecture.

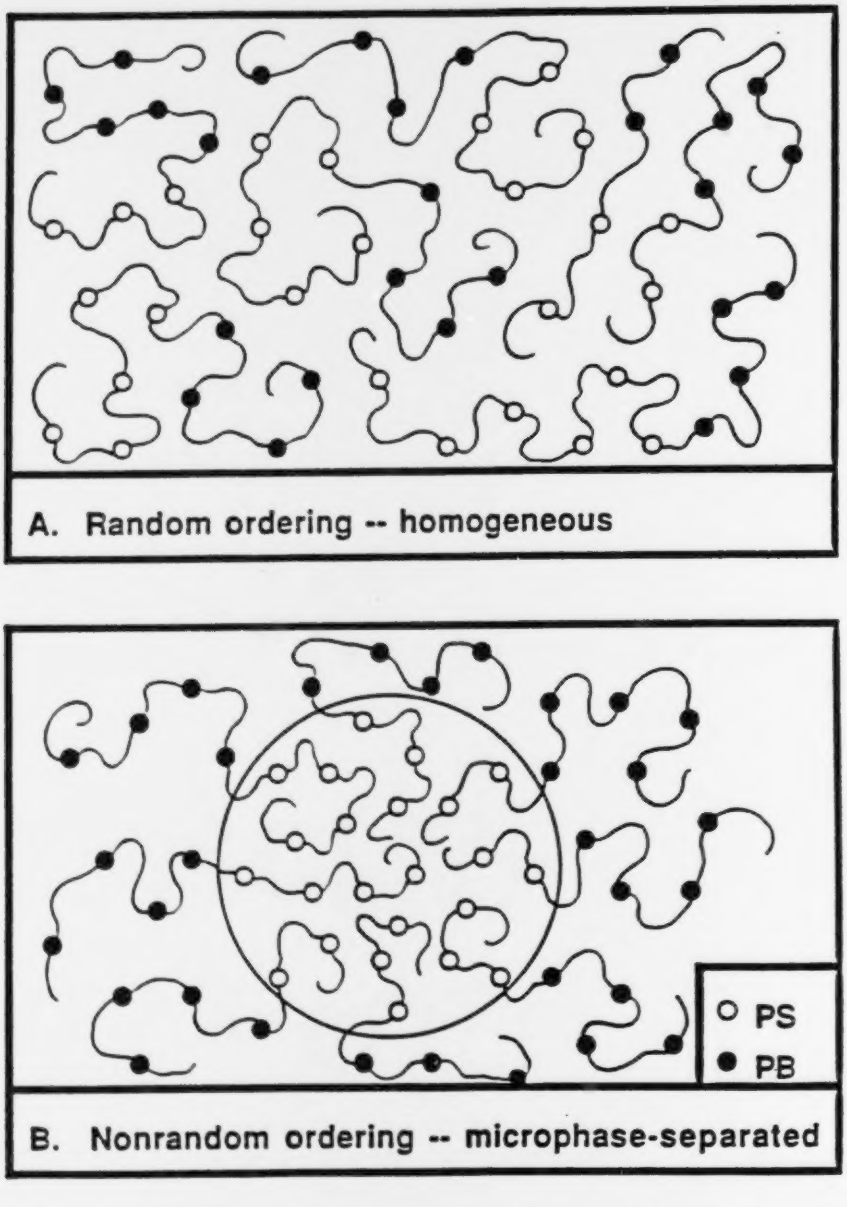
A. Random ordering -- homogeneous
○ PS
● PB
B. Nonrandom ordering -- microphase-separated

Figure 1.4 Schematic of block segregation in a monodisperse diblock (SB) copolymer upon microphase separation. Blocks of PS (light) and PB (dark) are randomly distributed in the homogenous state, $T>T_S$ (top). Upon microphase separation (bottom), the blocks (in this case PS) segregate to form microstructures, or domains, on the size scale of the block end-to-end distance.

copolymer will remain homogeneous and no phase separation will occur. However, at $T<T_S$, usually experienced in practice, microphase separation is thermodynamically favored, thereby allowing the formation of segregated microphases. It is clear from Figure 1.4 that the size scale of the styrene domains is on the same order as the S-block end-to-end distance.

The primary factor that influences the type of microstructure formed in phase-separated systems is the molecular composition (same as bulk composition), often expressed in terms of weight or volume fraction of either component in the copolymer. Microstructures in pure diblock and triblock copolymers will be discussed, as these systems are the most understood among all types of block copolymers.

When the composition is approximately 50/50, co-continuous lamellae are expected (under the condition of thermodynamic equilibrium); however, as the composition deviates from this midpoint, lamellae are expected to be replaced by discrete domains of the lesser component interspersed in a matrix of the other component. This variation of microstructural development is described in Figure 1.5. As the volume fraction of S increases (from left to right), the observed microstructures evolve in the following sequence: S spheres in a B matrix, S cylinders in a B matrix, co-continuous S and B lamellae, B cylinders in an S matrix, and B spheres in an S matrix. On each end of the composition spectrum in Figure 1.5, the fraction of the minor component is so small that microphase separation does not occur at the temperature of use. In this end range of composition, the copolymer behaves as a homogeneous mixture (similar to a random copolymer) dominated by the major component.

Consider a block copolymer with components polybutadiene, which is rubber at room temperature, and polystyrene, which is plastic at room temperature. In the case of styrene domains in the butadiene matrix, the block copolymer behaves as a filled rubber. Butadiene domains in the styrene matrix form morphologies referred to as "inverted" microstructures and are responsible for bulk mechanical properties analogous to those of a rubber-reinforced plastic.

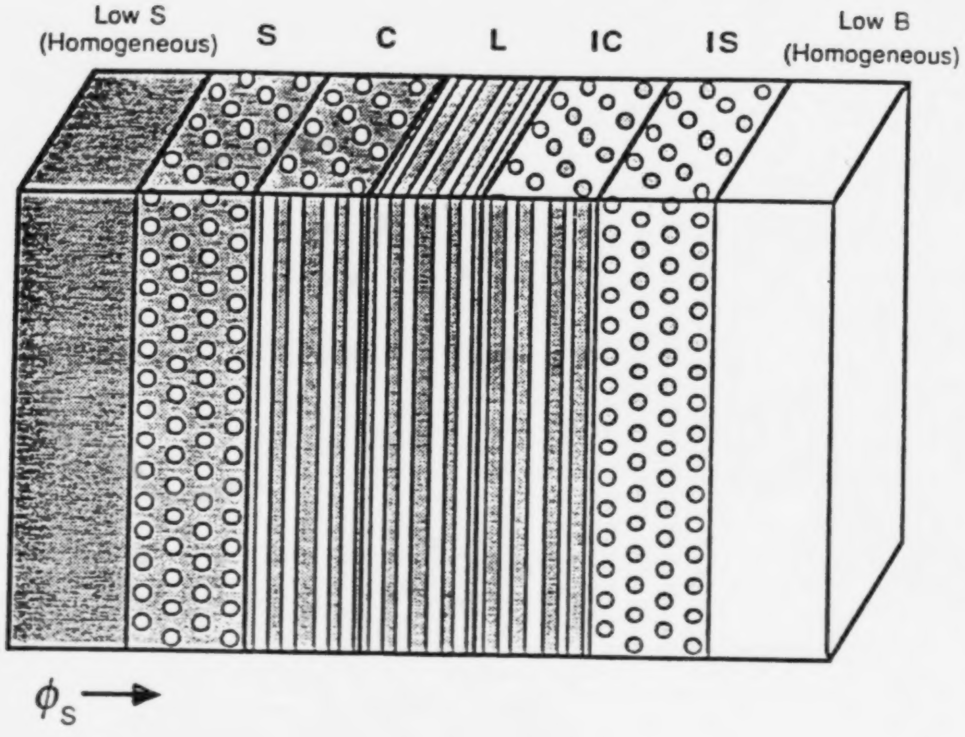
Low S
(Homogeneous)
S
C
L
IC
IS
Low B
(Homogeneous)
ϕ_S →

Figure 1.5 Morphologies observed in microphase-separated block copolymers composed of PS and PB. In the low-ϕ_S regime, spherical domains of PS form in a PB matrix to produce the equivalent of a "filled" rubber. As ϕ_S increases, the spherical PS domains yield to cylindrical PS domains and then to co-continuous lamellae. Inverted domains of PB in a PS matrix at observed at higher ϕ_S, where the copolymer behaves as a "high-impact" plastic.

Most of the work presented here will focus on SBS triblock copolymer with 44 wt% styrene and exhibiting co-continuous lamellar morphology. The unique feature of block copolymers (triblock and multiblock) is their thermo-mechanical behavior. They behave as filled crosslinked elastomers at application temperature and yet are processable as thermoplastic melts at elevated temperatures. This thermo-mechanical behavior associated with block copolymers is attributed to the fact that the styrene domains are glassy at room temperature and act as mechanical crosslinks in the rubbery matrix. Unlike crosslinked rubber, there are no chemical crosslinks [31]. This is most easily visualized for the SBS type of copolymers, in which both S-ends are anchored in these glassy domains and the middle B-chains endow the matrix with elastomeric qualities (The analogue to this for AB systems is shown in Figure 1.4, but here there is no 'crosslinking' because the S-domains cannot be mechanically connected.). When the temperature of the block copolymer is raised above the glass transition temperature of styrene (T_g^S), the styrene domains lose their rigidity and stop acting like rigid crosslinks. However, the system remains microphase separated and retains a soft solid-like character because of thermodynamic interphase barriers [32] while both phases are fluid. At still higher temperature even this sort of linkage is eliminated when $T>T_S$ (if this can be achieved without thermal degradation), thereby allowing facilitated processing because the microstructure is homogenized and the block copolymer behaves as a random copolymer.

The junction of the blocks (Figure 1.6) resides in a region designated as "interphase", measuring between 1nm and 4nm in ideal block copolymers. This region, denoted by "S+B" in the figure, has thicknesses of ΔT and ΔR in the lamellar and spherical/cylindrical morphologies, respectively. Research in block copolymer rheology has substantiated the significance of this interphase region [15].

Figures 1.5 and 1.6 represent the most common equilibrium microstructures that form in block copolymers. However, the actual block emplacements within these structures may be more complex and sometime different microstructures can form as a consequence of having a multiplicity of possible block configurations. The situation is most simple in a diblock copolymer, since one block is located within its microphase and the other block resides in its microphase, and no loops are possible. The triblock copolymer has one additional degree of freedom: in addition to restricting one end-block and the middle block to their respective microphases, the other end-block must find its microphase in order to minimize the free energy of the system. To do so, the second end-block can either reside in an adjacent domain (Figure 1.6) or loop back to the already-occupied domain. In the latter possibility, both ends of the triblock molecule are anchored in the same domain. As the number of block sequences increases, the complexity of this looping/linear molecular configuration also increases. In principle, the multiblock chain may be so extended that each of its segregating blocks resides in a different domain. However, due to diffusional limitations, chain looping is expected to occur frequently; interdomain connections can still exist through entanglements of loops belonging to adjacent domains.

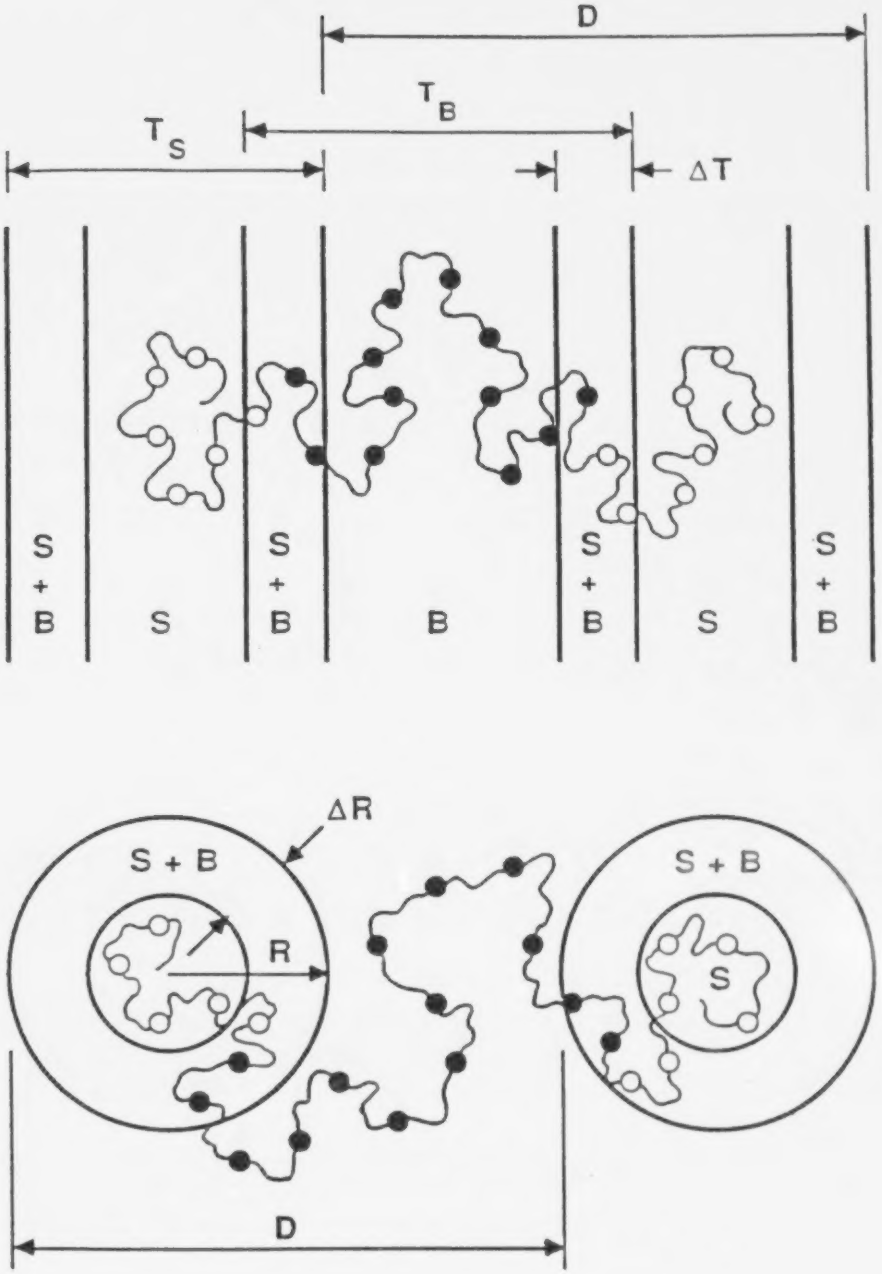

Figure 1.6 Schematic representation of the microstructural dimensions of the lamellar morphology (top) and spherically/cylindrical morphologies (bottom) in an SBS block copolymer. The block junctions are located within the mixed S+B interphase region (ΔR in spheres/cylinders and ΔT in lamellae).

1.5 Block Copolymers and Blends

One of the larger areas of application for block copolymers is in modifying the physical properties of other polymers. Alloys of block copolymer and a homopolymer (i.e., with hA or hB) are possible due to the compatibility of, or phase adhesion between, one segment of a block copolymer and its corresponding homopolymer. Within certain molecular dimensional limits, the homopolymer molecules are thermodynamically indistinguishable from the corresponding block segments. Based on similar arguments when hA and hB are both present, we find that block copolymers can also emulsify and thus "compatibilize" two macrophase-separated homopolymers. These characteristics have led to a number of applications for styrene-diene-styrene systems.

One motivation for developing block copolymer may have been the success of high-impact polystyrene (HIPS). One of the most important multicomponent polymers, HIPS is a copolymerized blend of hPS and the graft copolymer of styrene and butadiene. A clear parallel to the use of the graft copolymer would be to incorporate AB copolymer. However, whether this kind of effort will successfully result in more outstanding properties will depend on a thorough understanding of the miscibility behavior between the block copolymer and the corresponding homopolymers. A second motivation for studying block copolymer blends with homopolymers is that lack of adhesion between the component homopolymers (hA, hB) often makes it difficult to produce hA/hB blends with the desired properties by simple blending. The addition of the corresponding block or graft copolymers to the blends has been proved effective in improving interfacial adhesion, thus making possible the desired combination of properties in the macrophase-separated homopolymer blends. While the rules governing phase separation in the cases of either homopolymer blends or block copolymers are rather clear and defined, some ambiguity and discrepancy still exist in the cases of block copolymer / homopolymer blends.

There are numerous applications in which block copolymers are blended with homopolymers or random copolymers. In all of these cases, the block copolymer consists of both rubbery and rigid (glassy or crystalline) blocks. Four combinations are possible with block copolymer as either the minor or major component, and with a homopolymer having either rubbery or rigid (glassy or semicrystalline) character. All four possibilities have found applications. These can be further classified as (a) one block of the block copolymer being chemically identical to the homopolymer and (b) neither block being chemically identical to the homopolymer.

In the present work, blends of hPS and SBS block copolymer are considered representing case (a) above and the concentration range includes the two situations where the SBS is either the minor or major component. It happens that hPS is a rigid glassy polymer at room temperature, but the sample microstructures are formed from concentrated solutions wherein all microphases are liquid (rubbery).

1.6 Role of Solvent in Block Copolymer Studies

It is a challenging task to test various block copolymers at processing temperatures above their separation temperature [At these temperatures, block copolymers behave like random copolymers and are in a disordered state (ordered state is the microphase separated state)]. This is because most commercially available copolymers contain blocks that are highly incompatible and as a consequence T_S is very high. The disordered phase in bulk systems can rarely be accessed by increasing temperature, due to thermal decomposition. However this obstacle can be overcome in solvated systems.

Another important task is to achieve equilibrium in these systems. At T_S, block copolymers change from disordered state (viscoelastic fluid) to ordered state (a weakly bound elastic solid). Below T_S, it is not necessarily true that copolymers will form the morphology with the lowest free energy. The system could become 'frozen' in one of the many metastable structures. On further cooling of the copolymer, the transitions between ordered structures would not be observed for kinetic reasons, i.e., the system might become locked in the structures formed at T_S because the free energy barrier leading to the most stable structure is too large to surmount. The use of solvents for casting samples may provide sufficient chain mobility so that equilibrium states can be achieved.

1.6.1 Selective Solvent and Block Copolymer

It was recognized years ago that many of these experimental difficulties are greatly alleviated when a solvent component is added to the bulk copolymer, and a number of researchers used solvent in studying block copolymer morphology. However, if the solvent is selective for one of the components of the copolymer, then the solution can have an extremely complicated phase diagram (including micellar phases) that may differ entirely from that of the pure melt.

1.6.2 Neutral Solvent and Block Copolymer

If the solvent is a good solvent of roughly equal affinity for both types of blocks, one expects that the copolymer solution will have microphase separation similar to that of the pure melt but at a depressed T_S. That is, the solution plays a neutral role in the thermodynamics and serves primarily to separate the polymer chains, merely occupying volume in an unbiased fashion. In such solution, equilibrium is more easily attained than in the melt and, because the unfavorable interactions among the blocks are diluted by the solvent, order-disorder transitions (around T_S) can be more easily accessed [42].

1.6.3 Selective Solvent in Blends of Block Copolymer/Homopolymer

Experimental difficulties become more complicated in studying blends of block copolymer and homopolymer. Consider making a blend of SBS diblock copolymer and homopolystyrene using toluene as a solvent. Toluene is a preferential solvent for polystyrene and is thus a good choice for dissolving the hPS, while still being an adequate (though not neutral) solvent for SBS. In addition, homopolystyrene in the final blend will be a strongly biased 'solvent' for the styrene block of the copolymer, and this should affect the morphology obtained.

Consider, first the complications involving just toluene and the block copolymer alone. As solvent is slowly evaporated from the concentrated solution, polybutadiene will be the first to come out of the solvent, as toluene has lower affinity for polybutadiene. Micelles consisting of an internal PB phase with external solvated PS-chains, will form.

Upon further evaporation of solvent, this micellar butadiene phase will become leaner in toluene, and the solvated styrene phase will be the last phase for toluene to leave. A similar evolution should apply to solutions of blended PS and SBS. This can have significant effect on morphology. Once butadiene comes out of the solution, no further morphological transitions are possible between the phases, and the morphology is locked in (inspite of the presence of a substantial amount of solvent in the system). Thus, in the plasticized solid state, the solvent concentration profile in the SBS microphases would be inhomogeneous with a maximum in styrene domains, a sharp decrease in the interphase region, and a minimum in butadiene.

1.6.4 Neutral Solvent in Blends of Block Copolymer/Homopolymer

Use of a neutral solvent such as dipentene for the system described above would leave almost no effects on morphology of solution blends. Again, we consider first the case of the copolymer solute alone. As solvent evaporates, the PS and PB phases will both come out of solution at the same time, resembling the microphase separation of melts. For the highly concentrated (plasticized) copolymer solution in dipentene, dipentene leaves the PS and PB microphases at the same time, too, but traces will reside somewhat longer in the interphase which is the most favorable environment for a true neutral solvent. Thus, with $T < T_S$ and dryness approaching, we would observe homogeneous solvent concentration profiles everywhere except within the interphase and perhaps nearby. The solvent concentration would have a maximum at the interphase, decreasing away from the interphase into both component domains. Similar considerations would apply also to solutions of homopolymer and block copolymer, although drying would be slower if the homopolymer were hPS (low-permeability glass, for $T<T_S^{PS}$) than if it were hPB (high-permeability rubber, in the same T-range).

CHAPTER 2

INTRODUCTION TO ELECTRON MICROSCOPY

The domains formed in the microphase-separated block copolymers are on the same size scale as that of the polymer coils themselves. Thus the microstructural element sizes (domain sizes) are typically on the order of tens of nanometers, so small that they restrict the methods by which they can be studied directly. However, indirect methods of characterizing the microstructures from the bulk-property data have been accomplished and valuable information has been derived.

For example, researchers have successfully used dynamic mechanical testing (DMT) to relate linear viscoelastic properties of the bulk material to microstructural characteristics [16, 33]. In general, the rheology of the block copolymers is quite complex and is especially sensitive to temperature. For example, at ambient conditions, the hard block (e.g., S) may be in a glassy state and behave as a crosslink for the rubbery block. If the copolymer is heated above the T_g of the hard block, copolymer processing is facilitated due to the fluid nature of the material. For AB copolymers, which cannot form interdomain molecular linkages, the microstructure is then similar to that of a free emulsion and normal liquid fluidity is possible. For ABA and multiblock copolymers, the interdomain linkages (direct and loop-entangled) remain in place and can constitute considerable strength; e.g., a yield stress is established in the liquid state [100]. At still higher temperatures ($T>T_s$), the block copolymer loses its microstructure and behaves as a corresponding random copolymer. In fact, rheological data have been established as a criterion [33] for deducing T_S in diblock/triblock copolymers. In addition, attempts have been made to use DMT to indirectly determine the composition profile across the interphase region, since the interphase region significantly influences the bulk properties [50].

Another indirect method of characterizing the effects of microstructures on bulk properties is differential scanning calorimetry (DSC). One of the most important properties measured by DSC is T_S.

Detailed information about the average microstructural dimensions has been obtained using small-angle X-ray scattering (SAXS), either with block copolymers [34, 35, 37] or with blends of block copolymers and homopolymers [87, 112]. Small-angle neutron scattering (SANS) has been used in characterizing block copolymers [2, 38, 86] and blends of block copolymers and homopolymers [3, 82, 96]. Both techniques rely on the fact that scattering patterns of particles (whose wavelengths are smaller than the microstructural dimensions of interest) can be used to determine the domain size and repeat distance. One characteristic of these techniques is that average microstructural dimensions obtained from a specimen are representative of the entire bulk sample; local regions are not being probed individually. This can be an advantage in the sense of giving a fair representation of the whole sample, but a disadvantage in that specific structures cannot be observed directly. Another complication arises with certain assumptions commonly made in data analysis. For example, when attempting to apply either SANS or SAXS to determining the thickness of a very narrow region (e.g., the interphase), the most important assumption is that of the interphase composition profile [37].

While SAXS and SANS can prove useful in characterizing average block copolymer microstructures in both static and dynamic modes, direct observation of domains provides more detailed insight into their structural characteristics. Since the size of these domains is much smaller than the wavelength of ordinary light (380-760 nm), optical microscopy is not useful for this purpose. However, wavelengths used in electron microscopy are very well-suited to this task.

Electron microscopy is currently a very active field, and a complete description of its capabilities is beyond the scope of this introduction. Instead, the objective of this section is to provide some background on the modes of electron microscopy available, the principles of electron imaging, and interactions between the beam and the specimen. The various forms of electro-magnetic excitation emitted as an electron beam strikes an ultrathin specimen are shown in Figure 2.1. Each excitation mode will be described in terms of different branches of electron microscopy. First, consider the methods of electron microscopy developed to study the surfaces of samples. These include emission electron microscopy (EEM), reflection electron microscopy (REM), mirror electron microscopy (MEM), and scanning electron microscopy (SEM) [84]. In general, they are all alike in the sense that a beam is used to irradiate the surface of a specimen, thereby fostering the emission of secondary and back-scattered electrons (Figure 2.1). Due to its greater versatility, SEM is most commonly used to study the surface morphology of polymeric materials. The transmission electron microscope (TEM), which is used to image thin samples, will be described in the next section.

2.1 Scanning Electron Microscopy

The SEM is used to examine the surfaces of the specimens at high resolution. It utilizes a probe-forming electron optical system and probe beam scanning mechanism, secondary electrons (which provide detailed resolution of the surface), and back-scattered electrons (which provide depth to the topography of the sample) [111].

2.1.1 Image Formation in SEM

The probe spot, which is made as small and bright as possible since ultimate resolution depends on this, is scanned in a raster over the surface of the specimen. The incident primary electrons may themselves be reflected from the surface being examined (backscatter), or they may excite the emission of secondary electrons from just below the specimen surface. The image forming electrons are attracted into a detector placed close to the surface. Each captured electron gives rise to a flash of light in a solid scintillator. The light output corresponding to the secondary electron signal is amplified in a photomultiplier and the resulting electrical signal modulates the brightness of a display spot scanning synchronously with the probe spot. A direct image of the surface in the 'light' of emitted secondary electrons is thus produced on the face of the display tube, and may be photographed in the usual way to give a 'scanning electron micrograph'.

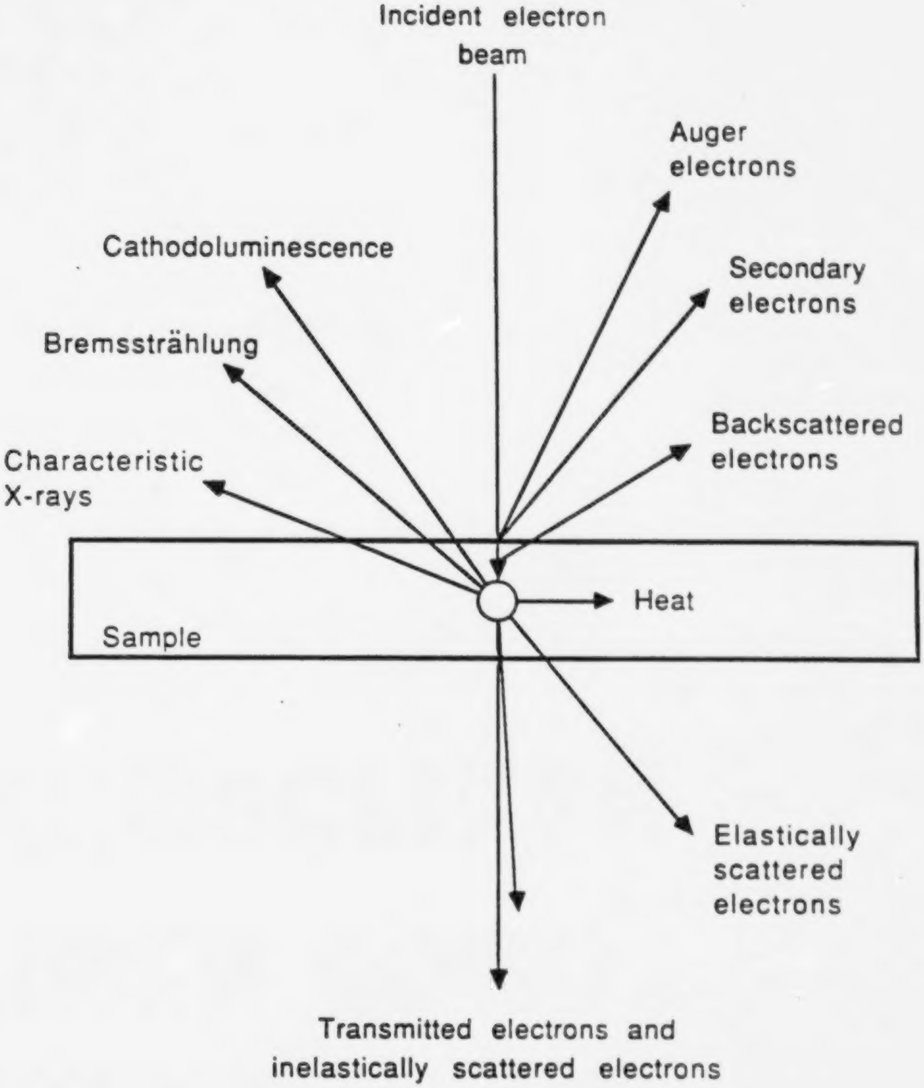
Incident electron beam
Auger electrons
Cathodoluminescence
Secondary electrons
Bremsstrählung
Backscattered electrons
Characteristic X-rays
Heat
Sample
Elastically scattered electrons
Transmitted electrons and inelastically scattered electrons

Figure 2.1 Various modes of beam-specimen interactions in an electron microscope. Scattered electrons from the surface region of the sample are used primarily in SEM, while those that penetrate through the sample are used in TEM. X-rays and inelastically scattered electrons are collected and analyzed to reveal elemental composition in EDX and EELS, respectively.

Secondary electrons are generally used rather than backscattered primaries, since these are emitted beneath the surface and one is able to 'see into' deep holes and re-entrant depressions in the surface. In both cases the number of electrons emitted is a function of the nature of the surface and its angle to the incident beam. By placing an electrically charged wire mesh grid in front of the detector and biasing it suitably, either reflected primaries or emitted secondaries can be collected. A picture of the surface is then built up on the face of the display tube by scanning the probe spot in a raster of 600-1000 individual lines.

2.1.2 Magnification and Resolution in SEM

Magnification in SEM is simply the ratio of the length of the display line on the final image tube to the length of the scan line on the specimen. The resolving power of the SEM depends primarily on the diameter of the probe spot, but it also depends on the signal to noise ratio in the final image also affects it. The latter depends on the speed with which the probe spot is scanned across the surface. The slower the scan, the greater the signal corresponding to each image point and the less the spurious signal due to random electrons or 'noise'. A micrograph at maximum resolution requires a total scan time of a minute or more, therefore the image must be recorded photographically by means of a camera (generally a polaroid) focused on the display tube-screen. A visual image of the whole field at "reasonable" resolution can be obtained on a separate long-persistence display tube with a scan time of few seconds. This enables the operator to select a field at a suitable magnification, focus the probe spot and set the correct brightness for the final photograph.

Resolving power is limited ultimately by the diameter of the probe spot. Conventional instruments using thermionic tungsten cathodes have resolving power of around 200 Angstroms, which limits top magnification to 10,000X. However, the new lanthanum boride point-source guns, which give a smaller, higher brightness virtual source under normal vacuum, are now being applied to commercial SEMs, with resulting improvement in claimed resolving power. 50 Angstroms resolution is common, and the cold cathode field emission gun should be able to give resolving power around 10-30 Angstroms.

2.1.3 Advantages and Limitations of SEM

The SEM has shown itself to be of great value to the polymer scientists, especially to those working in the areas of polymer processing and polymer blends. Specimen preparation is relatively simple, and can be accomplished in a rather short time. The depth of the field is extremely great due to the absence of imaging lenses, and the size of the specimen is limited only by the space available in the specimen chamber. The resolution obtained is at least 10 times as great as that of the light microscope. Thus, the surfaces of bulk specimens, measuring several millimeters thick, may be studied at magnifications up to about 50,000X.

The shortcomings of SEM include the fact that it is only possible to examine surfaces, and the resolution obtained is lower by an order of magnitude in comparison to TEM.

2.1.4 Sample Preparation for SEM

One of the great strengths of scanning electron microscopy is the fact that many specimens can be examined with virtually no specimen preparation. The SEM is a surface examination tool where information is carried by the backscattered and secondary electrons. Specimen thickness is not a consideration as is the case in transmission electron microscopy, where the information is carried by transmitted electrons.

Sample preparation techniques appropriate for different materials are available and described in many SEM related books [27, 28, 29].

2.2 Transmission Electron Microscopy

The principle behind TEM is that a significant fraction of electrons produced by the electron gun will be transmitted through the sample and some will show signs of elastic scattering (Figure 2.1). The operation of the transmission electron microscope (Figure 2.2) is similar to that of an optical transmission microscope[11]. The illumination source for an optical microscope is the lamp but for the electron microscope is an electron gun. The normal accelerating voltage for TEM is 60-100 kV for low-voltage (conventional) TEM, 100-400 kV for intermediate-voltage TEM, and 400-3000 kV for high-voltage TEM. The electron gun is usually a thermionic cathode possessing a filament composed of tungsten or LaB_6, although field emission guns are sometimes used [84].

2.2.1 Image Formation in TEM

Imaging in TEM is accomplished when the coordinated electrons are projected onto the fluorescent screen. In both light and transmission electron microscopes, four fundamental physical processes take part in the formation of the image. These are absorption, interference, diffraction and scattering. In general, all four contribute together to image formation. Absorption gives rise to amplitude contrast; the differences in intensity to which the eye is sensitive. It is generally the most important factor in the formation of the conventional light microscope image. Interference gives rise to phase effects, to which the eye is completely insensitive. These must first be converted to amplitude contrast before the eye can appreciate them; the effect is then known as 'phase contrast'. Diffraction effects in general degrade the image by the formation of fringes and haloes which reduce resolution and which may give rise to spurious images. Diffraction effects can be used to enhance contrast in both light and electron microscopes, but only at the expense of a certain loss of resolution. Scattering plays little part in the formation of the light microscope image but is the most important of all in the formation of the electron microscope image. Detailed descriptions of how these four processes give rise to the electron image are beyond the scope of this introduction, but are available in many books on electron microscopy [1, 11, 65, 84].

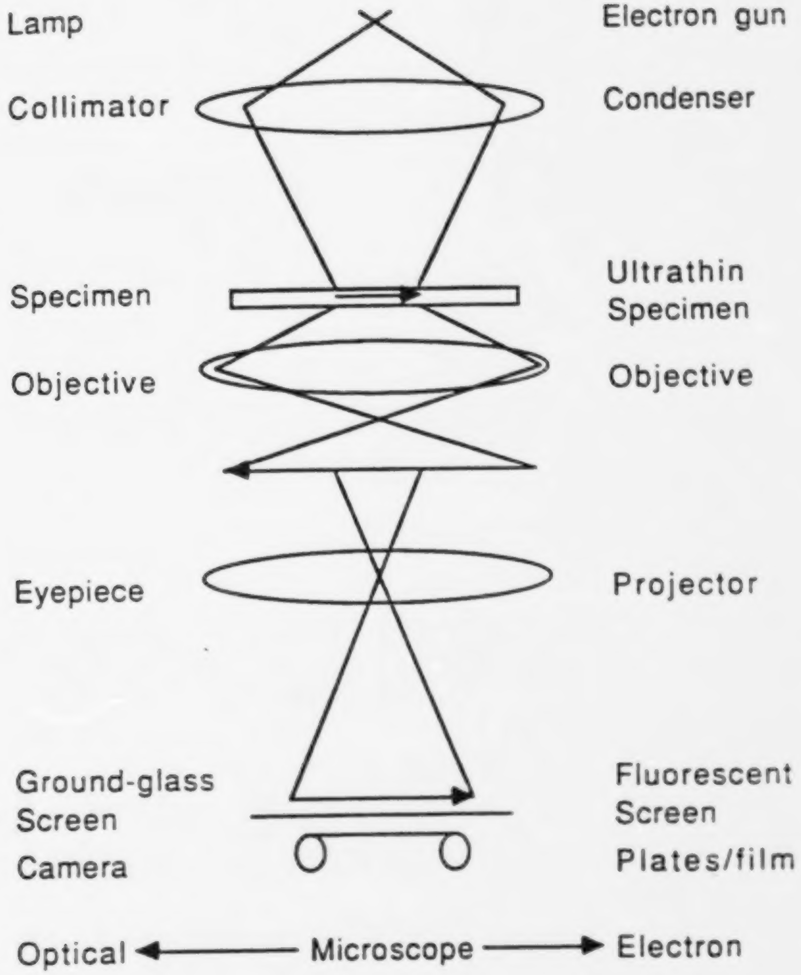
Lamp
Electron gun
Collimator
Condenser
Specimen
Ultrathin Specimen
Objective
Objective
Eyepiece
Projector
Ground-glass Screen
Fluorescent Screen
Camera
Plates/film
Optical
Microscope
Electron

Figure 2.2 Operation of the transmission electron microscope as compared to the operation of an optical microscope. In the former, electrons are generated rather than photons in the latter. Additionally, the glass lenses in the optical microscope are replaced by magnetic fields in the electron microscope.

2.2.2 Magnification and Resolution in TEM

The magnification needed to observe fine detail can be readily calculated. It is simply the ratio of the resolving power of the eye to the resolving power of the microscope. This enlarges the smallest resolvable detail up to the point where the eye can readily distinguish it. In the case of a light microscope, the resolving power is one-half-wavelength of light, which is approximately 250 nm. The unaided eye can resolve 250,000 (0.25 mm). Thus maximum magnification is simply the resolving power of the eye divided by the resolving power of the microscope, which gives a figure of 1000 times. Magnification in excess of this figure gives us no more information but merely magnifies a blur. Excess magnification is called 'empty magnification'. The resolving power of the electron microscope is about one thousand times better than that of the light microscope and thus calculation of maximum magnification comes to one million times. Any figure in excess of this is once again empty magnification.

Resolving power of the instrument is the ability to discriminate fine detail. The light microscope can discriminate fine detail, but only down to a certain limit which is imposed by the fundamental nature of the light itself. Unlike SEM, transmission electron microscopy (TEM) is operated so as to obtain image resolution on the order of 0.2-0.5 nm at the sacrifice of demanding ultrathin films less than 100 nm thick.

2.2.3 Advantages and Limitations of TEM

Since the electrons are transmitted through the ultrathin samples, information concerning the internal features of the samples -- e.g., internal morphology and crystallinity -- is revealed [95].

In addition to providing static information on two-dimensionally projected structures, some transmission electron microscopes are equipped with specialty equipment -- e.g., a tilting stage (goniometer), a heating stage, a cooling stage, a straining stage, and an environmental stage. Thus, the three dimensional nature of structures can be obtained by using a goniometer to obtain projections at varying degrees of tilt, and microstructural responses to heat or strain can be measured in-situ utilizing heating and straining stages, respectively. In some instances (for example, reducing the radiation induced heating effects of the electron beam on a sample), an ultrathin specimen must be cooled to the boiling point of liquid nitrogen, which is accomplished with a cold stage. In other cases, in-situ chemical reactions, especially oxidative reactions, can be monitored in the environmental unit. In addition to these specialty stages, many electron microscopes are equipped with microanalysis instruments. Characteristic X-rays and continuous (Bremsstrahlung) X-rays, along with Auger electrons, can be collected and used in energy-dispersive X-ray (EDX) microanalysis to discern the chemical composition of a relatively small region, depending on the size of the probe. Inelastically-scattered electrons can also provide composition information with electron energy loss spectroscopy (EELS) [109, 111].

The degree of transmittance (and hence the observed contrast) is inversely related to the atomic mass and the sample thickness. A number of conflicting factors govern the choice of specimen thickness and accelerating potential. The two requirements of 'maximum contrast' and 'highest resolution' are unfortunately mutually incompatible. Due to the electron transmittance requirement, ultrathin specimens and thus tedious methods of sample preparation are required.

2.2.4 Sample Preparation for TEM

Sample preparation is the most crucial part in the use of TEM. There are many methods of sample preparation and, in all cases, artifacts reflecting the preparation method will be found in the specimens. This point should always be taken into consideration while viewing micrographs presented here.

Specimens with the thickness of 50-100 nm thick are required for TEM work and can be obtained by either cutting ultrathin sections from a bulk sample or by dissolving the polymer in a suitable solvent and casting the dilute solution to form an ultrathin film.

Many methods exist for preparing an ultrathin film from a polymer solution [29], and almost all share one common feature: the cast film is floated on a clean fluid (e.g., water, mercury) surface. In some cases, the film is first cast on a carbon-coated glass slide and scored prior to the flotation step so that small sections may be picked up by TEM grids [86].

The above-mentioned methods share, in almost all cases, the appearance of non-equilibrium morphology due to fast evaporation of solvent leaving an ultrathin film behind. Representative bulk morphology can be obtained by cutting ultrathin sections from the bulk material using ultramicrotomy. SBS block copolymers with butadiene as a major component are rubbery at room temperature, and ultramicrotomy (which is carried out at room temperature) causes smearing (or tearing), thus disturbing the bulk morphology. This can be avoided with the use of cryo-ultramicrotomy where the sectioning is done at very low temperatures, usually below the glass transition temperature of butadiene. In this case all the polymer material is in the glassy state and thus smearing can be avoided during sectioning. Detailed processes of sample preparation are discussed in subsequent chapters.

CHAPTER 3

REVIEW OF LITERATURE

3.1 Theory of Microphase Separation in Pure Block Copolymers

As a block copolymer undergoes microphase separation, it seeks to reach a state of equilibrium, wherein the molar free energy change upon separation is minimized.

$$\Delta G \rightarrow \Delta G_{min} = (\Delta H - T\Delta S)_{min} \qquad (3.1)$$

Here, ΔG is the difference in free energy between the structured (microphase-separated) block copolymer and its homogeneous analogue at the same conditions of temperature, composition, molecular weight, and molecular architecture.

The energetic contributions to ΔG are found in the enthalpic term, ΔH, which incorporates information concerning the material properties (e.g., bulk composition, molecular weight, and chemical nature of the blocks) into the model by using a regular-solution approach to determine the enthalpy of demixing (ΔH_{demix})

$$\Delta H = \Delta H_{demix} = -\overline{V}(\delta_S - \delta_B)^2\left[\phi_S\phi_B - f\overline{\phi_S'\phi_B'}\right] \qquad (3.2)$$

Here, $\overline{V}$ is the molar volume; δ_S and δ_B are the solubility parameters for the styrene (S) and butadiene (B) blocks, respectively; and ϕ_S and ϕ_B are the volume fractions of S and B blocks, respectively. To account for the energetic effects of material remaining mixed within the interphase region, the average product of interphase compositions ($\phi_S'\phi_B'$) is multiplied by the volume fraction of material within the interphase (f), and the product is subtracted from the bulk composition product ($\phi_S\phi_B$).

Meier [72] developed a model for phase separation in diblock copolymers assuming the existence of spherical domains of A in a continuous matrix of B with a sharp boundary between the phases. The criterion for the phase separation was that the free energy difference (ΔG) between the random mixture of block copolymer segments and the domain system be negative.

Using this model, Meier developed a criterion for phase separation in terms of a critical 'separation' molecular weight (M_S) at a given composition and temperature. However, he did not take into account the effect of temperature on M_S.

Leary and Williams [59, 60] incorporated a third (mixed) region into the model. They termed this region "interphase" which is of significant dimensions (i.e., f can be quite large, perhaps 0.2-0.5) and has a great influence on copolymer properties.

Since the transition from a randomly mixed state to a phase separated state is a first order transition, the microphase separation temperature (T_S) is determined by setting $\Delta G_{min} = 0$, to give

$$T_S = \left[\frac{\Delta H}{\Delta S}\right]_S \tag{3.3}$$

3.2 General Features of Block Copolymer/Homopolymer Blends

Phase separation behavior is one of the decisive factors governing the properties of multicomponent polymer systems. One of the most important multicomponent polymers, high impact polystyrene (HIPS) is virtually a blend of homopolystyrene and the graft copolymer of styrene and butadiene. Some attempts have been made [89] to produce blends consisting of rubber and plastic components with new morphologies rather than the ordinary cellular structure found in HIPS or ABS. However, whether this kind of effort will successfully result in more outstanding properties will depend on a thorough understanding of the miscibility behavior between the block or graft copolymer and the corresponding homopolymers.

Lack of adhesion between two homopolymer components often makes it difficult to produce blends with the desired properties by simple blending. The addition of the corresponding block or graft copolymers to the blends has been proven effective in improving the interfacial adhesion, realizing the desirable combination of properties in the blends. This has stimulated some fundamental research on miscibility between the component polymers.

To illustrate how various microstructures can be promoted by the thermodynamics of block copolymer/homopolymer solubility, the simplest possible case is illustrated here: the addition of homopolymer A (hA).

As an increasing volume fraction of hA (ϕ_{hA}) is added to the ordered state of block copolymer ABA. Initially, hA will be dissolved in the microdomains of block A of the copolymer (Figure 3.1). After a solubility limit ($\phi_{hA}*$) is reached, macrophase separation between pure hA and swollen block copolymer occurs. For $\phi_{hA} < \phi_{hA}*$, we can anticipate a thickening of the A lamella but no morphological change. Swelling stabilizes at $\phi_{hA} = \phi_{hA}*$ and the additional hA (for $\phi_{hA} > \phi_{hA}*$), simply forms another phase of unbounded extent. However, is it really as simple as this?

Homopolymer A is chemically identical with block A chains of the copolymer and by intuition we expect they should be compatible with each other. However, experimental results show that the solubility limit $\phi_{hA}*$, depends on the relative lengths of the blocks of the copolymer and the corresponding homopolymer molecules as indicated in Figure 3.1.

3.3 When the Copolymer is Dilute: The Micelle Concept

Suppose a small amount of block copolymer AB or ABA is dissolved in an excess of 'solvent' (hA) homopolymer in which one of the block components is soluble and the other component is insoluble. Aggregation of the insoluble blocks may occur, resulting in the formation of micelles, just as is found when ordinary surfactants exceed their critical micelle concentration(CMC).

Leibler et al. [64] and Whitmore and Noolandi [115] offer theoretical descriptions of micelle formation in block copolymer-homopolymer blends. Both approaches consider

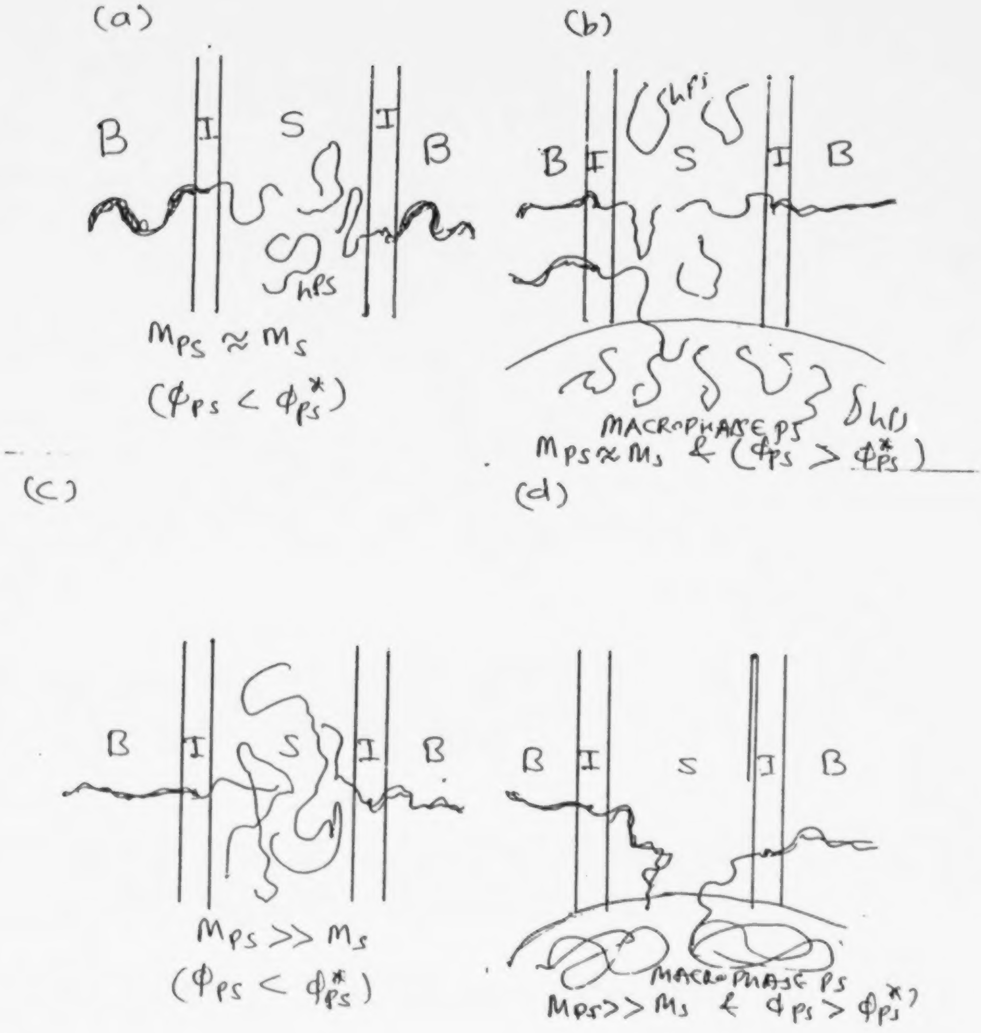
(a)
B
I
S
I
B
hPS
Mps ≈ Ms
(φps < φ*ps)
(b)
hPS
B
I
S
I
B
hPS
MACROPHASE PS
Mps ≈ Ms & (φps > φ*ps)
(c)
B
I
S
I
B
Mps >> Ms
(φps < φ*ps)
(d)
B
I
S
I
B
MACRO-PHASE PS
Mps >> Ms & φps > φ*ps ?

Figure 3.1 Schematic representation of microphase and macrophase separation in blends of SB diblock copolymer (having lamellar morphology) and hPS homopolystyrene.

a model of micelles consisting of a spherical core, of block B, surrounded by a spherical shell (usually termed the corona), in which block A of the copolymer intermixes with homopolymer A.

Mayes and Olvera de la Cruz [67] presented a theoretical treatment of micelle formation in dilute solutions of AB diblock copolymer in homopolymer A. The effects of varying copolymer block lengths and homopolymer molecular weight on micelle morphology were analyzed. The minimum concentration required for the formation of micelles was determined for cylindrical and spherical micelles. A trend toward cylinder formation was predicted with increasing B block fraction and increasing homopolymer molecular weight.

It is worth mentioning that the above-mentioned theories for the micelle formation in block copolymer-homopolymer systems assume the homopolymer chains to be shorter than the corresponding block of the copolymer, thereby restricting predictions to simplest most-miscible case. No attention is paid to the case of possible macroscopic phase separation between homopolymer and the block copolymer micelles, as would be common when homopolymer chains are much longer and particularly when $M_{hA} >> M_A$.

3.4 When the Homopolymer is Dilute: Swelling of the Microstructure

Meier [71] made the first attempt in making a theoretical description of the miscibility of hA into a matrix of AB block copolymer as an extension of his theory of microphase separation in block copolymers. The free energy change associated with the solubilization was considered to be composed of change of interfacial energy and placement entropy. Entropy change was due to constraints and perturbations of both homopolymer and block copolymer chains, and also due to the entropy of mixing. The theory predicted a decrease in the solubility limit of the homopolymer in the corresponding microdomains of the copolymer with increasing homopolymer molecular weight. For example, for lamellar domains of copolymer AB, only 5% of homopolymer A is expected to be solubilized in the domains of block A, when the molecular weight of homopolymer A is equal to that of block A in the copolymer.

This predicted trend is in agreement with the experiments; however, the predicted miscibility is very limited. This predicted miscibility is about one order of magnitude less than that found by electron microscopic [45] and SAXS [92, 120] studies.

In Meier's theory it is assumed that in the block domains where homopolymer is solubilized, the segment densities of both the free (homopolymer) and bound (corresponding block) chains are uniform. This assumption can be realized only if the bound chains adopt some rather improbable conformations, which would cause high entropy loss, especially in the cases when large amounts of homopolymer chains are dissolved. This is believed to be the main cause for the prediction of low miscibility.

Tucker and Paul [105] developed a simple model assuming a lamellar domain morphology. The model follows conceptually along the lines used by Meier [71], except a finite enthalpic interaction between the dissolved homopolymer and copolymer segments was added. This model predicts improved solubility in comparison to Meier's model, but still falls much short of experimental results.

Xie et al. [119] proposed a density gradient model in their study on the miscibility of block copolymer-homopolymer systems. In the case of pure block copolymer , the requirement of uniformity of the segment density in the domains can be fulfilled only by adjusting the conformations of the blocks of the copolymer. For the case of block copolymer-homopolymer blends, this requirement can be satisfied by changing the conformations of both the bound and free chains as well as the spatial distribution of the homopolymer. In contrast with block chains of the copolymer, homopolymer chains with two free ends are able to assume suitable spatial distributions to compensate partially for nonuniformity of segments caused by localization of the A-B junctions. It is assumed that a constant total density of segment is maintained within the whole domain, but the blocks form a distribution of segment density decreasing from the interphase to the center of the domain, and the segment density of the homopolymer decreases from the center to the interphase of the domains. In other words the homopolymer is permitted to occupy preferentially the centre-core position, staying away from the interphase, but the block segments are 'tied' to the interphase and can not get far away.

The calculated free energy of mixing of this system shows that the predicted miscibility is much larger than that obtained by Meier[71] or Tucker and Paul [105]. In particular, the density gradient model predicts solubilization of homopolymer by corresponding blocks in the whole composition range, provided that the molecular weight of the former is less than that of the latter ($M_{hA} < M_A$).

Three important features of all the above-mentioned theories are that (1) the molecular weight of homopolymer is always lower than the corresponding block molecular weight in the copolymer, (2) only AB diblock copolymer is considered in the theoretical derivations, and (3) all predictions are for the equilibrium morphology of bulk AB polymer (no effect of preferential solvent (hA) on the morphology is taken into consideration).

3.5 Experiments

3.5.1 Disorder and Micelle Formation in Block Copolymer/Homopolymer Blends

Due to segregation effects between blocks, mesophases and micelle structures are observed in most cases of copolymer/homopolymer blends.

Cohen and Torradas [13] observed that microphase separation occurred in otherwise homogeneous block copolymer upon addition of homopolymer. This was the case when molecular weight of homopolymer was smaller than corresponding block of the copolymer. However, homopolymer-induced microphase separation did not occur when the added homopolymer molecules were very much longer than the corresponding block of the copolymer. In this case two homogeneous phases were formed (macrophase separation); i.e., the copolymer separated from the high molecular weight homopolymer but did not undergo microphase separation itself.

Selb et al. [96] studied blends of SB diblock copolymers (M_w = 43000, 29000, 21000, 137000, 69000 with 32, 48, 66, 16, and 33% butadiene respectively) and hPB, using copolymers whose PS block was deuterated. Low molecular weight hPB's had average molecular weights of 1600, 3300 and 4500. SANS study of dilute solutions of SB copolymer (the SB copolymer concentration in the blends ranged from 0.5% to 10% by weight) in PB, revealed the morphology consisted of spherical micelles with the cores composed of PS blocks and coronas consisting of PB blocks and dissolved hPB chains. The authors found that the core size increased with molecular weights of PS (M_S) block and PB homopolymer matrix but decreased with that of PB (M_B)block. The authors also reported an unexpected decrease of the core size with increasing copolymer concentration.

Rigby and Roe [87, 89], using SAXS techniques, studied a similar system containing low molecular weight homopolymer hPB (M_n = 2350) and smaller amounts (0.5-8%) of SB diblock copolymers (M_n = 25000, 52.2% styrene). They investigated the effects of temperature and molecular parameters of both the component polymer and blocks on critical micelle concentration (CMC) and the structure of the micelle. The CMC of the blends generally increased as the temperature was raised and as the content of PB block (increasing the molecular weight of PB block at constant copolymer molecular weight) in the copolymer is increased, which is attributed to an increasing solubility of the copolymer in the PB homopolymer matrix. A detailed comparison of these results with the predictions of the theories by Leibler [64] and by Whitmore and Noolandi [115] was made by Roe [88].

Kinning et al. [51], using TEM, found new morphologies in the micellar phase in blends of diblock copolymers (M_n = 22000, 41000, 87000, 33900, 73800 with 51, 46, 45, 27, 13% styrene respectively) and homopolystyrenes (M_n = 2100, 3900, 17000, 35000). The new morphologies included cylindrical micelles, spherical and multilamellar vesicles, and lamellar type structures. The transitions in micelle geometry were found to be correlated with the relative volume fractions of the core and corona regions of the micelle, which are in turn dependent on block molecular weights in copolymers.

Kinning et al. [55] analysed the micellar structures of SB diblock copolymer/homopolystyrene blends using SAXS and TEM. Results showed that at small copolymer concentrations in homopolystyrene, a homogeneous solution occurred.

However, increasing the concentration of copolymer beyond the CMC resulted in the formation of micelles having polybutadiene cores surrounded by coronae consisting of polystyrene block chains swollen with homopolystyrene. The CMC was observed to increase (i.e., the copolymer became more soluble) with decreasing homopolymer molecular weight, fraction of polystyrene in the copolymer, and decreasing overall copolymer molecular weight.

Although the theories for the formation of micelles in diblock copolymer / homopolymer blends assume micelles of spherical geometry, Sardelis et al. [104], Eastmond and Philips [21], Bradford [4] and Bates et al. [6] reported transitions (from one to another) in the geometry and and the appearance of new mesophase morphologies (i.e cylindrical micelles, vesicles and other lamellar type structures). However, in these reports, due to a limited variation of composition, concentration and molecular weight in the blends studied, it was difficult to make clear conclusions dealing with the effects of these parameters on the transition of the micelle geometry.

Kinning et.al. [56] systematically studied micelle transitions in a blend of diblock SB and homopolymer PS, with special attention to their dependence on the particular molecular parameters of the blends. The transitions in micelle geometry were found to be correlated with the relative volume fractions of the core and corona regions. Any variations leading to increase of core volume fraction promoted the geometry transition from spherical to non-spherical structure. For example, increasing the core-forming B-block molecular weight, increasing the molecular weight of the homopolymer matrix would lead to the transition. Increasing the molecular weight of the block forming micelle cores, with respect to that of the corona blocks, will directly increase the micelle core volume fraction. The reasoning for the effect of homopolymer is not straightforward but is understandable: a high molecular weight homopolymer will mix with the PS block in the corona to the lesser extent than a lower molecular weight PS, which will reduce the corona volume and lead to an increase in the core volume fraction. The micelle core volume fraction can also be increased by raising the block copolymer concentration, which will results in a higher aggregation number.

3.5.2 Block Copolymer/Homopolymer Blends: Effect of Molecular Weight on Solubility

Riess [94] used optical turbidity of blend films as a criterion of the degree of mixing between the component polymers. Such results are summerized by Paul [78]. A series of blends composed of a diblock copolymer of styrene and isoprene (SI) and homopolymers PS and PI of different molecular weights covering a broad composition range, were examined. The turbidity results showed that when the molecular weights of both PI and PS were less than those of the corresponding blocks, the blend films in most compositions were almost transparent, indicating absence of phase separation on a macroscopic scale. However, when the molecular weights of PI and PS were larger than those of the corresponding blocks, most of the films (except those with very small concentrations of homopolymers) were opaque, indicating the presence of macroscopic phase separation. Optical turbidity is only a rough indication for the degree of mixing in the blends; however, this result does present a clear trend with respect to the effect of molecular weight of the homopolymer on the miscibility.

Inoue et al. [45] were the first to study the miscibility of block copolymer and homopolymer blends using transmission electron microscopy (TEM). Their diblock copolymer (SI) with molecular weights of PS and PI blocks being 230 and 310 kg/mol respectively, had the characteristic feature of lamellar microdomains as expected for copolymers with a 42/58% composition. This was solution blended with PS of different molecular weights. When PS of molecular weight 180 kg/mol was used at low concentrations, the lamellar structure of the PI block remained separated by PS domains swollen with homopolymer PS. This mesophase structure without apparent macrophase separation was maintained even at high concentrations; it remained stable until the volume ratio of homopolymer PS to PS blocks in the blends approached 5. In the second series of blends composed of copolymer SI having a spherical PS microdomain structure (as expected with molecular weights of PS and PI blocks being 50 and 227 kg/mol respectively), the PS domain size increased as low molecular weight (18 and 33 kg/mol) PS was added. In contrast, when PS of high molecular weight (600 kg/mol) was blended, two different phases coexisted, indicating clear macrophase separation between the SI and PS. One of these macrophases had the characteristic spherical microstructure of the SI block copolymer and the other appeared to be without any internal structure.

Thus, it was found that in copolymer/homopolymer blends, substantial solubilization occurs only when the molecular weight of the homopolymer is less than or similar to that of the corresponding blocks. When the homopolymer molecular weight is larger than that of the corresponding blocks, the homopolymer forms a separate phase and is not solubilized in the microdomains of the like blocks.

Selb et.al. [96] reported substantial miscibility of block copolymer with a larger amount of homopolymer. The SANS results showed that in the blends composed of SB block copolymer having PS spherical domain structure and low molecular weight PB homopolymer, PS spheres were randomly arranged in a matrix consisting of PB blocks and a large amount of PB homopolymer.

Cheng et al. [12] reported some blends with rather limited apparent solubility. In the SANS study, SB diblock copolymer (molecular weights of the blocks being 90 and 11 kg/mol) and two perdeuterated PB homopolymers of molecular weights 8.9 and 23.7 were used. It was found that in spin-cast films of SB/PB blends, the relatively short PB (8.9) homopolymer was completely solubilized by PB microdomains only up to the point at which about 15 mol% of the repeating units in the domains came from the homopolymer. At about 18 mol% of the same homopolymer, phase-separated homopolymer PB regions appeared outside the PB microdomains. The SANS data seemed to suggest that rejection of homopolymer from the microdomains observed at this moderate concentration was a kinetic phenomenon reflecting the conditions used in the solution-casting procedures. The longer PB chains are found to behave in a similar manner except that the observed kinetically-controlled solubility limit was even lower, lying somewhere between 3 and 6 mol%.

3.5.3 Blends of AB and Homopolymer A (where A is the 'rigid' block in AB)

Jeon and Roe [47] studied the blends containing SB diblock copolymer and polystyrene using light scattering, TEM and SAXS. Two diblock copolymers containing ~ 50 wt% of styrene, one almost exactly twice the size of the other (M_n = 25,000 and 47,900, M_w/M_n = 1.04), were used in this work. The polystyrene homopolymers were in the molecular weight (M_{hPS}) range of 14,000 < M_{hA} < 45,500, some smaller and some larger than the styrene blocks in the copolymer.

It was found that the solubility of polystyrene in the styrene lamellar microdomains of copolymer was governed by the ratio M_{hPS}/M_S. When this ratio was about equal to or less than one, no limit to the solubility of polystyrene was found. The solubilities obtained in this work, in which the block copolymer formed a lamellar structure in its pure state, were much greater at the same M_{hPS}/M_S ratio than those in the block copolymers exhibiting spherical or cylindrical morphologies [6]. With increasing polystyrene concentration, the thickness of the butadiene layer remained constant while the lamellar repeat period expanded linearly. Thus, added polystyrene simply squeezed into the pre-existing styrene lamella but was unable to expand the lamellae laterally and to force the average interfacial area occupied by a copolymer junction point to increase. On the other hand, other workers [112] have found that when the added homopolymers were much smaller than the block lengths, the area per junction point increased with increasing homopolymer concentration.

Hasegawa et al. [43] used SANS and SAXS to investigate blends of diblock copolymer (SI) and deuterium -labeled homopolystyrene. The SANS results suggested that the homopolymer chains in the microdomain space (as well as the block copolymer chains) were more compressed in the direction perpendicular to the interface than the corresponding unperturbed polymer chains with the same molecular weight.

Matsushita et al. [73] employed SANS to measure single-chain conformations of styrene homopolymers dissolved in a polystyrene lamellar microdomain of a styrene--2-vinylpyridine diblock copolymer in bulk. The molecular weights of the styrene homopolymers were 13,000, 29,700, and 76,700. The molecular weight of diblock copolymer was 63,300 with $M_S = 34{,}200$ for the polystyrene block (54 wt% styrene). The homopolymer contents of the blends were kept low, 10% with lowest molecular weight (13,000), 5% for the intermediate molecular weight (29,700), and 1% with highest molecular weight (76,700), so as not to give rise to macrophase separation.

Homopolymer chains in styrene lamellae were found to have unperturbed dimensions, at least in the direction parallel to lamellae, in contrast to block chains which were contracted in that direction. This result is different from a previous conclusion [43] that a homopolymer chain is extended and contracted in the same manner as block chains in the perpendicular and parallel directions, respectively, so that the homopolymer dissolves uniformly in lamellae.

Winey et al. [113] summarized the equilibrium morphologies observed in over 130 diblock copolymer/homopolymer blends using two new types of isothermal morphology diagrams. Blends were prepared from homopolystyrene and either SI or SB diblock copolymers by slow solvent evaporation from a single-phase solution followed by annealing.

The recently-discovered morphology known as ordered bicontinuous double-diamond (OBDD) was produced by Winey et al. [114] in binary blends of SI or SB diblock copolymers and a homopolymer. If a diblock copolymer which formed the lamellar morphology was used in the blend, the homopolymer was found to reside in the matrix region of the OBDD morphology. However, if a diblock copolymer with cylindrical morphology was used to prepare the blend, the homopolymer resided inside the OBDD channel regions. Attempts to prepare the OBDD blend morphology with homopolymer in the matrix region, when using diblock copolymer with cylindrical morphology, failed and blends underwent macrophase separation.

Spontak et al. [97] employed TEM to identify morphologies developed in a series of blends which had potential to generate OBDD morphologies. OBDD morphology was indeed produced in most of the blends, and additional morphologies such as lamellar catenoid, cylindrical and disordered state were also found.

A block copolymer with a star-shaped molecular architecture was used by Hashimoto et al. [40], who observed 'mesh' and 'strut' microdomain structures in a copolymer/homopolystyrene mixture. The mesh structure consisted of alternating parallel sheets composed of A and B in which one type of sheet (e.g. A) was fused by catenoidal channels of A traversing through the other type of sheet B. The strut structure was a three-dimensional tunnel network characteristic of bicontinuous microdomain structures of A and B. They were found only in a narrow composition 'window' around 30%hPS where the system styrene content was around 83-86% between the lamellar and spherical phases.

A new catenoid-lamellar morphology was reported by Disko et al. [18] in blends of SB diblock copolymer (M_S and M_B being 25,500 and 24,500 respectively) and homopolystyrene ($M_{hPS} = 26,000$). We note that $M_S \approx M_{hPS}$ and that the total styrene composition was close to the region of 65-67 vol% styrene where Winey et al.[114] and Spontak et al. [97] observed the OBDD morphology in blends of diblock copolymer and homopolymer.

Winey et al. [112] used DSC, SAXS and TEM to investigate the lamellar morphology in 14 binary blends of a lamellar (SI) diblock copolymer (molecular weight = 753,000 and 35 wt% styrene) and several polystyrenes (molecular weights in the range 2600-36,700). As the homopolymer concentration increased, the PS layer thickness increased and the PI layer thickness decreased. When low-M_w homopolystyrene was added to the copolymer in small amounts (5%), the lamellar repeat distance reduced below the value for pure diblock copolymer. A similar phenomenon was observed by Quan et al. [83] for a blend of triblock copolymer and homopolymer when 20% low-M_w homopolymer was added.

Eastmond and Phillips [21] extended their conclusions about blends of crosslinked AB polymers and homopolymers to systems of noncrosslinked block copolymer/homopolymer blends. They discussed possible morphologies which might exist in block copolymer/homopolymer blends, and it was proposed that unusual morphologies in block copolymer blends reported by various workers were the direct consequences of combinations of macroscopic phase separation and subsequent microphase separation within phases of different composition.

The effects of solvent-casting conditions, the presence of homopolymer in the continuous phase, and the magnitude of block molecular weights on the structural features of SB diblock copolymer/homopolystyrene blends were investigated by Bates et al. [6]. Interphase thickness, domain size, and domain packing order were determined using SANS.

Glass transition temperatures of mixtures of styrene-dimethylsiloxane diblock copolymers with polystyrene were measured by Lu et al. [62] using refractive index-temperature measurements and DSC. The T_g's of these mixtures (measured by refractive index-temperature method) obeyed the inverse mixing rule within 1 K except when the mixtures had either large or very small values of M_{hPS}/M_S molecular weight, either ≥ 2.5 or ≤ 0.23.

3.5.4 ABA (Triblock) and Homopolymer (A or B) Type of Blends

Toy et al. [108] reported that SBS with $M_S = 78{,}000$ formed a homogeneous blend on a macroscopic scale with low molecular weight PS (10,000), but macrophase separation occurred when M_{hPS} was high (330,000).

Similar results were reported by Kotaka [51] who studied morphologies of a series of blends of SBS (15.7-63.7-15.7 kg/mol) with hPS or hPB having high or low MS's: (MS =26 or 10.2 and MB = 1.9 or 95.5).

Quan et al. [83] employed SANS to examine the effect of homopolymer molecular weight on the morphology of blends wherein the SBS middle block matched the homopolymer type and the latter was dilute. A series of samples containing 20% by weight of hydrogenated butadiene homopolymer in a matrix of styrene-hydrogenated butadiene-styrene triblock copolymer were used. $M_{SBS} = 115{,}000$ with 49 wt% styrene (hence, $M_B = 57{,}000$). M_{hPB} ranged from 11,000 to 130,000. For the blend $M_{hPB} =$ 130,000, the microdomain spacing reverted to the value for the pure triblock copolymer. This demonstrated the existence of complete macrophase separation since virtually all of the homopolymer was excluded from the microdomains in the blend. When M_{hPB} = 58,000 corresponding to that of the copolymer midblock, the homopolymer solubility become finite, and the microdomain spacing became larger, apparently expanding to accommodate the homopolymer within the midblock lamellar domain. A further decrease in M_{hPB} below that of M_B produced interesting results. The characteristic size of the microdomains was seen to decrease. For the blend with lowest M_{hPB} (11,000), which was expected to have the highest homopolymer solubility), the domain spacing fell below that of the pure triblock copolymer. That is the overall microdomain structure contracted to a repeat distance of a lower value than that of pure copolymer even though it accommodated essentially all of the homopolymer.

Spontak et al. [101] solution-blended linear $(SI)_n$ multiblock copolymers which consist of n ($2 \leq n \leq 4$) perfectly alternating SI block pairs with homopolystyrene. These blends were prepared under conditions identical to those used to generate the OBDD morphology in $(SI)_1$/ polystyrene blends [46]. However, none of the blends produced [95] exhibited OBDD morphology. Multiblock copolymers with varying molecular weight, varying 'n", and constant styrene wt% (50%) were synthesized. In some cases, homopolystyrene was solubilized within the copolymer microstructure, resulting in either dispersed isoprene cylinders or swollen lamellae. Macrophase separation also occurred, depending on copolymer architecture and block length.

Melt blending was employed by Park et al. [81] to prepare mixtures of block copolymers (diblock and triblock) with homopolystyrene. Their objective was to study the effects of the molecular architecture of (SB, SBS) on effectiveness of toughening a brittle polystyrene. Toughening appeared to be controlled mainly by the blend morphology, which is determined by the rheological characteristics of the block copolymer relative to that of the matrix. The formation of dispersed particles during melt blending in a Brabender plasticorder was strongly influenced by the ratio of the matrix and block copolymer viscosities (estimated by Brabender torque). The extent of toughening of this matrix appeared to increase strongly with M_S, whereas the architecture seemed to have no significant effect in toughening polystyrene.

Flosenzier et al. [23, 25] measured tensile, cyclic, and tear properties in blends of several SBS with monodisperse polystyrene of various molecular weights. Tear test results were observed to be similar to the results for pure SBS of the same total polystyrene content.

Folkes and Reip [24] investigated the microstructure of extruded samples of SBS and polystyrene blends using light microscopy and electron microscopy (SEM and TEM). For some compositions, the separated homopolymer phase was in fibrillar form. These fibrils were dispersed throughout the block copolymer matrix with a surprisingly high degree of spatial ordering. The authors proposed that this ordering arose from a molecular association of homopolymer polystyrene with the block copolymer, which itself underwent a transformation from a cylindrical to lamellar microphase morphology.

Baek et al. [5] experimentally constructed phase diagrams for mixtures of a styrene-isoprene-styrene (SIS) triblock copolymer and a homopolymer polystyrene. Two SIS triblock copolymers (M_{SIS} = 113,800 and 13% styrene and 39,000 and 30%styrene) were blended individually with hPS (M_{hPS} =: 1500-3700). Various mixtures were prepared by first dissolving the block copolymer and homopolymer in toluene in the presence of antioxidant (Irganox 1010, Ciba-Geigy Co.) and then evaporating solvent slowly.

At a fixed M_{hPS}/M_S ratio, a greater amount of homopolystyrene was solubilized in SIS (30 wt% styrene) than in SIS (13 wt% styrene) indicating the influence of the block length ratio (M_S/M_I, i.e. composition of block copolymer) on solubility limits of added homopolymer. Results of dynamic viscoelastic measurements and turbidity measurements were combined in constructing phase diagrams and experimental results were compared with predicted results.

Diamant et al. [19] measured linear viscoelastic properties and nonlinear stress-strain properties of SBS triblock copolymers and their blends with several homopolystyrenes. Cyclic tests, with each cycle advancing to a larger strain, showed progressive structural alterations with blend behavior resembling host properties (SBS copolymer) more closely with each new cycle.

Table 3.1 Review of block copolymer/homopolymer blends

Block Copolymer(s)	Homopolymer(s)	Blend preparation	Characterization techniques	References
SB (7-21)	PS (2.4, 3.5)	Solution blended using toluene	SAXS	92, 120
SB (14-29, 14-15, 14-7, 23-114, 23-46)	PB (16, 33, 65)	Solution blended using benzene	SANS	96
SB (13-12)	PB (2.4)	Mechanical mixing at 220^{0}C using magnetic stirrer	SAXS	87, 89
SB (10-10, 20-20, 40-40, 10-23, 10-65)	PS(2.1, 3.9, 7.4, 17.0, 35.0)	Solution blended using toluene	TEM	51
SB	PS	Solution blending using toluene	SAXS, SANS	3
SI (40-60)	PS, PI	Solution blending	TEM	45
SB (79-11, 77-21, 85-45, 149-20, 126-46, 122-66)	PS (64, 116, 390)	Solvent spin casting benzene, toluene or mixture of THF/MFK	TEM, SANS	6, 9
SB (13-12, 24.5-23.5)	PS (15, 18, 25, 30, 45)	Solution blending using benzene	TEM, SAXS	47
SI (27-22, 13-34, 13-51, 45-12) and SB (20-20, 10-23, 23-10)	PS(2.6, 4.0, 5.9, 14.0, 17.2, 30.1)	Solution blending using toluene	TEM, SAXS	114
SBS (19.5-91-19.5)	PS (330) PB (600)	Melt blending in a two roll	DSC	116

Table 3.1 Review of block copolymer/homopolymer blends (Continued)

Block Copolymer(s)	Homopolymer(s)	Blend preparation	Characterization techniques	References
SI (10-10, 15-15, 20-20, 24-25, 30-30, 40-40, 60-60, 90-90)	PS (6.5, 9.5, 15, 20, 30, 42, 45)	Solution blending using toluene	TEM	97
SB starblock (60-20)	PS (2.8)	Solution blended using toluene	TEM	40
SB (25.5-24.5)	PS (26)	Solution blending using toluene	TEM	18
SI (27-22)	PS (2.6, 6.0, 14.0, 37.0)	Solution blending using toluene	SAXS, DSC, TEM	112
S-DMS	PS	Solution blending using toluene	RI, DSC	62
SBS (16-78-16)	PB (330, 10)	Solvent spin casting using benzene	DMT, TEM	108
SBS (15.7-63.7-15.7)	PS (26, 10.2) PB (95.5, 1.9)	Solution blending using THF/MEK and Cyclohexane/benzene mixtures	DMT, TEM	51
SBS (14-30-14,16-78-16, 7-36-7)	PS(3.6,4,4.8,10.3,20)	Solvent spin casting using THF/MEK (9:1)	Rheology	19

Table 3.1 Review of block copolymer/homopolymer blends (Continued)

Block Copolymer(s)	Homopolymer(s)	Blend preparation	Characterization techniques	References
SBS (28-59-28)	PB (11, 32, 58, 130)	Solution blending using dichloromethane	SANS	83
(SI)$_2$ (30-30-30-30,18-18-18-18) (SI)$_3$ (20-20-20-20-20-20, 18-18-18-18-18-18) (SI)$_4$ (15-15-15-15-15-15-15-15)	PS (6.5, 10, 15)	Solution blending using toluene	TEM	101
S-EP (36-61,37-96) SBS (7-67-7)	PS (350)	Melt blending in a Brabender Plasticorder (240 ^{0}C, 60 rpm) 15 minutes	SEM, Impact strength measurements	81
SBS (45-210-45)	PS (520) PB (550)	Melt blending in a two roll mill (145^{0}C, 10 rpm, 20 min)	SEM, Capillary rheometer	14
SBS (19.5-91-19.5)	PS (330) PB (600)	Melt blending in a two roll mill (147^{0}C, 10 rpm, 10 min)	DSC	116
SBS (14-30-14, 17-84-18, 16-78-16,10-51-10,7-36-6)	PS(2,4,9,17,51)	Solution blending using Toluene		23,25
SBS (5-55-5)	PS (20)	Melt blending in a two roll mill (130-170^{0}C)	LM, SEM, TEM	24
SI (14-12,29-21) SIS (29-43-29)	PI (6,8,9,17,21,35 61,89,119)	Solution blending using Benzene	TEM	46

CHAPTER 4

MATERIALS AND METHODS

Different methods were used for preparation of blends of block copolymers with homopolymers. As a result different techniques were used for electron microscope specimen preparation and for morphology examination. Brief descriptions of these methods are presented in this chapter.

4.1 Blend Preparation

Blending methods for polymers include: mechanical melt blending, fine powder mixing, dissolution in co-solvent followed by film casting, freeze or spray drying (solution blending), use of monomer(s) as solvent for another blend component followed by polymerization etc. Mechanical melt blending predominates for economic reasons. Mechanical blending and solution blending are both used in the present study.

4.1.1 Mechanical Blending (Melt Blending)

Melt blending is the simplest route to incorporate rubber into plastics for purposes of preparing a toughened (less brittle) plastic or a stronger elastomer. However, for simple gum rubbers, this approach seldom leads to the desired toughening or strengthening effect in these two phase materials. The reason is that property enhancement requires some level of adhesive coupling between the rubber and plastic phases and a degree of control over phase morphology which is usually not possible with simple elastomers. In addition, it is often desirable for the rubber phase to be crosslinked, which further limits the use of blending gum (melt) elastomers.

Block copolymers, on the other hand, can circumvent these limitations and consequently have received some attention as toughening agents for a number of plastics, especially polystyrene, and also as thermoplastic elastomers (see Chapter 1). In the former, the block copolymers soft segments provide the low modulus needed for the dispersed particles to act as effective stress concentrators, while their hard segment can lead to microdomains that act as physical crosslinks and can provide a mechanism of physical adhesion to the rigid matrix phase.

Homopolystyrene used in this work was provided by Dow Chemical, Sarnia, Ontario. According to the supplier, M_w = 315,000 and polydispersity (M_w/M_n) = 2.6. This polystyrene was melt blended with SBS triblock copolymer (supplied by Fina-Finaprene) having M_W = 150,000 and total styrene content of 30%. Both the polystyrene and the block copolymer used are commercial products and therefore contain the antioxidant necessary to stabilize them at high temperatures during melt blending.

Blend preparation

Blends of the block copolymer with PS were prepared using a Brabender Mixing Head (Docorder) with roller type blades. The total amount of material used in each loading was 40 gm. To prevent oxidation during melt mixing, dry nitrogen was fed continuously into the mixing chamber. No antioxidant was added. The mixing chamber of the Docorder was heated to 160 ^{0}C and roller blade speed set to 30 rpm. Hand-mixed pellets of polystyrene and block copolymer were added into the mixing chamber. At the end of the operation, the Brabender rollers were turned off and the blend was peeled off from the blades and cooled to room temperature through natural convection in open air. No oxidative degradation was observed in the blends.

Rheological tracking

Torque-time traces recorded on a chart from the Brabender Docorder were used to track the blending process to a steady state, and also for rheological characterization of the blends and their components. As a general rule, melt blending was terminated after a steady state torque value was achieved. However, torque response for all blends in this series showed minor fluctuations (like 'noise') throughout the blending process. Although the major melting/blending treatment subsided in about 20 minutes, we waited as long as 55 minutes for long-term stability to be established.

4.1.2 Solution Blending

So far, most of the studies on blends of block copolymers and their homopolymers have been carried out using solvents which dissolve both types of polymers forming the blocks. There are several reasons for studying blends of block copolymer-homopolymers using carefully selected good neutral solvents. The major motivation is to achieve a molecular-level uniformity of mixing that is possible only when all components are dissolved in an excess of solvent. However, solvents may also be added deliberately (e.g., as plasticizers) in a commercial operation, or they may be residues of polymer synthesis. The presence of solvent will change the separation temperature (T_S) and glass transition temperatures (T_g) by an amount depending on the fraction of solvent present in the system and thus can influence processing strategies. From a research standpoint, it is essential to have a framework to classify the great variety of solvent-based experimental studies being reported, and only a neutral solvent can provide this reference point..

Consider a case of ABA block copolymer. Its solvents can be classified in several ways, as shown below:

Solvent having equal affinity for both blocks ("neutral solvent")

This condition may be represented conceptually in terms of solubility parameters (δ) of polymer PA, polymer PB and solvent S:

$$(\delta_{PB} - \delta_S) = - (\delta_{PA} - \delta_S) \qquad (4.1)$$

and thus δ_S is precisely intermediate between δ_{PA} and δ_{PB}. In practice, the true equal-affinity case may not be quite in accord with Equation 4.1, which requires that

$$\delta_S = (\delta_{PA} + \delta_{PB}) / 2 \qquad (4.2)$$

This is due to differing types interactions between PA- solvent and PB- solvent pairs, such that the true neutral solvent could have δ_S slightly larger or slightly smaller than given in Equation 4.2. By definition, a neutral solvent is uniformly distributed within pairs of macrophases, as well as throughout each microphase structure, and has two types of limiting behavior.

(i) Strong affinity

This can occur only when (δ_{PA} - δ_{PB}) is itself small, as is fortunately the case here when PA is polystyrene and PB is polybutadiene.. When the solvent is added to the bulk ABA, complete miscibility prevails on the macroscale (solvent is uniformly absorbed), but the pre-existing microphases initially retain their identity. As solvent fraction increases, T_s for block copolymer is reduced and mechanical properties weaken as the microphases are solvated. Eventually, $T_s(\phi_S) < T$ and the unstable microphases vanish into a homogeneous solution. This thermodynamic transition can happen when solvent is still the minority component--i.e., when the solution is still far from dilute. For example, Hugenberger and Williams [42] found that S-EB-S ["EB" means ethylene-butylene (random) copolymer, a rubbery polymer at room temperature with properties similar to those of PB but more stable at high temperatures because double bonds are absent.] in dipentene becomes homogeneous at 30^0C when polymer concentration is only about 0.32 g / cm^3.

(ii) Strong incompatibility

In this case, solvent does not dissolve either PA or PB -- i.e., it is equally poor for both. Actually, the polymer will take up a small amount of solvent, with both microphases swelling equally. However, Ts (ϕ_S) can never be depressed to room temperature because ϕ is too small, and no homogeneous solution can result. This corresponds to the case where (δ_{PA} - δ_S) and (δ_{PB} - δ_S) have equal large values, while in (i) they have equal small values.

Solvent preferentially biased

(i) End (A) blocks favored.

(i-a) End block in domain (disperse phase)

In the limit of absolute PB/solvent incompatibility, no solvent could penetrate the matrix and an apparent (nonequilibrium) macrophase separation would occur -- i.e., supernatant solvent and unswollen polymer. Even with more realistic PB/solvent incompatibility, solvent permeation through the matrix will be quite slow. Ultimate polymer swelling will depend on how much spatial accommodation for the expanding A domains will be provided by the resilient matrix, but no dissolution of the sample will be possible unless the PB matrix can ultimately dissolve.

(i-b) End block forming matrix (continuous phase)

In this case, solvent uptake is not so restricted. After an initial delay, during which the favored matrix absorbs enough solvent to become plasticized and lose its glassy character, the matrix swells rapidly and becomes soft enough to make mechanical breakup (e.g., by stirring) very easy. When geometric limits on A-block extensibility are reached, the polymer morphology is disrupted as the A-chains are solubilized. A separation occurs, characterized by formation of aggregates which have a gel-like nature but retain an internal microphase structure consisting of micelles (PB interior, PA exterior). These aggregates are dispersed in solvent. Further increase of $\phi_{solvent}$ serves only to move the aggregates further apart, but does not immediately affect their solvent content or size. These aggregates could be quite large, containing many domains, and should cause considerable turbidity in the fluidized mixture. With sufficient time, solvent would penetrate into the gels and allow the PA to be completely solubilized, releasing the micelles (with insoluble cores) to be distributed uniformly in the fluid.

(ii) Middle (B) block favored

(ii-a) Middle block in domain (dispersed phase)

Permeation of solvent through the glassy PA matrix, which also is chemically incompatible, will be extremely slow. Solvent uptake in the compatible domains will be slight because of extreme mechanical resistance to PB swelling in the rigid environment. Macrophase separation (nonequilibrium) will occur at very low $\phi_{solvent}$, the system being composed of a still glassy plastic (PA) with supernatant solvent. In less extreme cases, when the glassy matrix is sufficiently plasticized, the plastic could crack or disintegrate under the internal pressure generated within swelling domains.

(ii-b) Middle block forming matrix (continuous phase)

The rubbery matrix is favored and takes up solvent extremely rapidly, ultimately being limited by the existence of anchoring points (glassy domains of A) at both ends of the B block. The polymer will always be in a gel-like solid state, with maximum volume determined by the maximum attainable swelling of the middle blocks. Further increase of $\phi_{solvent}$ results in macrophase separation, with supernatant solvent plus a gel retaining its microphases.

4.1.3 Blend Protocol (SBS + PS) Using Neutral Solvent

Pico and Williams [77] found cyclohexane and dipentene to be solvents in the category of 'strong equal affinity'. Solubility parameter (δ) values (δ_{PB} = 8.1, δ_{PS} = 9.1, $\delta_{Cyclohexane}$ = 8.2, $\delta_{Dipentene}$ = 8.5 cal $^{1/2}$/cm $^{3/2}$) would indicate an off-center solubility bias towards B. Therefore, the unique neutral character of these solvents seems to be related to their unusual structural similarities (Figure 4.1) to both polystyrene and polybutadiene, beyond mere energetic considerations embodied in the solubility parameter.

Cyclohexane has a low boiling point of 80.74^{0}C and dipentene has 178^{0}C. I selected dipentene as a solvent, since its slow evaporation (related to its very high boiling point) avoids solvent gradient formation in the blend. That is, dipentene molecules can diffuse to the polymer surface faster than they can evaporate from that surface. The resulting morphology is therefore either at equilibrium or near to equilibrium.

The casting protocol for blend preparation was designed to produce blends having the same history but of different composition. All the blends in this category were prepared in an identical manner: a weighed mixture (roughly of about 4 gm) of granulated block copolymer and powdered homopolystyrene was dissolved in 35-40 ml of dipentene (neutral solvent for PS/PB systems). The solution was stirred at room temperature, using a magnetic stirrer, for an hour and then poured into a Petri dish which was placed in a heated vacuum oven. Slow evaporation of dipentene at 60^{0}C for eight weeks formed a ~2 mm thick polymer layer at the bottom of the Petri dish. The blend was then annealed as shown in Table 4.2. At the end of annealing, blends were somewhat brown in color due to oxidation at the higher temperatures of annealing.

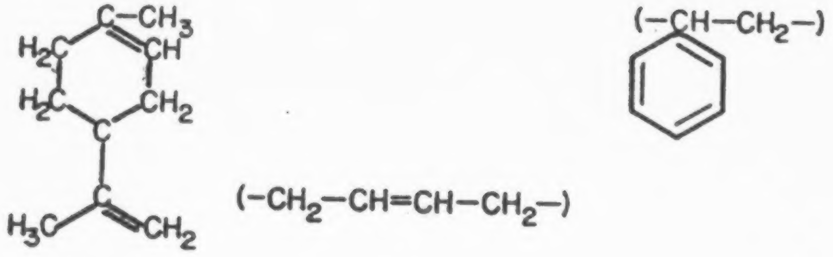
(−CH₂−CH=CH−CH₂−)
(−CH−CH₂−)

(a) (b) (c)

Figure 4.1 Chemical Structures (a) Dipentene (b) Polybutadiene (c) Polystyrene.

Table 4.2 Solvent removal and annealing procedure

Steps #	1	2	3	4
Temperature (^{0}C)	0	75	110	1108
Time	8 weeks	1 week	3 days	1 week

4.2 Preparation of Specimens for Electron Microscopy

4.2.1 Specimens for SEM

I used the freeze-fracture technique to examine the solid surface of melt-blended binary (hPS and SBS) and ternary (hPS + SBS + hPB) blends. Small pieces of these blend materials were cooled down to liquid nitrogen temperature by dipping in a liquid nitrogen dewar for 15 minutes and then fractured at that temperature. Fragments were taken out of the dewar, air-dried, coated with a thin layer of gold in a vacuum chamber, and placed in a SEM specimen chamber where their fracture surfaces were examined.

4.2.2 Specimens for TEM

Specimen preparation is one of the most important factors in TEM studies of materials. The two methods employed in this research work were direct solution casting and microtoming of the bulk sample.

For TEM work, the thickness of either polymer film (direct solution casting) or section of the bulk sample (microtoming) should be 10 to 100 nm thick for working with conventional electron microscopes operating at accelerating voltages up to 100 kV. These sections are termed ultrathin sections. Using microscopes operating at higher accelerating voltages (up to 200 kV), it is possible to work with thicker sections.

TEM copper grids (300 mesh) were first coated with a formvar film (0.25 vol% formvar dissolved in ethylene dichloride). Formvar film gives mechanical support to the block copolymer film produced by direct casting of solution followed by evaporation of solvent and to the sections cut through bulk material using ultramicrotomy. Next, a molecular layer of carbon was deposited on top of the formvar. This deposition of carbon was done in a Balzer BAE-120 High Vacuum Coating Unit. The layer of carbon isolates formvar from the sample material and provides additional mechanical strength. Carbon deposition also helps in minimizing the beam damage of the specimen by distributing the electron charge uniformly over the specimen (due to high intensity of electron beam, the specimen is heated up, resulting in change of structures). The grid at this stage (grid + formvar + carbon) was treated by a Balzer CTA 010 Glow Discharge Unit where negative charge was added on the surface by ionizing the air. Ionization of the surface helps in adhesion of frozen sections (cryo-ultramicrotomed sections) to the grid. Once a specimen film was cast on the grid (in case of direct casting from solution) or microtomed sections were placed on the grid, the sample was stained for four hours by vapors of osmium tetroxide (OsO_4). Polybutadiene is selectively stained by osmium tetroxide and shows dark regions of polybutadiene domains under the microscope. After staining, an additional layer of carbon was deposited for additional stability of the specimen during extended exposure under the electron beam. At this stage, the specimen assembly consist of Cu grid + formvar + carbon layer + polymer film or sections + carbon layer.

The usual solution casting technique involves putting a drop of polymer solution (volatile solvent) on top of clean liquid (nonsolvent) such as distilled water, mercury, etc. The polymer film formed on the surface of liquid is carefully lifted on the top of the TEM grid. Since the polymer film deposited on the liquid surface is in a state of non-equilibrium with respect to the ultimate solvent-free system, the most representative morphology is obtained by allowing the solvent to evaporate slowly over a period of a day or so. When this procedure was used (using toluene or dipentene solvents), most of the film agglomerated to a thickness greater than the 100 nm necessary for high-resolution TEM studies.

Direct solution casting on the grid does provide advantages over the solution-casting procedure described above. A major advantage is avoidance of orientation variations in the phase-separated microstructures due to flotation medium (nonsolvent) used in solvent casting. Here, the polymer is dissolved in a suitable solvent such as toluene (toluene being able to dissolve both polystyrene and polybutadiene completely) or a mixture of solvents. A dilute solution of the polymer (0.5%) is prepared and a drop of it deposited on the top of a treated TEM grid (+ formvar + carbon + glow discharge). The solvent is allowed to evaporate at room temperature, leaving behind a thin film of polymer, and the specimen is kept in vacuum at room temperature for 3 days. The polymer film is formed on the top of grid and, unlike solution casting, excessive handling of sample film and transference from liquid surface to grid surface is avoided.

The morphology obtained for block copolymers using this technique with toluene was far from equilibrium, due to using the PS-biased solvent with high volatility. Attempts to use this technique with dipentene as the solvent failed; the polymer formed a thick layer instead of thin film on the formvar surface when dipentene was evaporated, perhaps because of the long times needed for this low-volatility solvent to evaporate.

Direct solution casting is easy and fast. However, if the solvent evaporation is too fast, the ultimate solvent-free system will have nonequilibrium character, and slow evaporation of the solvent (e.g., dipentene) forms thick film making high-resolution TEM work impossible. Due to the above limitations of direct solution casting, representative bulk morphology characterization for blends could not be carried out and only pure SBS block copolymer morphology was studied by this method.

Since the density difference between styrene and butadiene is not sufficient to give the desired contrast, the samples were stained using vapors of osmium tetroxide which selectively stained the rubbery butadiene phase. In order to get representative microstructures of the bulk materials, thin sections were produced by microtomy (see section 4.3) from bulk material.

Ultramicrotomy is the term used to describe the technique of producing sections of material thin enough for examination in the electron microscope. Cryo-ultramicrotomy is the technique of producing ultrathin sections (10-100 nm) for electron microscopy study where the material is hardened at low temperatures before cutting. Cryo-ultramicrotomy was used for most of the blends in this work and is presented as a separate section, below.

4.3 Cryo-ultramicrotomy

To permit the cutting of ultrathin sections, material under study must be fairly hard. Triblock copolymers (SBS) having end use as thermoplastic elastomers are rubbery at room temperature. Thus some means of hardening these materials must be employed. Conventional techniques used in hardening biological materials such as plant and animal tissues involve embedding these materials into hard resins. I tried this technique using a number of epoxy and other resins as embedding medium. Additionally, block copolymers (styrene-butadiene-styrene) can be drenched in aqueous osmium tetroxide where block copolymers get hardened due to osmium penetration into butadiene region. Stiffness acquired by block copolymers due to osmium penetration and the embedding action of resins was found to be inadequate for ultramicrotomy, and the cutting of the section resembled tearing of the material. Osmium penetration was found to be non-uniform, resulting in hardened surface and rubbery core in block copolymers. Osmium, being a heavy molecule, creates a diffusion barrier across the hardened surface, preventing additional penetration of osmium into the polymer.

Cryo-ultramicrotomy solved the hardness problem and was found to be suitable for my work. Actual operation involves a blend of science and art, and training should be received from a skilled person before beginning cryo-ultramicrotomy. Detailed description of cryo-ultramicrotomy is a subject by itself and beyond the scope of this thesis. However, critical points pertaining to cryo-ultramicrotomy of block copolymer blends are mentioned.

The two most important items in ultramicrotomy are the preparation of the specimen (acquiring the desired hardness) and the manufacture and use of the knife.

4.3.1 Preparation of the specimen

When dipentene was completely evaporated in the vacuum oven, a thin circular disc of diameter 8 cm and thickness of ~2 mm of SBS-homopolystyrene remained at the bottom of the Petri dish. A rectangle about 5 mm long and ~2-3 mm wide, was cut out using a sharp razor blade; stressing of the material was avoided as much as possible. At this stage, the cut piece had dimensions of 5 x 3 x 2 mm. At one end of the rectangle (in the long direction), the specimen was trimmed to a point. Carefully, the upper and lower edges were trimmed away so as to avoid sectioning from the artifact-ridden surfaces and in order to achieve a relatively sharp "tip".

These pieces can be glued with sucrose solution to a flat tip pin called 'stub' and then transferred in an insulated container filled with liquid nitrogen where the specimen is allowed to equilibrate for about 5 minutes. Once at equilibrium, it is mounted on the sample holder.

Alternatively, a trimmed piece is transferred to an insulated container filled with liquid nitrogen. Once at equilibrium, the specimen is inserted into a specially made specimen chuck which resembles a miniature vice. (This specimen chuck is called " gripping chuck for cryo-ultramicrotomy".) The jaws of the chuck are tightened with a screw after making sure that the specimen is completely glassy.

Additional trimming of the specimen is necessary when the edge of the specimen is blunt. During trimming, the glued specimen may fall off the stub and re-alignment of another specimen is needed. Aligning of the specimen is a time consuming task, and it is advisable to use the 'gripping chuck assembly'.

The production of sections by ultramicrotomy involves a type of cutting action similar to that used in the machining of metals. A prepared specimen is moved past a cutting edge and forces are transmitted from that cutting edge to the specimen, causing a thin layer of the material to be detached. Unlike machining, the primary concern in ultramicrotomy is with the section and not with the surface finish.

The first contact between the specimen and the knife is most important as both can be damaged if care is not taken. The specimen arm of the ultramicrotome is operated by either the manual or automatic control and the knife is advanced in very small increments, approximately 1 micron, between each stroke. It is impossible to judge accurately by eye the distance between the specimen face and the knife edge, and thus if the advance is too great there is a danger of cutting a very thick section which will blunt the cutting edge. The choice of cutting speed will vary for different specimens. An average speed of 2-3 mm per second can be used as a starting point, and the speed is varied according to the properties of the material being sectioned. Once contact has been made, low speed is set and the specimen arm movements continued automatically. While sectioning is in progress, attention should be paid to avoiding any disturbances that are likely to affect it. Sectioning operation is never a smooth operation, and various adjustments are necessary throughout the operation. Any adjustments that have to be made on the ultramicrotome should be done gently. As the advance takes place automatically between each stroke, it is important that a section is produced at every stroke once contact has been made; otherwise, the specimen block will rub against the clearance facet of the knife, thus quickly damaging the knife edge.

4.3.2 Knives

Early knives included objects made of metal, such as sharpened steel knives and razor blades. These knives lost their sharpness after cutting relatively few thin sections, and the tedious process of sharpening had to be started again. In 1950, Latta and Hartmann [61] discovered that a freshly broken piece of plate glass produced an edge suitable for cutting ultrathin sections and because of its relatively low price could be discarded once it had become blunt.

In 1953, Fernandez-Moran [26] made a knife from a single crystal of diamond. The crystalline structure provides a very sharp, stable edge of molecular thickness and of unsurpassed hardness. Diamond knives are capable of cutting almost any material. Use of a diamond knife in cryo-ultramicrotomy offers many advantages over use of glass knives. Glass is a supercooled liquid and the freshly broken edge of molecular thickness is subject to molecular flow that results in a rounding of the edge and therefore loss of sharpness. For this reason, glass knives lose their sharpness over a short period of time and cannot be stored for a relatively longer period.

The great advantage with a diamond knife is that the cutting edge remains sharp for a considerable period of time (proper cleaning, handling and storing procedures would ensure its life for years). This make it ideal for use when it is inconvenient to keep changing knives (as in cryo-ultramicrotomy), with the subsequent realignment of the specimen and knives that would be necessary if glass knives were used. A good diamond knife will also be capable of cutting thinner sections needed for very high resolution work.

However, a few points should be kept in mind while using a diamond knife. Although a diamond knife edge is extremely hard, it can easily be damaged by misuse. The cost of a diamond knife is very high ($ 2000-4000) compared to that of a glass knife and is due to exacting processes involved in its production. Thus, it is advisable for a neophyte to begin cryo-ultramicrotomy (or ultramicrotomy) with a glass knife. A diamond knife may be used once the user is confident with the whole operation using a glass knife. Care should be taken to avoid cutting sections thicker than 1 μm on a diamond knife. This is especially important when fast sectioning speeds are used or the cutting force is produced by a motor. Diamond knives should never be used for trimming unless they have been discarded from normal use. The edge should never be touched by anything other than the specimen or the cleaning tool. It is advisable for an operator to have his own knife, if possible, to ensure good care.

Glass knives are discarded after one use. However, diamond knives are retained and therefore good care must be taken in storing and cleaning them. After use, unwanted sections should be removed immediately while the knife is still wet. The knife is carefully rinsed with distilled water and allowed to dry. Acid should never be used to clean a diamond knife. If debris remains, acetone or alcohol can be used to clean the knife edge, but the knife should be thoroughly rinsed again with water before drying. The clean knife should then be placed in its holder and stored in its box or in a safe dust-free environment.

I learnt ultramicrotomy using glass knives and continued to use glass knives throughout this work, due to unavailability of a diamond knife. However, wherever available, a diamond knife is a preferred choice. Glass knives perform better at the lower temperatures used in cryo-ultramicrotomy than at room temperature used in normal microtomy. I recommend the use of glass knives prepared on the same day and their temporary storage in an airtight desiccator, as was the case in this work.

Glass knives were made with balanced brake method using LKB 2178 Knifemaker II [91]. Knives were then tungsten-coated by sputtering a monolayer of tungsten in a vacuum chamber to minimize static charge. This is because the presence of liquid nitrogen makes air very dry in the cryo chamber, resulting in an increase in static charge and thus many times sections fly off once they are cut. Tungsten coating also improves usability of the knives by maintaining sharpness.

4.3.3 Temperature Selection for Cryo-ultramicrotomy

The cryo-ultramicrotome assembly used was capable of controlling temperatures at three points. Temperature of specimen, temperature of knife, and temperature in the cryo-chamber could be controlled. All the blends (SBS and polystyrene) made using dipentene were cryo-ultramicrotomed and the temperature of the specimen varied from -90^0C to -135^0C. Spontak [98] observed a correlation between the rubber content in SBS samples and the optimum temperature of microtoming. No such correlation was observed in our case. Knife temperature was kept constant at the same temperature as that of the specimen. Cryo-chamber temperature was kept at 20 degrees below specimen and knife temperatures. The desired temperatures were maintained within $\pm 5^0$C.

4.3.4 Collection of Sections

As the specimen passed over the knife edge, a thin section was generated and care was taken in removing sections from the cutting edge to avoid knife damage and flying of the sections. Sections are pulled down away from the knife edge to make space for new sections. This can be accomplished with the help of any ultrathin soft material such as brush bristles, hair, etc. I preferred using an eye-lash. The eye-lash was glued to a thin wooden stick with fingernail enamel (lacquer) at the one end. While handling the sections with this eye-lash, care should be taken in not touching the wooden stick to the knife edge, which would damage to both knife edge and eye-lash brush. Once 15-20 good sections were generated on the knife, they were ready to be collected. A 3 mm diameter loop made out of thin platinum wire was dipped in 0.2 M sucrose solution and then lightly touched over the sections. Sections get stuck to the sucrose solution in the loop. Sucrose solution freezes at the low temperature of microtoming, and thus this collecting should be done at fast speed and with great care. The loop must touch sections before the sucrose solution freezes; when it does freeze, the loop is taken away from the knife where the frozen solution is allowed to melt. Sections are transferred to the treated TEM grid (grid + formvar + carbon) by transferring the sucrose drop. The grid is washed in water 4-5 times to get rid of sucrose and then observed under a light microscope to detect the presence and orientation of sections.

4.3.5 Osmium Staining

Osmium tetroxide is a poison and therefore the whole staining procedure was carried out in a fumehood. TEM grids with mounted sections were placed on a clean glass slide, kept at the center of a Petri dish, and a few drops of 2% aqueous osmium tetroxide were deposited on both sides of the glass slide. The Petri dish was covered for the next 8 hours, kept at room temperature, and then grids were taken out and stored in a referigeter.

4.3.6 Cryo-ultramicrotome Equipment

Reichert-Jung Ultracut E cryo-ultramicrotome was used in this work, made available to us by the Electron Microscopy Laboratory, Department of Biological Sciences, University of Alberta. This microtome can be used either at room temperature or at cryogenic conditions. Cryochamber ‘Cryo-attachement FC-4D’ was installed for cryo-microtomy work and can be removed when doing work at room temperature.

4.4 Differential Scanning Calorimetry

A DSC 2910 differential scanning calorimeter (TA Instruments) in our laboratory was used for all DSC measurements. Calibration was done using indium at the beginning of each set of experiments and no further calibration was done. Various scanning rates were used in the experiments, in the range 1-10^{0}C/min. Additional details are discussed in chapter 6.

4.5 Electron Microscopes

Phillips EM 201 E (100 kV) and Philips EM 400 T (125 kV) were the two transmission microscopes used, available at Electron Microscopy Laboratory, Department of Biological Sciences, University of Alberta. Some of the high resolution work was done at Electron Microscopy Laboratory, Department of Physics, University of Alberta. SEM work was performed at SEM laboratories in Department of Geology, University of Alberta.

4.6 Brabender Do-corder

C.W. Brabender Plasti-Docorder (C.W. Brabender Instruments, Inc., New Jersey, USA) was used for melt blending of polymers. The temperature in the mixing bowl is controlled with the help of two thermocouples, one at the inner surface of the mixing bowl (this thermocouple measures the temperature of the polymer melt) and another at the wall of the mixing bowl (this thermocouple measures the temperature of the wall of mixing bowl). A nitrogen stream was used to create an inert environment inside the mixing bowl. Two roller-type of mixing blades were used and torque readings were recorded on a chart recorder. Nominal volume of the mixing bowl was 60 cm^3. Additional details are given in Appendix A.

4.7 Materials

The following block copolymers and homopolymers were used in the present study. All characterization data were supplied by the manufacturers.

SBS (Styrene-butadiene-styrene) Triblock Copolymer samples

Sample	Company and Product	Molecular weight (Mw x10^3)	%Styrene	Specific
S127	Dow Vector 8508-D	69.4	30.4	0.92
S129	Dow Vector 4461-D	61.2	44.0	0.92
S130	Doe Vector 2510-D	101.2	31.3	0.92
S145	Fina-Finaprene 416	150.0	30.0	0.94

Homopolymer (Polystyrene) samples

Sample	Company and Product	Molecular weight (Mw x10^3)	Polydispersity
S191	Pressure Chemical	13.0	<1.06
S192	Pressure Chemical	65.0	<1.04
S189	Dow Chemical Canada	315.0	2.60

Homopolymer (Polybutadiene) sample

Sample	Company and Product	Molecular weight (Mw x10^3)	Polydispersity
S165	Firestone Company	197	1.9

CHAPTER 5

TRANSMISSION ELECTRON MICROSCOPY

5.1 Morphology in SBS Block Copolymers

Microphase-separated morphologies of the SBS block copolymers observed by TEM vary considerably depending on techniques used in sample preparation (direct casting from solvent, cryo-ultramicrotomy of the bulk material cast from solvent). For casting, results can depend on solvent preference for one of the blocks as well as on the conditions of evaporation.

For example, SBS sample S129, which is 44 wt% PS, is expected to exhibit a lamellar morphology; this type of morphology is shown in Figure 5.1 which depicts a film cast from toluene (good solvent for polystyrene). The dark regions indicate the osmium-stained polybutadiene domains. Fast evaporation of the volatile solvent caused kinetically controlled morphology consisting of imperfectly developed lamella and only short-range order. Additionally, variations in background light intensity prove that the film is not of uniform thickness.

This sample preparation effect is even more pronounced for sample S127, which contains 30 wt% PS. At this composition, either cylinders or spheres or a combination of the two can be expected. Figure 5.2, which also depicts a toluene cast film, reveals a cylindrical PS morphology. Small circles of PS are seen which can be interpreted as either spheres or the end view of cylinders, but cylinders are expected due to the PS fraction.

When block copolymer is dissolved in a suitable solvent and solvent is evaporated slowly enough; near-equilibrium morphology is obtained. Moreover, morphologies will be free of preferential solvent artifacts if a "neutral solvent" is used. Theoretically, "neutral solvent" is equally attracted to "A" blocks and "B" blocks: $|\delta_A - \delta_S| = |\delta_S - \delta_B|$ [79]. Dipentene is a true neutral solvent for SBS block copolymer [77] as will be discussed further in Chapter 7. Figure 5.3 is a typical micrograph of pure SBS (S129) having 44%

Figure 5.1 TEM micrograph of SBS copolymer (S129) having 44% styrene. The sample was prepared by 'direct casting technique' from 0.5% polymer solution in toluene. The butadiene blocks, stained with OsO_4 to enhance contrast, constitute the dark regions. Imperfectly developed lamellae with short range order are seen.

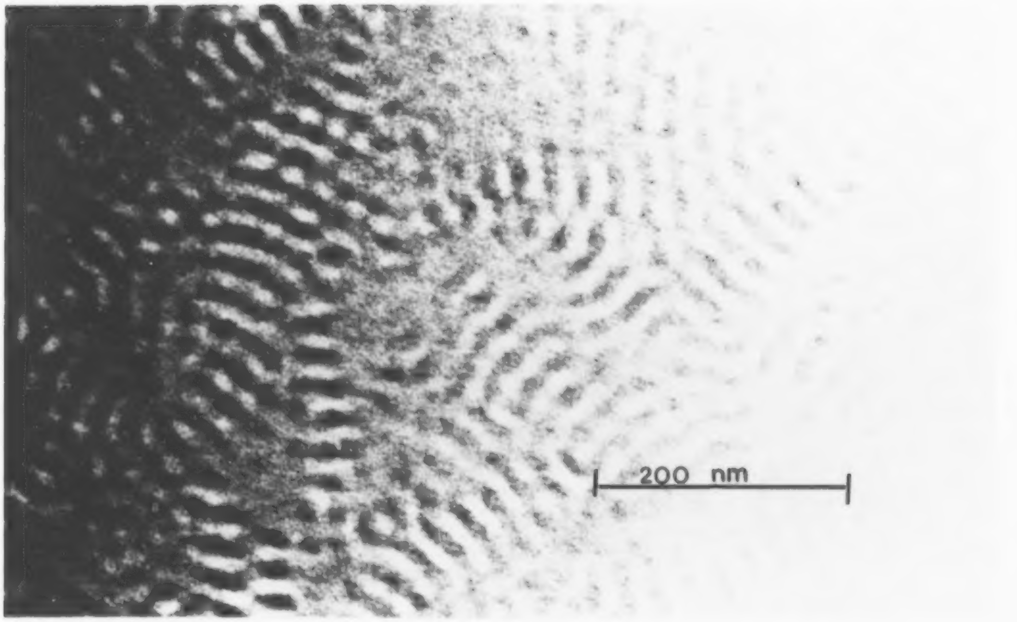
200 nm

Figure 5.2 Typical electron micrograph of SBS copolymer (S127) having 30% styrene. Initial and developing cylindrical structures of PS in butadiene matrix.

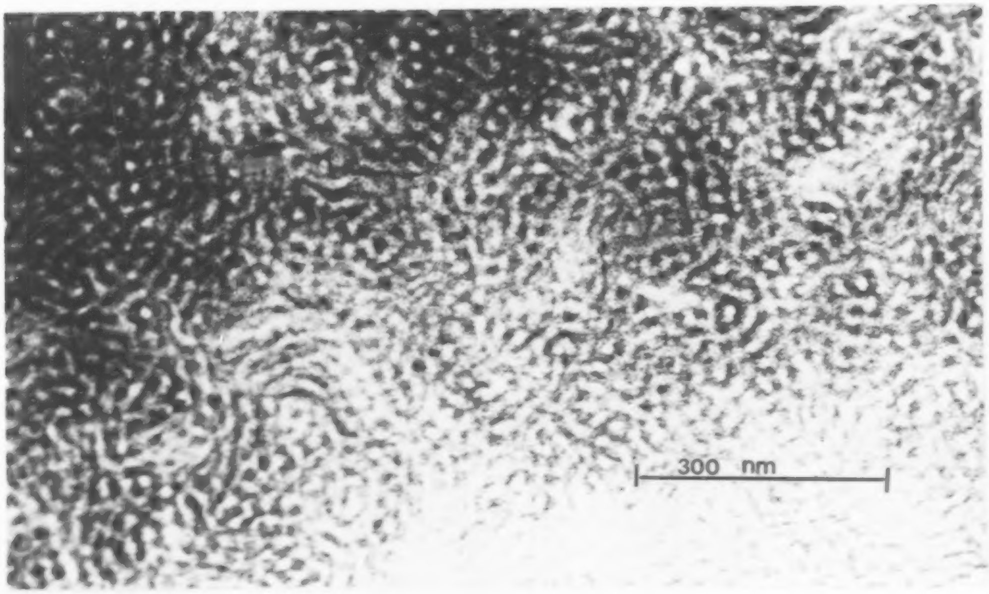
300 nm

Figure 5.3 TEM micrograph of block copolymer (S129). The section was obtained by cryo-ultramicrotoming of the film cast from solution with dipentene as a solvent. Co-continuous lamellae of styrene (light) and butadiene (dark) run parallel to each other for long distances.

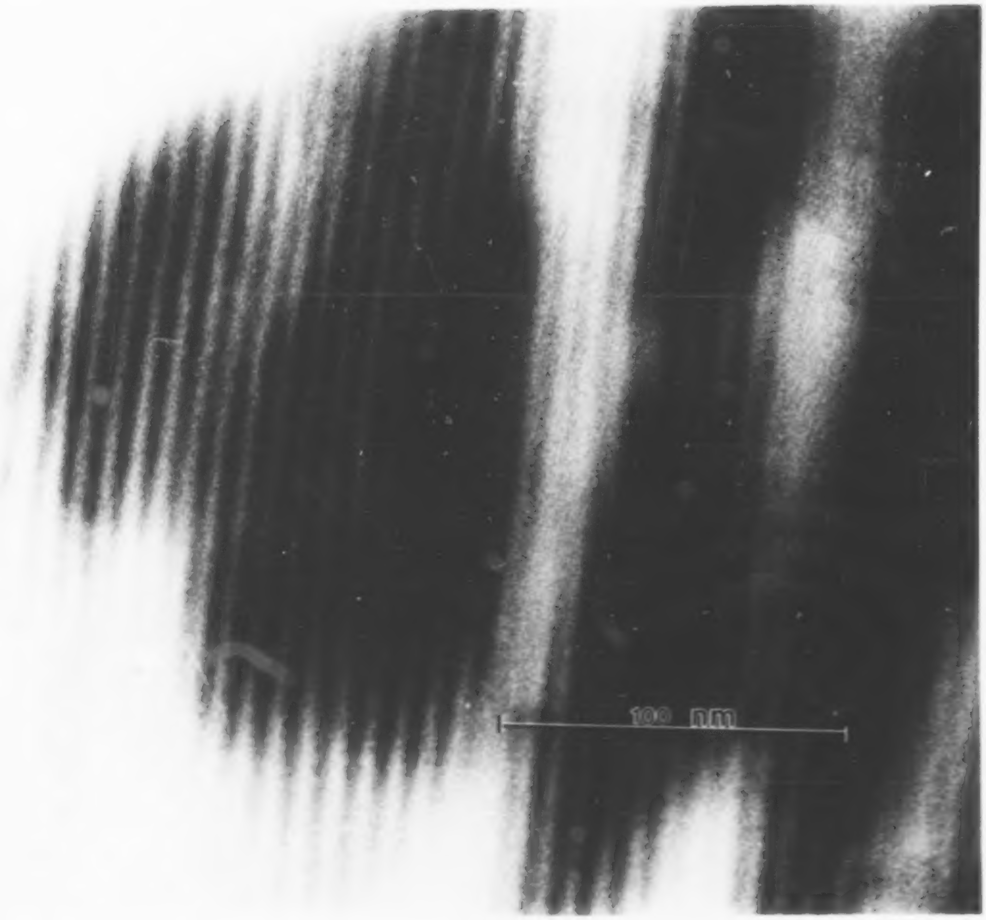
100 nm

styrene, cast from dipentene. The lamellar morphology consists of alternating layers of polybutadiene and polystyrene and thickness of individual lamella is about 5 nm. Lamellae run parallel to each other for long distances.

Another important way of characterizing the sample is by studying morphology of "as-received" commercial product, where process history is unknown. S127 sample (All block copolymers used in this work were supplied generously by Dr. Kevin Mackay of Dow Chemical Company, Louisiana, USA) initially appears as irregularly shaped chunks. A thin polymer film of roughly 2 mm thickness was obtained by pressing the irregular chunks in a heated press at 225^0C (below the separation temperature T_s, which is around 240^0C), under a ram force of 2 tons in a platen press for 45 minutes. This was sufficient to cause interdiffusion of the polymer granule boundaries and eliminate all visible air bubbles, thus forming uniform samples. Figure 5.4 shows morphology of an ultramicrotomed section of this sample. Irregular dark and bright specks are seen all over the micrograph. This sample having identical process history was later on used in rheological studies [100].

5.2 Solution Blending: Morphology in Blends of Block Copolymer and hPS

Table 5.1 (A and B) lists the blends of SBS block copolymer and pure homopolystyrene (PS). Each blend in Table 5.1-A is designated by a number and letter code hPS indicating weight percent of homopolystyrene in the blend, whereas blends in Table 5.1-b are designated by a number and letter code SBS indicating weight percent of copolymer in the blend. Below, we discuss separately the blends made with PS13 (M = 13,000) and with PS65 (M = 65,000).

Figure 5.4 Section of compression molded block copolymer (S127). Irregular shaped flakes of butadiene (dark) and styrene (light) are observed indicating that morphology is far from its equilibrium state.

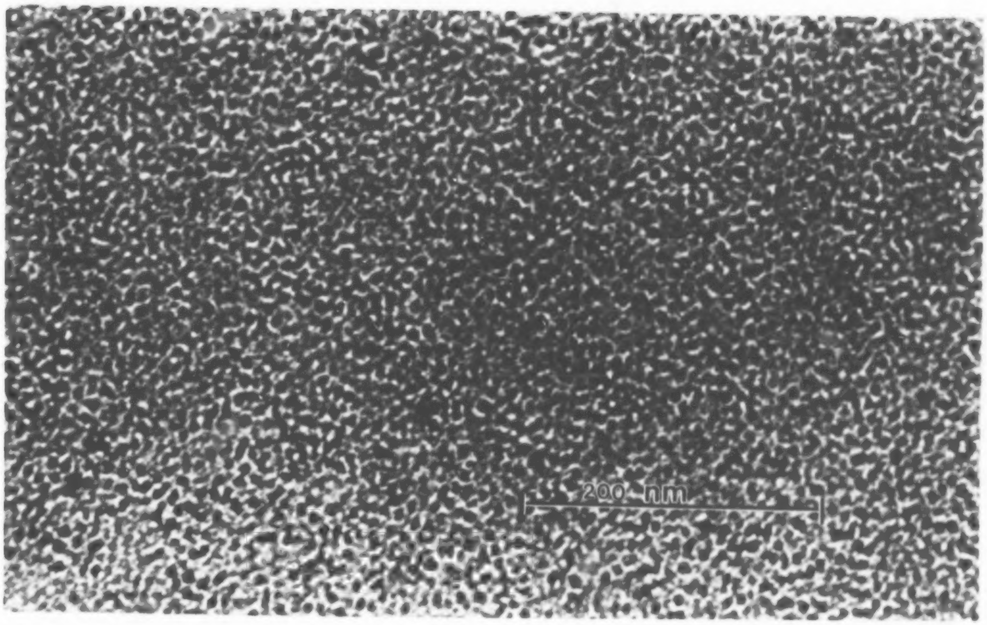
200 nm

Table 5.1-A Solution Blends of Polystyrene PS13 (S191) with SBS Block Copolymer (S129). SBS (S129) molecular weight = 61,000

Blend Designation	Homopolystyrene molecular weight (M_w)	%SBS	%Polystyrene	%Homopolymer
60% hPS	13,000	39.9	77.7	60.1
44% hPS	13,000	55.5	68.9	44.5
37% hPS	13,000	62.6	64.9	37.4
18% hPS	13,000	81.5	54.4	18.5
8% hPS	13,000	91.4	48.8	8.6
4% hPS	13,000	95.9	46.3	4.1
Pure SBS	13,484[z]	100.0	44.0	0.0

[z] molecular weight of polystyrene block in the copolymer

Table 5.1-B Solution Blends of Polystyrene PS65(S192) with SBS Block Copolymer (S129)

Blend Designation	Homopolystyrene molecular weight (M_w)	%SBS	%Polystyrene	%Homopolymer
4-SBS	65,000	4.6	97.4	95.4
8-SBS	65,000	8.8	95.1	91.2
16-SBS	65,000	16.2	90.9	83.8
32-SBS	65,000	32.6	81.8	67.4

5.2.1 Solution Blends with Molecular Weight of S-block Being Equal to Added hPS

When a small amount of hPS is added to the block copolymer, hPS is thermodynamically driven to occupy space in domains of styrene, and swelling of styrene domains was observed [47, 112]. In the case of a block copolymer having lamellar morphology, a small addition of hPS might be expected to cause insignificant quantitative change to the copolymer morphology (say, by proportional thickening of the styrene lamella) and no qualitative change. However, Figure 5.5, shows wavy lamellar morphology in bulk, where only 4% hPS is added to the copolymer. In other regions of this same blend, alternate globules of styrene and butadiene form a regular network pattern (Figure5.6), a surprise for this composition of blend (4% hPS) and apparently never seen before. Figure 5.7 shows another micrograph of this blend, resembling wavy-rod morphology (with network character) but still keeping its overall lamellar microstructure intact.

Increasing the amount of hPS in a SBS with lamellar morphology leads to further increase in the thickness of styrene domains. Butadiene domains may either experience some shrinkage [112] or remain constant. Addition of 8.5% PS13 to SBS leaves morphology in a distorted lamellar state as shown in Figures 5.8 and 5.9. The material appears to be under stress as if unable to reach its lowest energy state at this composition, leading to long-range rinks and whorls which can be observed at long range in Figure 5.10. We call this a "quasi-transition state" morphology. Also evident in Figures 5.8 and 5.9 is the localized thickenning of the polystyrene lamella, sometimes to 80% of the local volume, but progression is smooth.

Further addition (18.5%) of PS13 pulls the morphology out of the "quasi-transition state" and establishes a distinctive new structure, which may be driven either by kinetics or thermodynamics. Figure 5.11 shows large-scale lobes, with internal lamellar morphology. The lobes are converging towards the center, where the lamella are grossly distorted. Excess hPS appears to be packed within the styrene lamellae, but there is no

Figure 5.5 TEM micrograph of 4%hPS blend with SBS (S129). Co-continuous lamellar morphology was predominant in this blend. No significant swelling of styrene domains was observed.

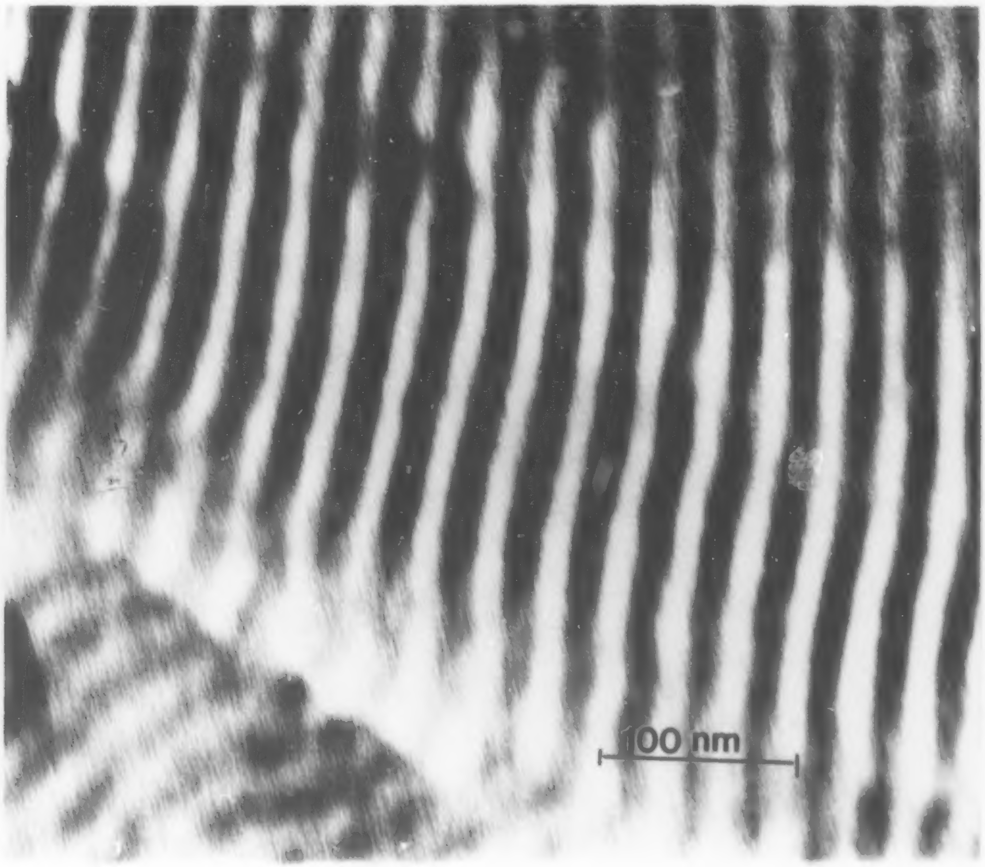
100 nm

Figure 5.6 Typical micrograph of 'alternate globule morphology' observed in some parts of 4%hPS blend. It had resemblance of a lattice structure and catenoid arrangement was prevalent between the globules.

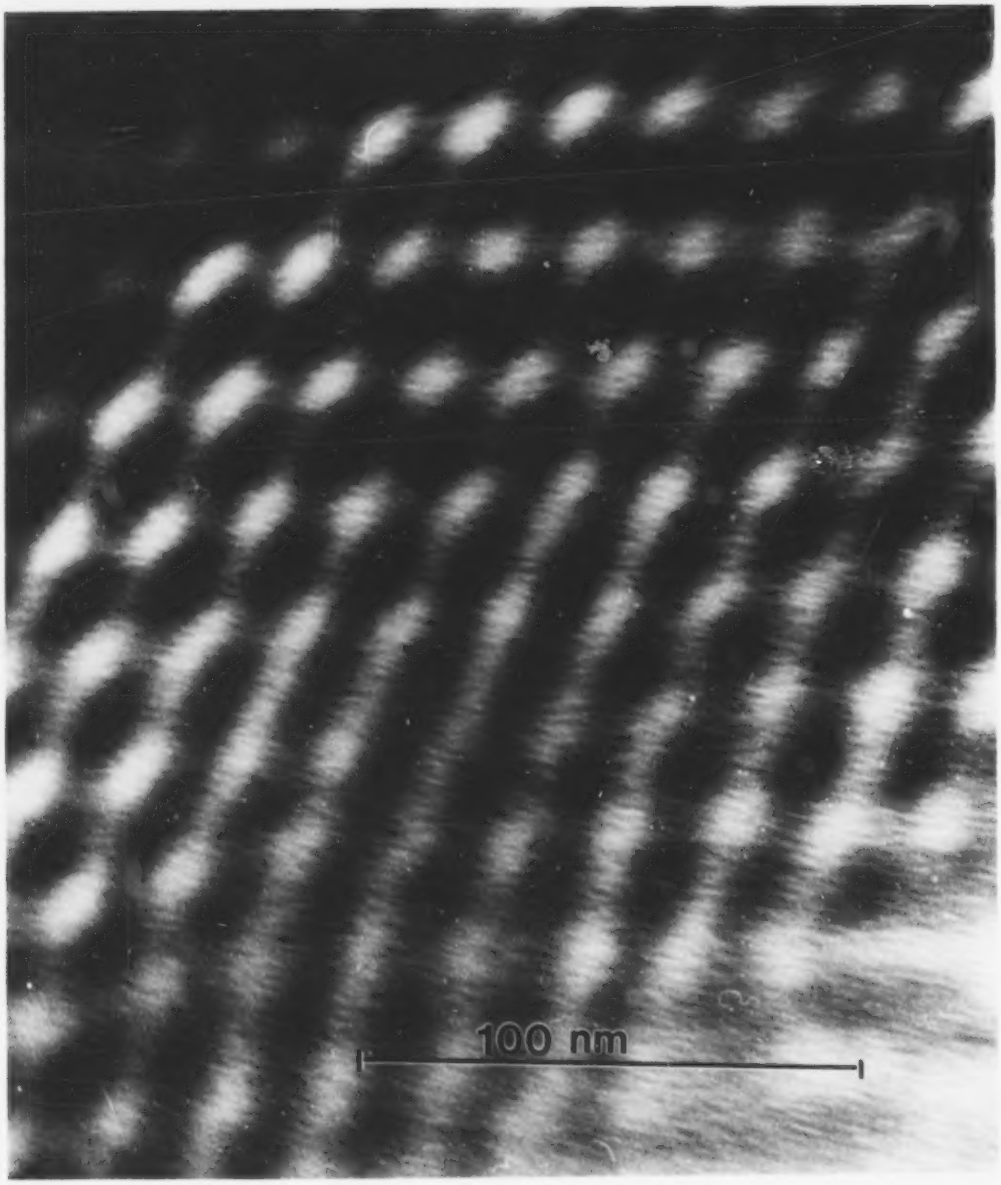
100 nm

Figure 5.7 TEM micrograph showing broader region of 'alternate globule morphology' in 4%hPS blend..

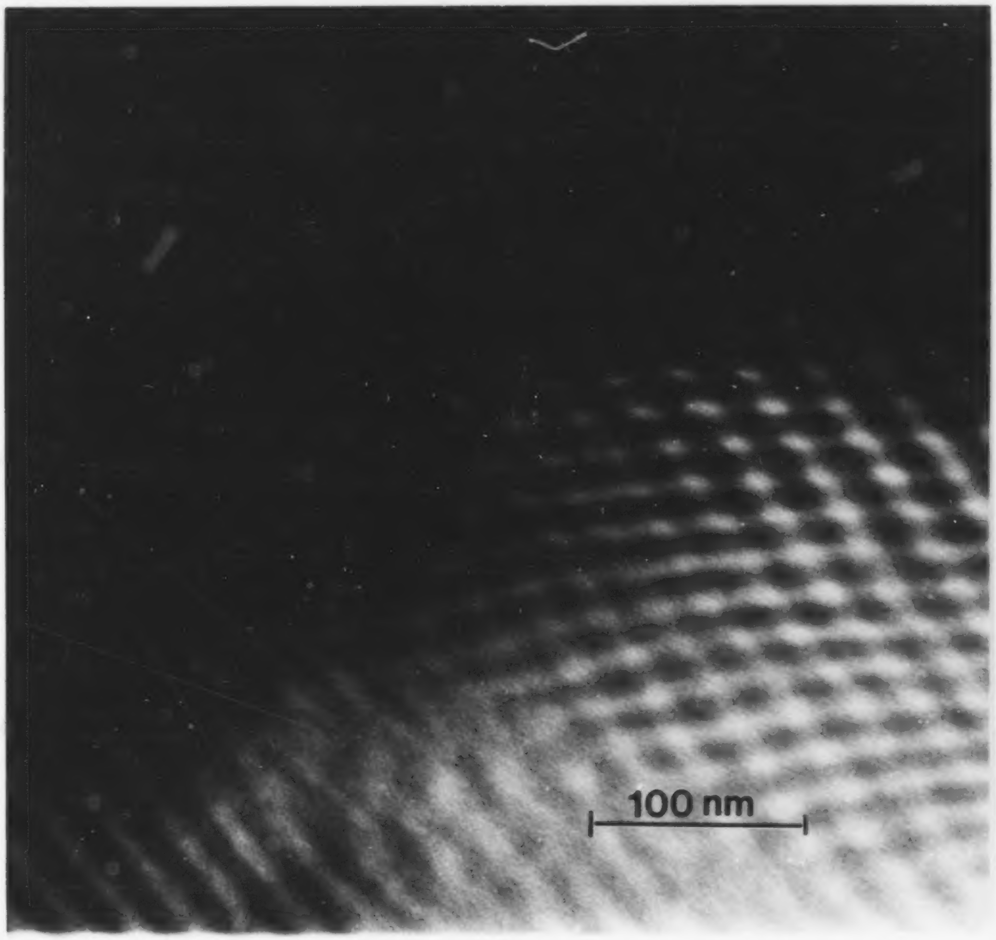
100 nm

Figure 5.8 Typical electron micrograph showing lamellar morphology for 8%hPS blend.

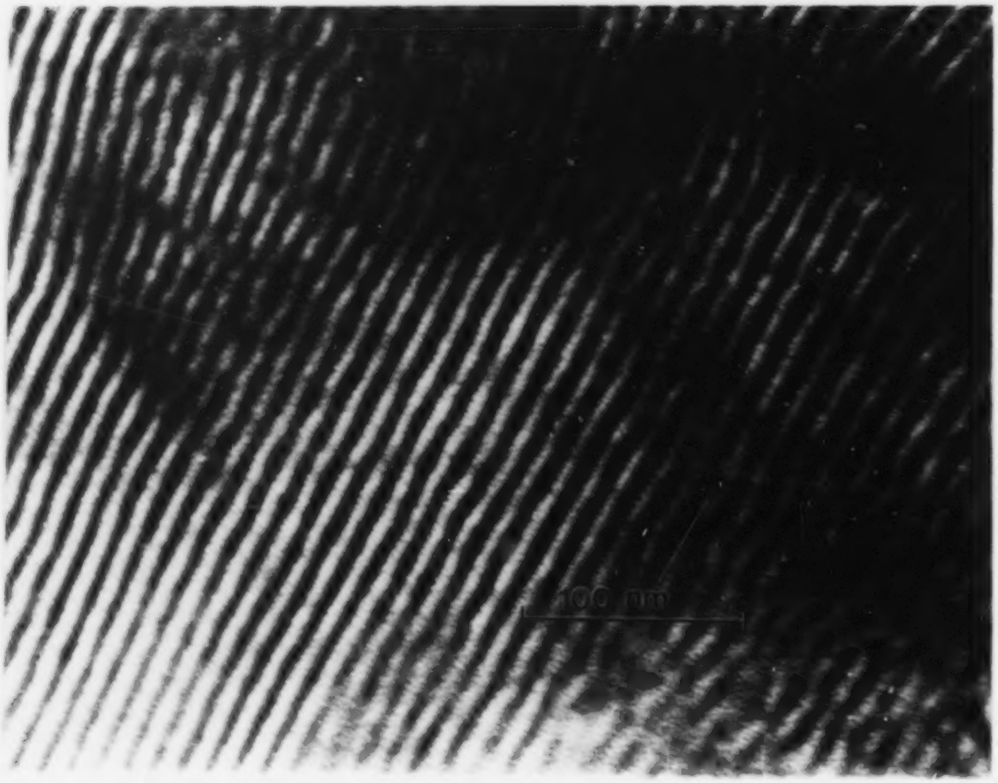
100 nm

Figure 5.9 High magnification electron micrograph of 8%hPS blend. The light styrene domains have experienced some swelling due to added hPS and overall morphology is lamellar.

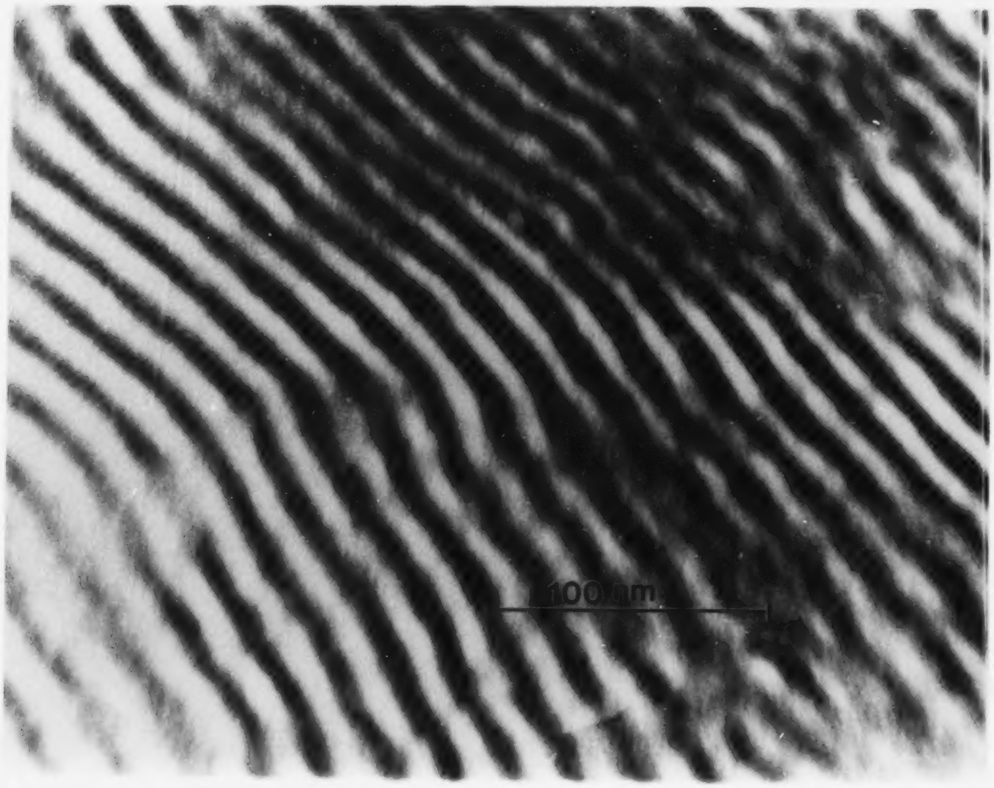
100 nm

Figure 5.10 Low magnification electron micrograph of 8%hPS blend giving a broader view of the blend morphology. Material in the blend appears to be under stress (still keeping its overall lamellar nature) and rinks and whorls were observed (e.g. top right corner).

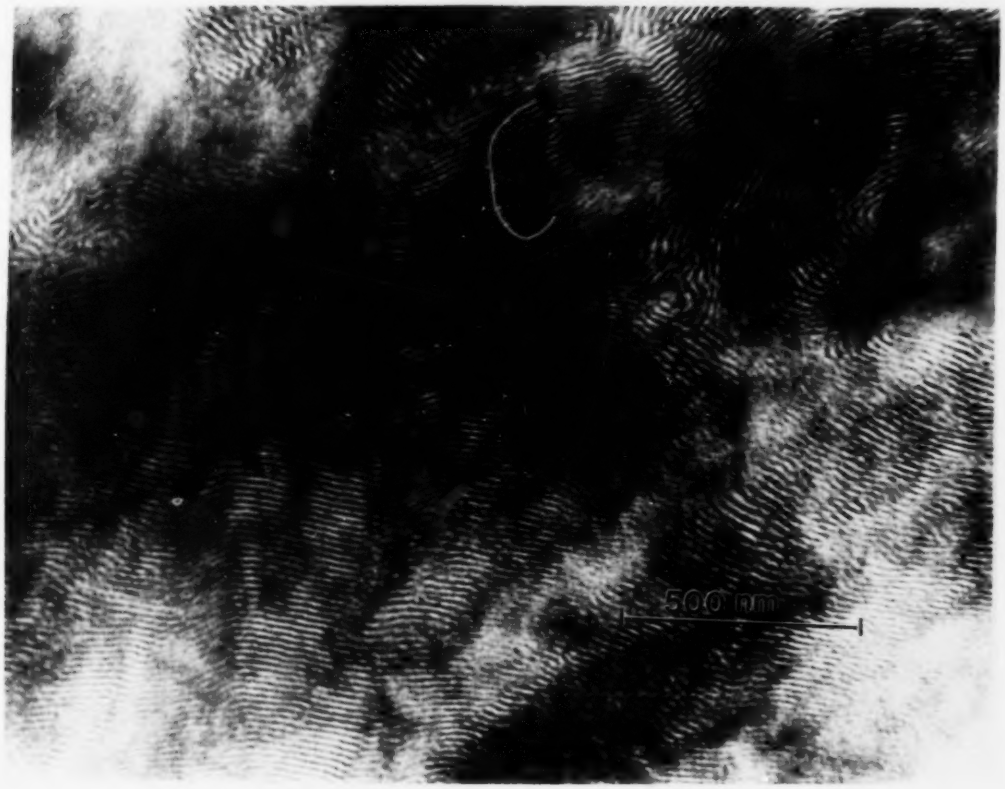
500 nm

Figure 5.11 Electron micrograph of 18%hPS blend. The lobular structures observed here were thought to be the extensions of 'whorls of 8%hPS blend' as more hPS was added to the system.

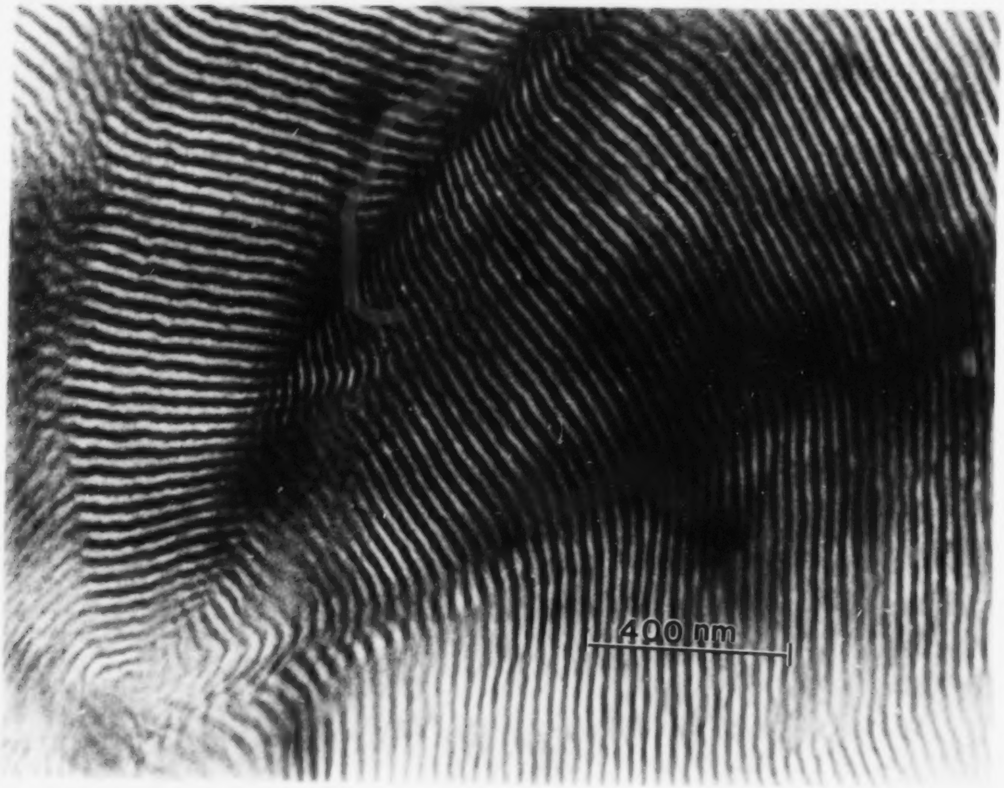
400 nm

Figure 5.12 High magnification micrograph of 18%hPS blend. Butadiene domain thickness remained constant and swelling of styrene domains was excessive and nonuniform indicating onset of macrophase separation.

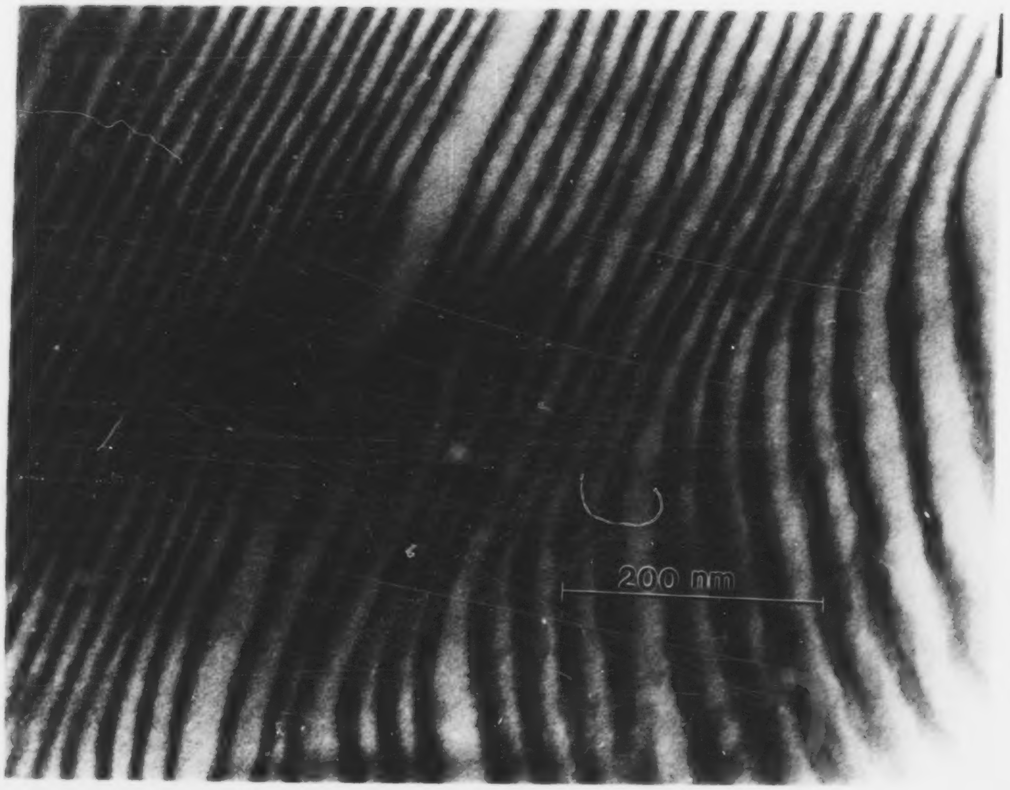

200 nm

macrophase separation evident. The lobe structure might occur because microphase separation started at many points and grew until colliding to form the "grain boundaries" (lobe boundaries) visible in the micrograph. Figure 5.12 is a high magnification micrograph showing considerable local variation in styrene domain thickness, whereas butadiene domains have uniform thickness. Figure 5.12 is a clear indication of instability of the system in accommodating additional styrene, since styrene regions change thickness abruptly rather than smoothly and gradually as in Figures 5.8 and 5.9..

Addition of hPS (M_{PS} = > and < Block M_S) above 30% in block copolymers (diblock, triblock) have resulted in macrophase separation in previous studies [46]. Figure 5.13 where 37% PS13 is added to SBS, shows a region of more or less parallel lamellar morphology with substantial local distortation. Styrene domains are much thicker than butadiene domains as additional styrene finds its way into styrene-rich domains. In another region we find some defects (shown by arrows in Figure 5.14 in the growth of butadiene lamellae, which are interrupted by pockets of excess PS). In contrast to this, there were also some regions of greater smoothness and order (Figure 5.15).

Extreme variations in the thickness of styrene as well as butadiene lamellae were found in this blend. In order to investigate this in detail, we tried to obtain sections cut in the parallel direction to the disc surface, unlike all other micrographs in this study which were obtained by cutting in normal direction to the disc surface. Figure 5.16a and Figure 5.16b show micrographs obtained from sections cut in the parallel direction, with unexpected and remarkable results. In the absence of these two micrographs, we would have been tempted to consider this blend morphology as being lamellar with mesophase separation, but this is clearly not the case in the regions of Figures 5.16 (a and b).

Central dark butadiene cores are surrounded by bright styrene rings and this whole assembly is embedded in a matrix of grey (mixed styrene-butadiene). When seen at lower magnification, as in Figure 5.16b, irregular patches of light and dark seem to indicate distinct regions of polystyrene-rich macrophase and polybutadiene-rich macrophase, each with its own internal microphases. This suggests co-existing overall macroscopic phase separation and local microscopic phase separation. The addition of PS13 has forced the

Figure 5.13 TEM micrograph of 37%hPS blend showing regular lamellar morphology. Styrene domains are swollen due to added hPS.

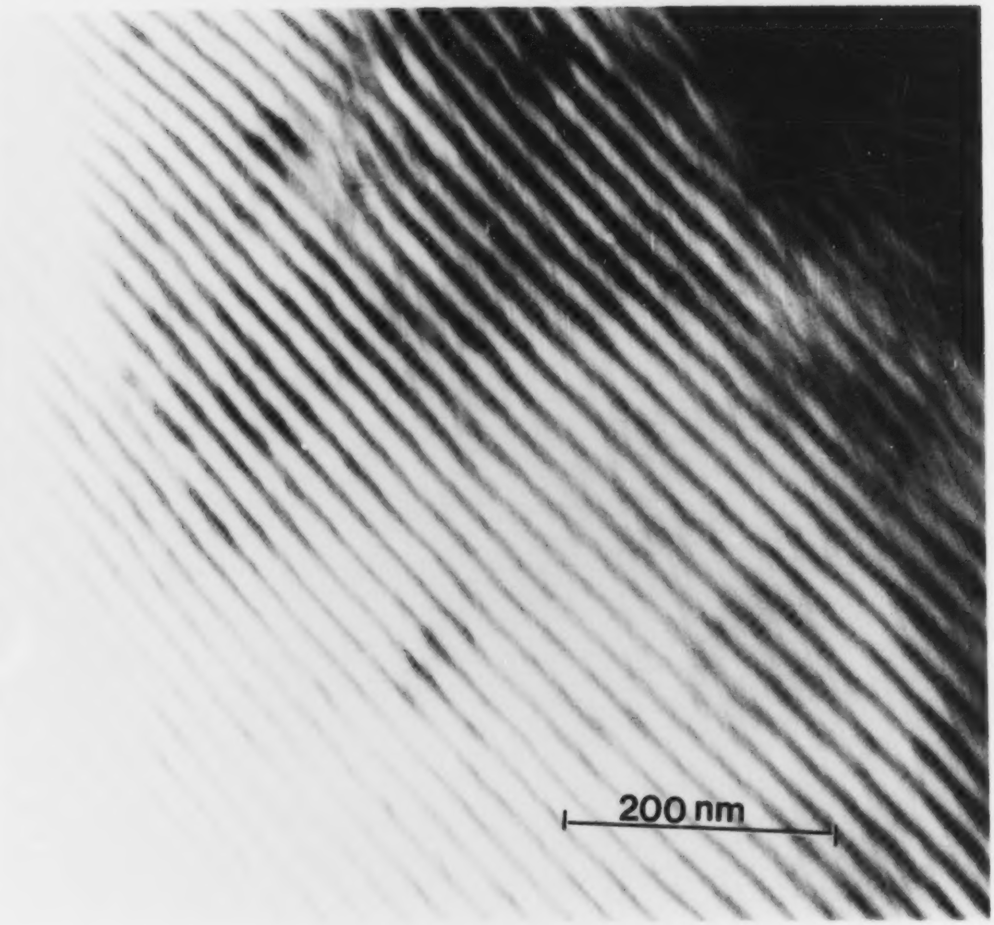
200 nm

Figure 5.14 Another micrograph for 37%hPS blend showing small pools of macrophase separated hPS (shown by arrows). Defects in growth of polybutadiene lamellae is shown by arrows.

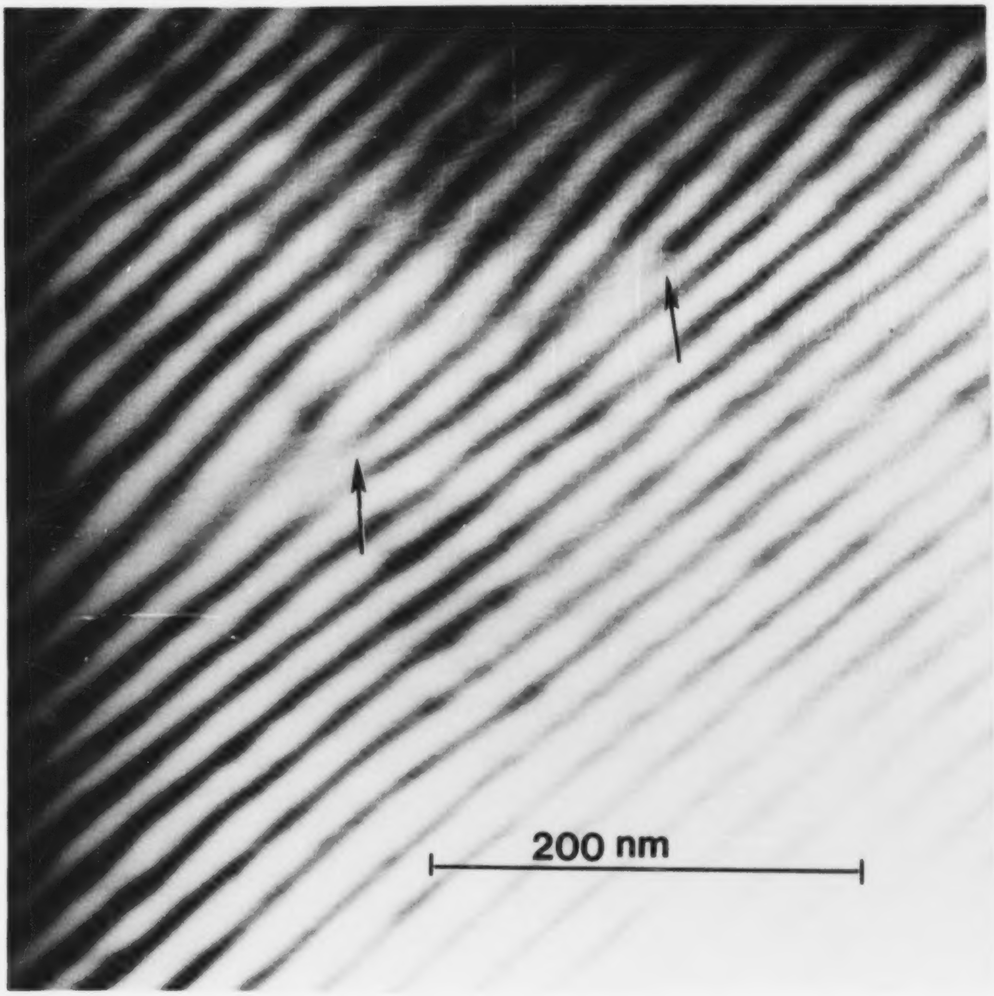

200 nm

Figure 5.15 Electron micrograph of 37%hPS blend showing nonuniform swelling in styrene domains and much thicker butadiene domains. (This and many other similar micrographs led us to carry out more work on this blend (as shown in next two micrographs).

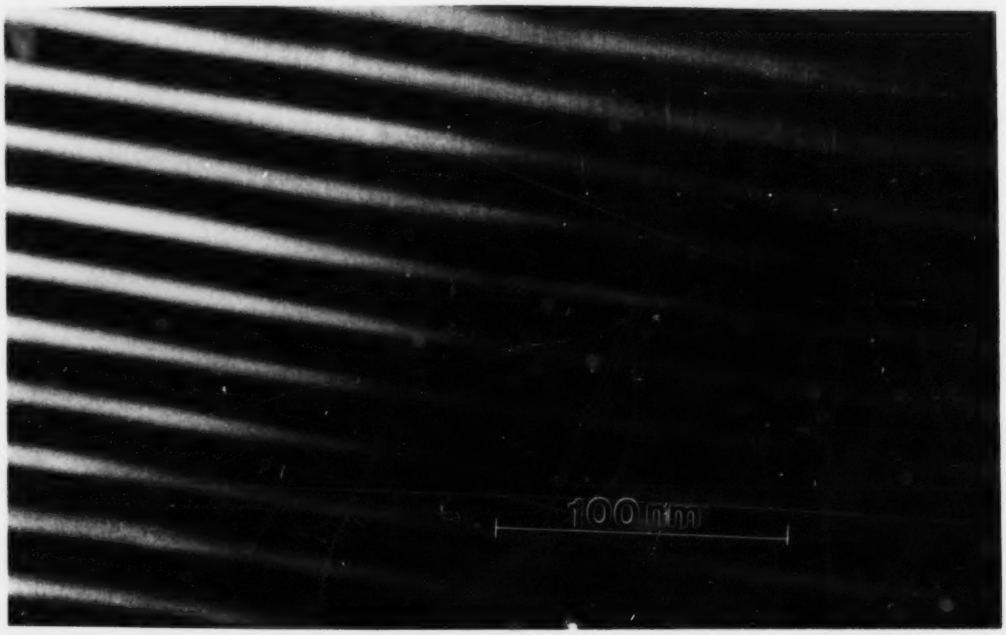
100 nm

Figure 5.16-a High magnification view of 37%hPS blend. The section was cut in direction parallel to the polymer film surface to observe the morphology at 900 with respect that observed in Figures 5.13-15. The region appears to be rich in polybutadiene and central core of butadiene is surrounded by ring of styrene.

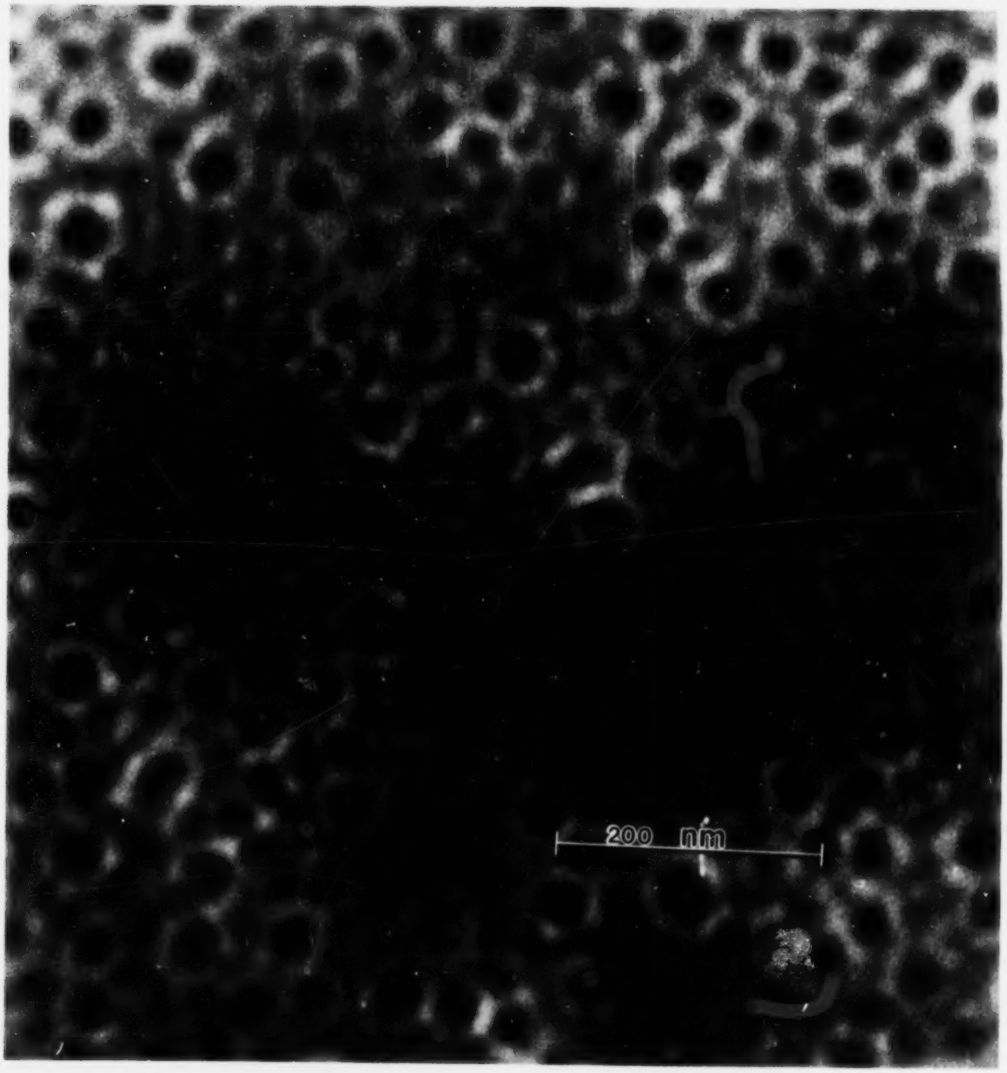
200 nm

Figure 5.16-b Low magnification micrograph of 37%hPS taken in an identical fashion as in Figure 5.16-a. Irregular shaped hPS-rich and copolymer-rich phases are seen. The styrene core surrounded by butadiene sheath which is in turn surrounded by styrene annlus was the type of morphology observed in some areas (shown by arrows). However, major feature was that of central butadiene core surrounded by styrene sheath in both macrophases.

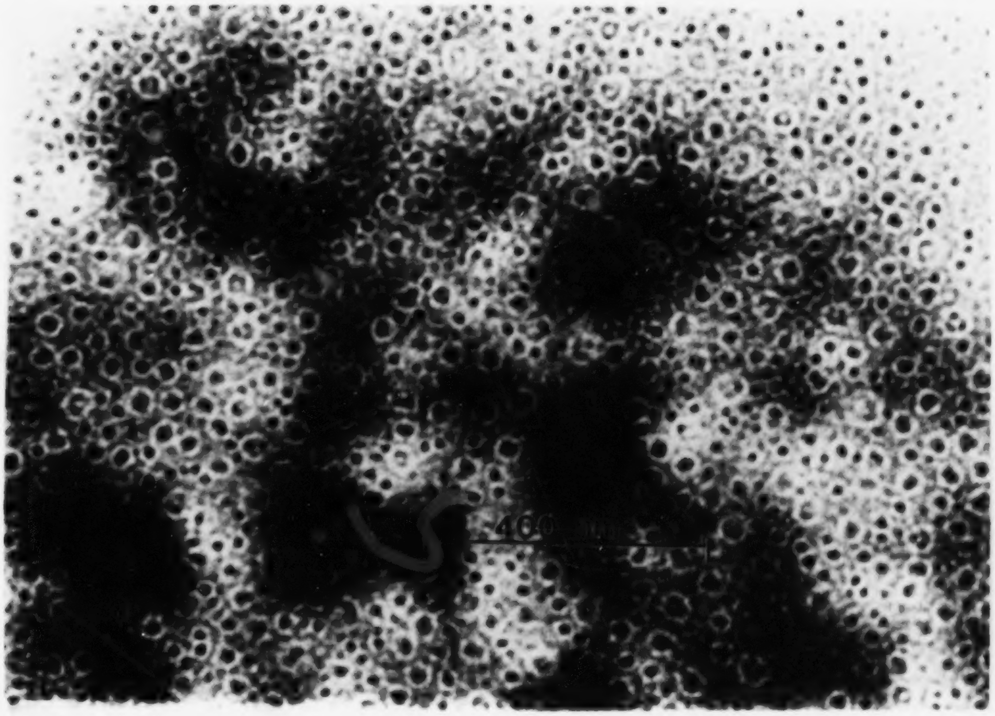

400 nm

Figure 5.17 TEM micrograph of 44%hPS blend. Here amount of added hPS is same as styrene content of the copolymer. Macrophase separated hPS and copolymer-rich phases are seen. Lamellar morphology is seen in copolymer-rich region with some swelling of styrene lamellae. Macrophases of hPS are virtually free of trapped copolymer.

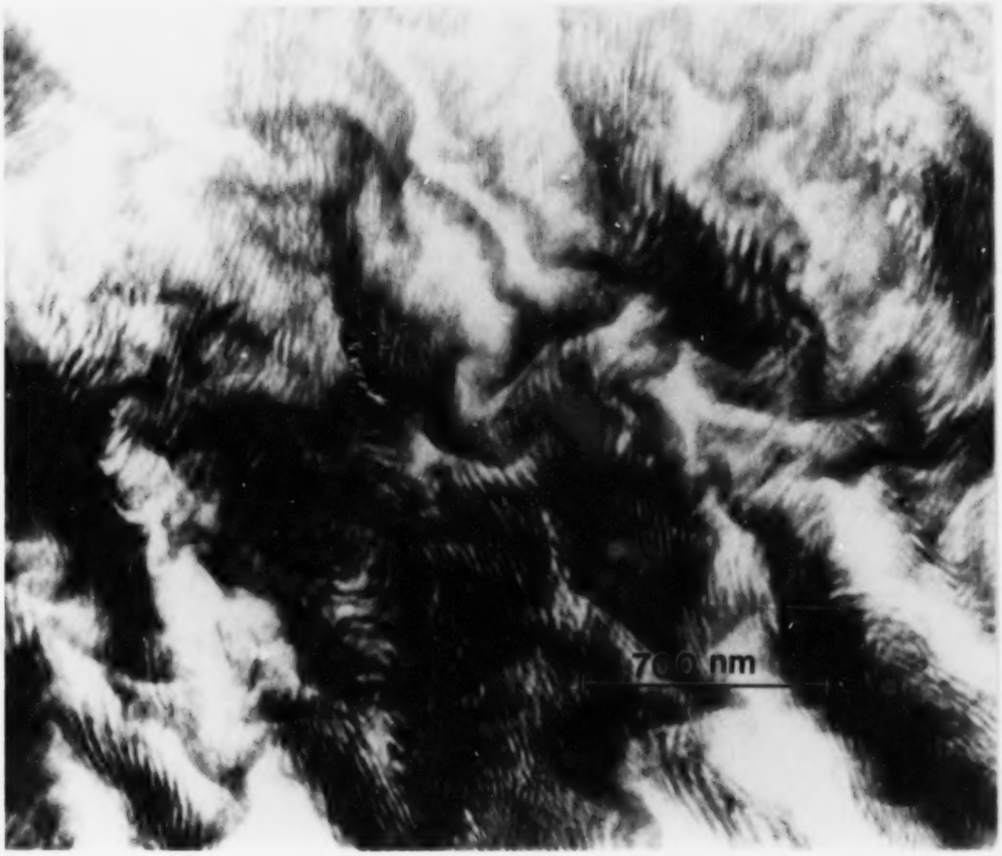
700 nm

continuous butadiene lamella into long cylinders of butadiene, and the ends of cylinders are represented by the central dark cores of butadiene in Figures 5.16a-16b. In some regions (marked by arrows in Fig 5.16b), light circles appear in dark cores, suggesting a cylindrical core of styrene surrounded by a butadiene annulus and then a styrene sheath. In these styrene-rich systems, there is no case found wherein the outermost layer is butadiene. If this alternating arrangement of concentric rings (or annuli) of styrene and butadiene continued to a large number of rings, we would have what is commonly termed as "onion ring" or "alternating concentric shell" morphology [64, 55] when dealing with spherical-domain microstructures. However, Figures 5.13-5.15 clearly show that spherical domains do not exist here, so the cylindrical morphology must prevail. This leads to describing the structures as "soda straws", with Fig. 5.15 being the side view of the assembly of straws.

Macrophase separation is clearly evident at 44.5% addition of PS13. Figure 5.17 shows a localized lamellar morphology within regions of approximately 50/50 average composition, as well as the presence of unstained areas due to macrophase separated hPS. Thus, Fig. 5.17 indicates another transition (from mesophase to macrophase separation). Within the ordered 50/50 macrophases, the composition as well as the lamellar thickness indicate these to be pure or nearly-pure SBS phases.

The last blend in this series has 60% PS13. Lamellar morphology has completely vanished as shown in Figure 5.18 which is a low-magnification micrograph. The initial impression is of totally chaotic microstructure, but closer examination shows this not to be so. What is seen as debris consists of irregular large bodies set in a medium of regular, but imperfect lattice structure morphology. Lamella seems to be absent, but there is a background pattern of styrene domains dispersed in orderly fashion in a continuous butadiene matrix; this appears to support large-scale domains of styrene-rich macrophases. At high magnification (Figure 5.19) the orderly background can be observed in greater detail. Figure 5.20 shows one of the many macrophase-separated lobes of hPS. Block copolymer, identified by the black striations, has been trapped in this styrene-rich region, with styrene end blocks anchored in hPS. The copolymer has preserved its lamellar

Figure 5.18 Low magnification electron micrograph of 60%hPS blend showing irregular lattice copolymer-rich phase and big blobs of hPS with trapped copolymer.

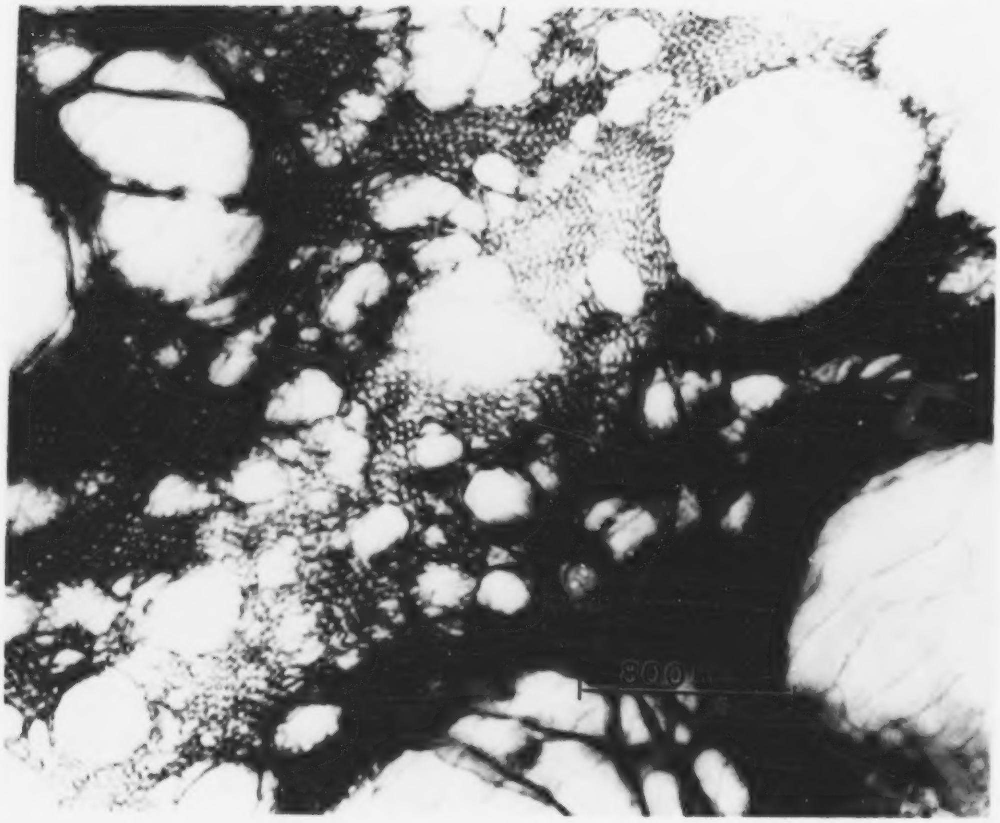

800

Figure 5.19 High magnification micrograph of copolymer-rich phase showing irregular lattice arrangement in a greater detail.

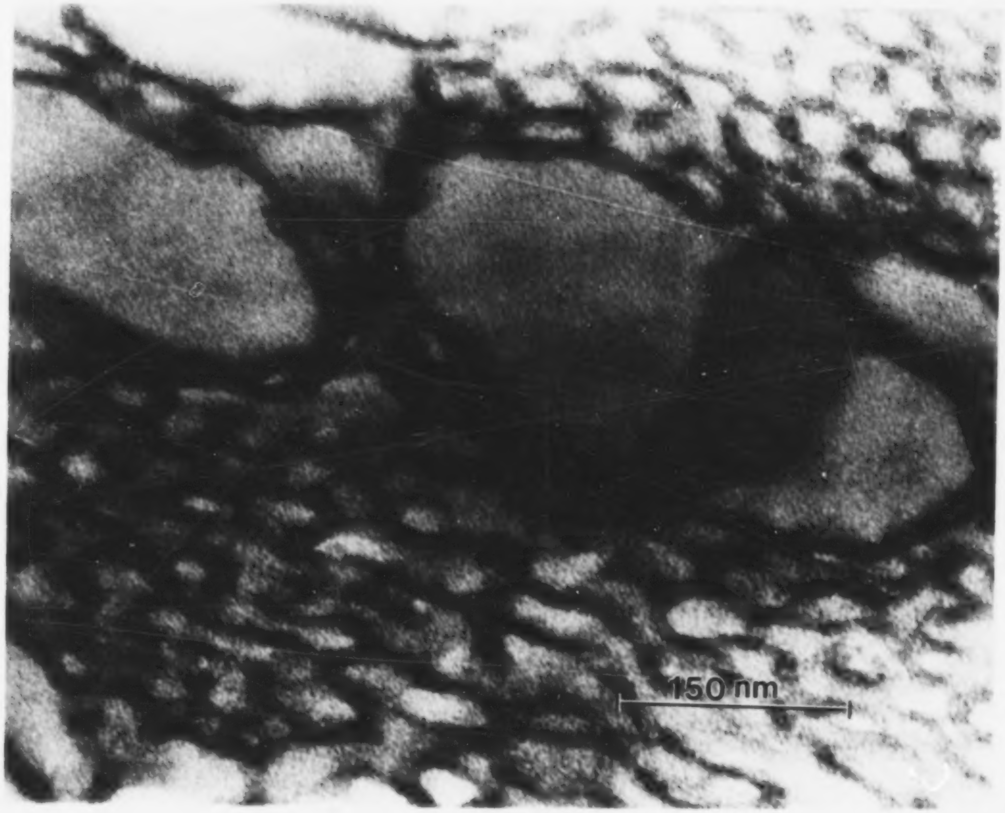
150 nm

Figure 5.20 High magnification micrograph of hPS-rich phase. Big blobs of hPS have in them trapped copolymer seen as ribbons of butadiene running parallel to each other.

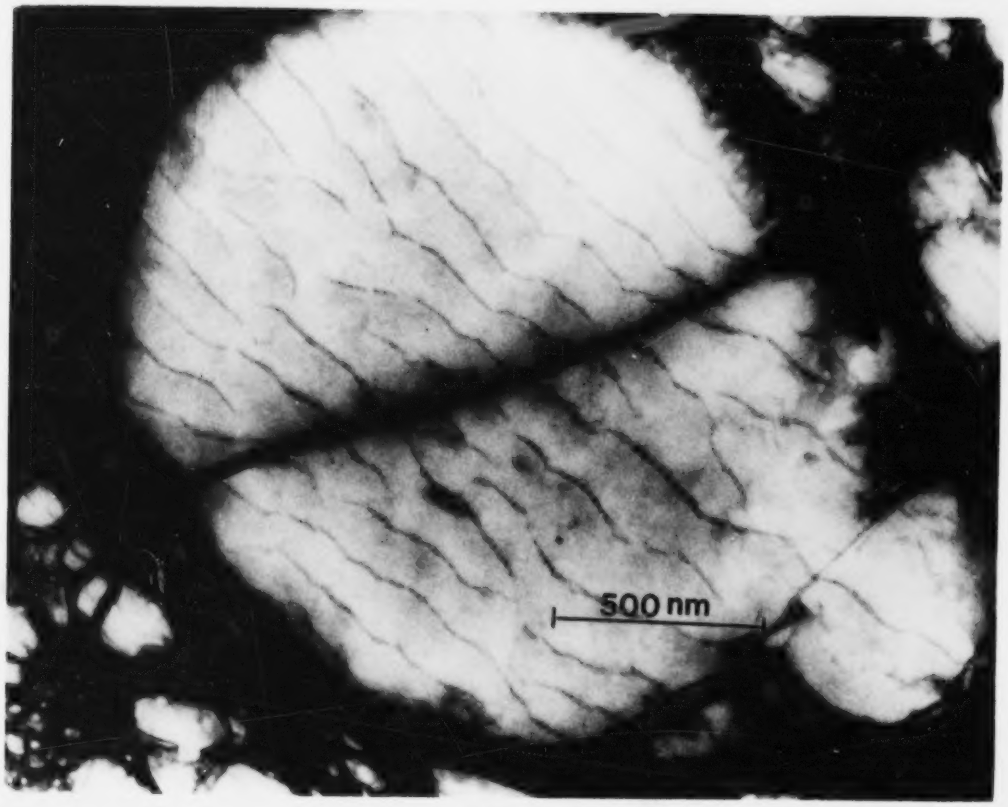
500 nm

domain structure, as indicated by the continuous butadiene ribbons running all through these styrene-rich domains. These ribbons run almost parallel to each other, as might be expected if the macrophases are the end result of packing hPS between SBS lamella. The PS macrophase is almost spherical, but is fractured almost perfectly in half with a planar cleavage at an angle of roughly 45^0 to the butadiene striations. Indeed, all the styrene macrophases appear to form as spheres and then fracture along planes to produce hemispheres (Figure 5.20, where two sizes of these can be seen) or other sections of spheres (Figure 5.18).

5.2.2 Solution Blends with Block Copolymer Molecular Weight Equal to Added hPS

In another series of blends, where higher molecular weight homopolymer (PS65) was used, no distinguishable microstructure was found for the 4.6% and 8.8% addition of block copolymer in matrix homopolystyrene. Thus we presume that the SBS was dissolved in the hPS. At 16% SBS, (Figure 5.21) the morphology is in a state of disorder, signaling macrophase separation but with the SBS-containing phase still not concentrated enough to achieve its own microphase separation.

The last blend in this series of four blends, where 32.6% SBS was added to hPS, the blend exhibited a dispersed grainy microstructure (Figure 5.22) of uncertain origin and micrograin size of about 5 nm. The latter size scale is consistent with a colloidal dispersion of microphase-separated SBS molecules, with the colloidal particles not aggregating. Another micrograph (Figure 5.23) showed lamellar microstructure in localized regions. Lamellar thickness measurements were identical to pure SBS block copolymer used in this blend, indicating complete macrophase separation (i.e., no hPS entrained between lamella). Irregular shaped dark-white regions shown by arrows look like some contamination at a first glance. However, close examination indicate microphase separation of SBS in the presence of hPS, where butadiene core is surrounded by styrene on all sides.

Figure 5.21 TEM micrograph of 16%SBS blend. No ordered structure is seen.

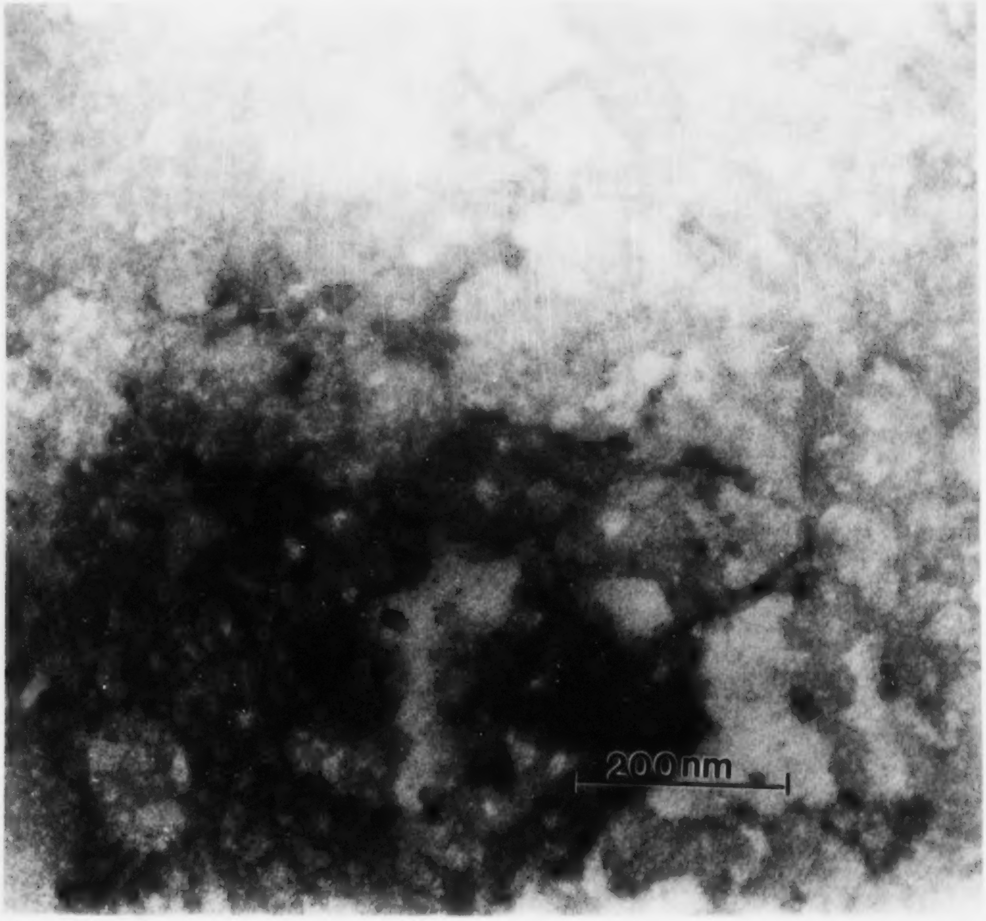
200 nm

Figure 5.22 Electron micrograph of 32%SBS blend. Dispersed grainy microstructure is seen.

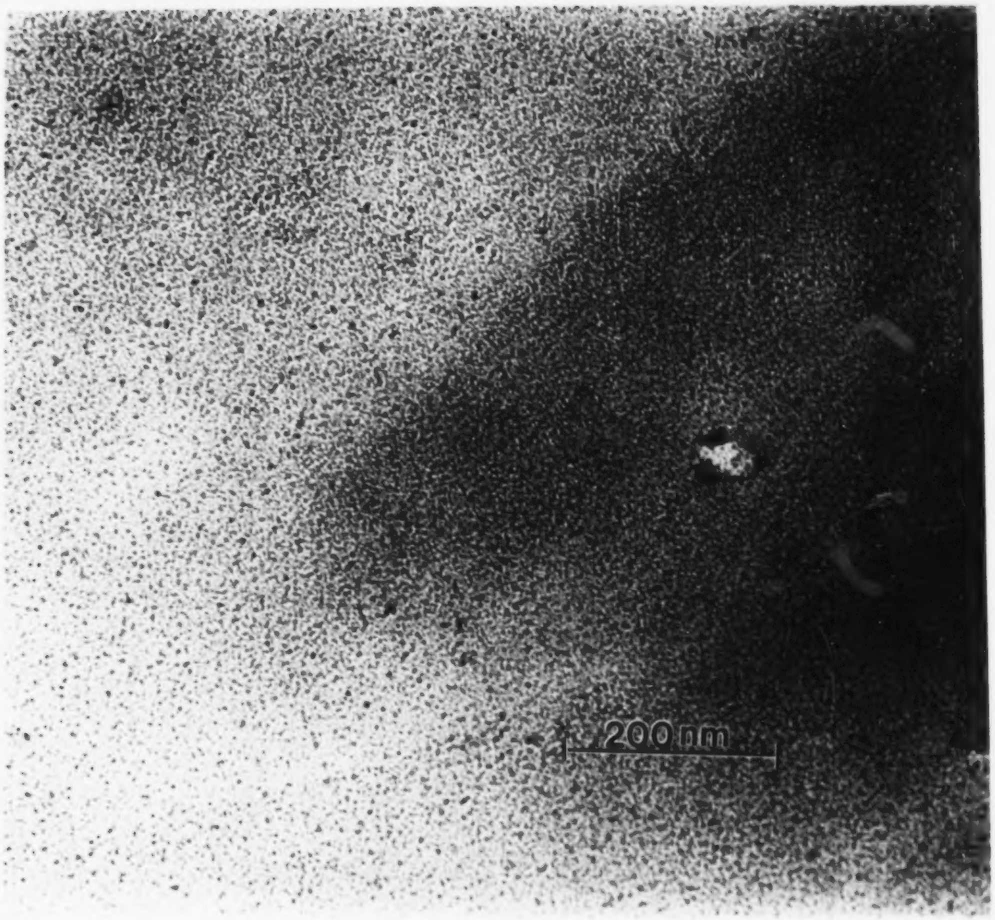
200 nm

Figure 5.23 TEM micrograph of 32%SBS blend showing macrophase separated block copolymer forming lamellar morphology upon microphase separation. Lamellar thickness was found to be equal to that of pure copolymer indicating complete macrophase separation between hPS and copolymer.

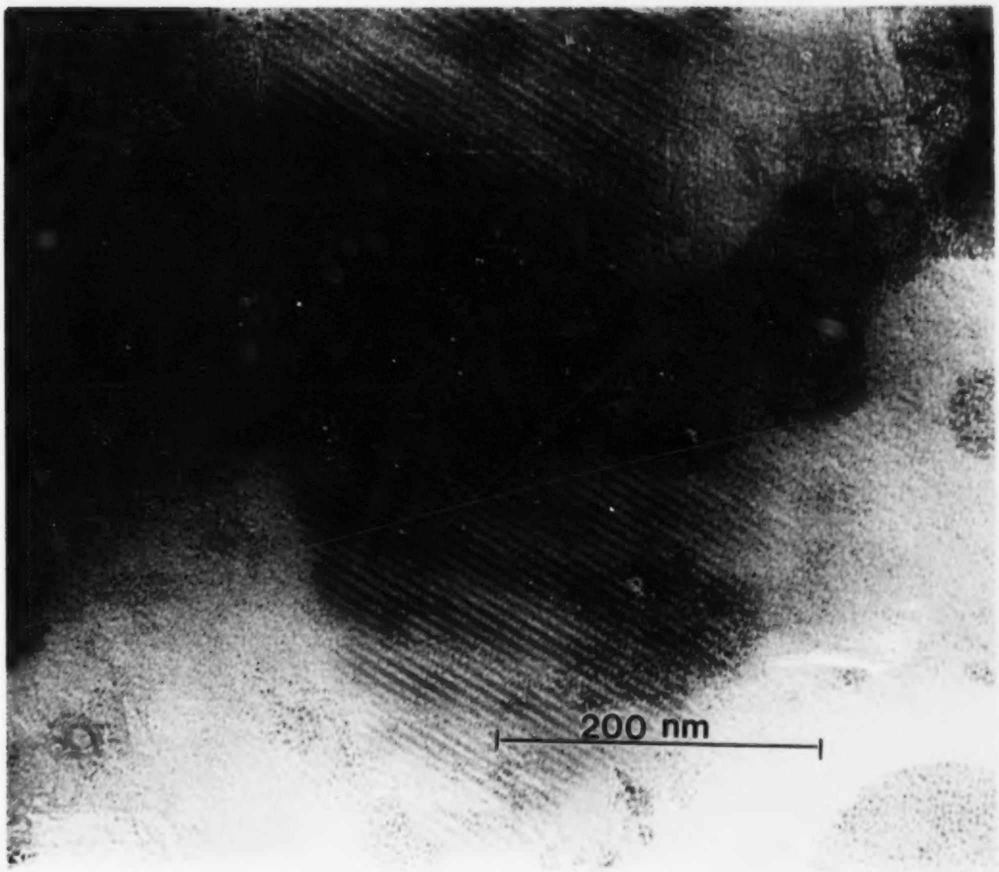
200 nm

5.3 Microdomain Spacings in Copolymer/Homopolymer Blends

Since lamellar morphology prevailed in the pure block copolymer (S129), measurements of microdomain spacings were easy. Domain repeat distance of ~10 nm and individual domains of ~5 nm each for both styrene and butadiene phases with long range order of lamella were observed. Depending on the angle of cut through the domains, morphological spacings could get exaggerated, but they will never be underestimated.

No significant variation in microdomain spacings was observed for 4% PS blend in comparison to pure copolymer, however, further addition of PS (8.5%. 18%, 37%) up to 37% increased the thickness of styrene domain. In a given blend, the increase in domain thickness was found to be nonuniform and average increment in thickness of the styrene domain increased with increasing PS in all three blends. The variation in the ratios of thickness of styrene lamella to that of butadiene lamella (T_S/T_B) allows us to compare this swelling of styrene domains in a consistent manner. There is no apparent change in this ratio for the 4% PS blend from pure copolymer. As more hPS is added, this ratio becomes 1.2 (8% PS), and then jumps to 2.54 (18% PS). It seems that the maximum limit for the accommodation of hPS into the styrene block domain reached its limit around 18% hPS. In 18% hPS blend, morphology observed was a lamellar morphology but some areas were excessively swollen with hPS which would qualify as pools of macrophase separated hPS. This could be supported by the fact that T_S/T_B ratio in 37%hPS blend (~2.55) was identical to that of 18%hPS blend. We do not like to emphasize the absolute values of these T_S/T_B ratios, but these ratios are been of help in deciding the saturation limit for added hPS in styrene block domains. Above this limit (T_S/T_B ~2.55), additional hPS could no longer be accommodated into the styrene domain and in finding its low energy state the system fell into soda straw morphology.

Nearly pure macrophases were formed in 44%hPS blend and ratio T_S/T_B returned to ~1.0. Microphase separated copolymer had lamellar morphology with short range order and trapped hPS pools in copolymer -rich phases.

Lamellar morphology was completely dismantled in 60%hPS blend (Figure 5.18) and still no pure copolymer (Figure 5.19) and pure homopolymer (Figure 5.20) phases were found as in 16%SBS blend (Figure 5.23).

In another series no distinguishable structures were found up to 16% SBS addition in high molecular weight hPS. At 32%SBS addition, complete macrophase separation was observed and microdomain dimensions of copolymer in the macrophase separated blend reverted to those of pure copolymer (Figure 5.23) as would be the case for complete macrophase separation. This demonstrated that virtually all of the high molecular weight hPS was excluded from the microdomains in the blend.

CHAPTER 6

DIFFERENTIAL SCANNING CALORIMETRY

6.1 Introduction to Differential Scanning Calorimetry

The glass transition temperature (T_g) is the temperature at which an amorphous glassy solid becomes rubbery when heated. The glass transition is accompanied by a change in the heat capacity of the sample. In differential scanning calorimetry (DSC), this change (change in heat capacity) is observed as a change in the baseline. The another transition is the separation temperature T_S above which copolymer is in disordered state. This can also be measured by DSC and is observed as a change in the baseline.

The glass transition temperatures of blends of SBS triblock copolymer and homopolystyrenes were measured by DSC. The calibration of DSC was carried out using Indium at the beginning of the experiments and no additional calibration was done for different heating rates (5-10^{0}C/min) used in this study. All polymer samples weighed between 5-20 mg when packed and pressed in the non-hermetic sample pan.

All the solution-blended mixtures (using dipentene as a solvent) of block copolymer and homopolystyrene as well as pure copolymer used in DSC have gone through a process history given in chapter 4 (section 4.1.3), with evaporation of solvent and annealing of samples as described in Table 4.2. Unless specifically stated, fresh samples were used for all DSC experiments.

All the DSC runs reported in this chapter were carried out in both the presence and the absence of a nitrogen stream (nitrogen stream in the sample chamber of DSC creates an inert atmosphere that surrounds sample pan) and the results were identical.

6.2 DSC Scans for Pure SBS Triblock Copolymer (S129) and Homopolymers

Glass transition temperatures were measured for block copolymer (Dow Vector 4461-D, Dow Chemical USA, LA) both in (a) as-received state from the company and (b) as-cast from dipentene solvent. As-received sample was in the form of small rubbery chunks whereas sample obtained after evaporating dipentene was in the form of a thin circular film. Two scanning rates were used (5^0C/min and 10^0C/min). Thin film samples were cooled to -140^0C, held at this temperture for a minute and then heated at scanning rates of (5^0C and 10^0C) per minute to 300^0C. Figure 6.1 shows DSC scans and Table 6.1 summarizes the results.

For as-received SBS (S129) the glass transition temperature corresponding to the butadiene microphase observed by DSC at scanning speeds of 5^0C/min and 10^0C/min was a steep transition at -90.0^0C. On the other hand, for the SBS (S129) films, T_g^B increased and became scan rate dependent: T_g^B = -84.64^0C at 10^0C/min and T_g^B = -88.56^0C at 5^0C/min. Styrene phase glass transition was a broad transition with hysteresis for both as-received and as-cast SBS copolymer and, higher values were obtained at 10^0C/min (68.0^0C for as-received and 70.0^0C for as-cast) in comparison to values obtained at 5^0C/min (65.15^0C for as-received and 65.37^0C for as-cast). Unexpected exothermic peaks were observed in case of as-received SBS at 226.48^0C (10^0C/min) and at 209.52 (5^0C/min). These peaks were not observed in dipentene-cast SBS copolymer. Also unexpected was the appearance of an intermediate glass transition observed in dipentene-cast SBS: at -22^0C when the scan rate was 5^0C/min, and -13.2^0C with 10^0C/min. The transition strength was also rate-dependent, being stronger at the slower rate.

Glass transition temperatures obtained for the block copolymer (dipentene-cast) butadiene and styrene phases also deviated from those of polybutadiene and polystyrene homopolymers as shown in Figure 6.2. Glass transition temperature of hPB is ~ -91.11^0C and of hPS is ~ 96.77^0C, as contrasted with -85^0-88^0 and +65^0-70^0C, respectively, for the block copolymer.

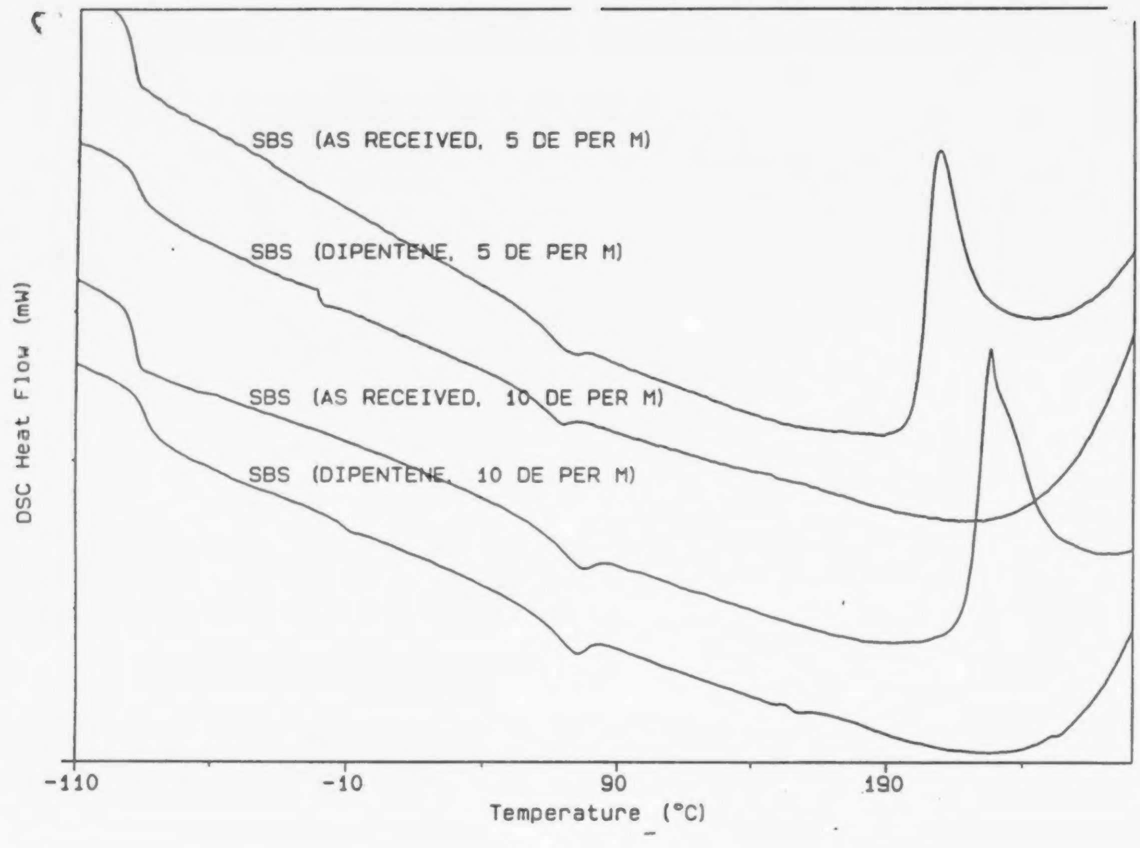

Figure 6.1 DSC scans of as-received and as-cast SBS block copolymer (scanning rates 5^0C/min and 10^0C/min). DSC scans are moved in the vertical direction in this and rest of the figures in this chapter for the sake of clarity.

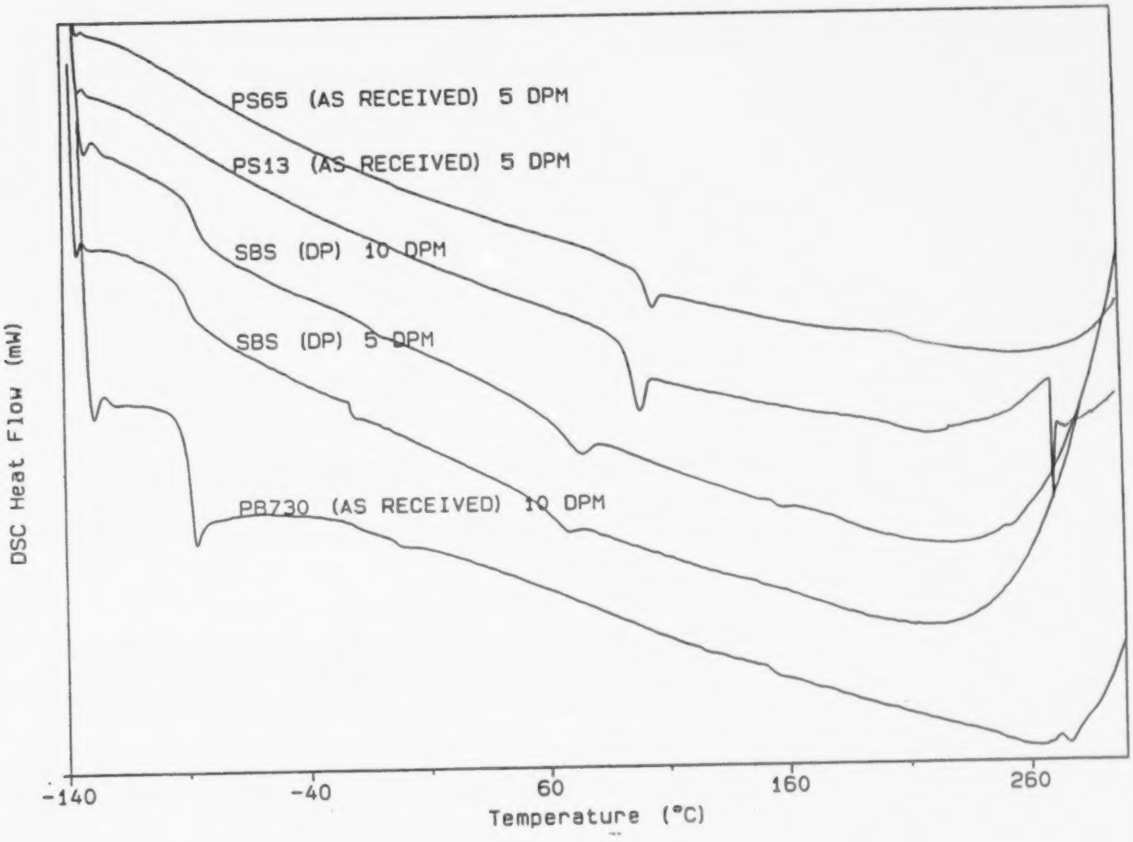

Figure 6.2 DSC scans for pure polystyrenes (PS13 and PS65) and pure butadiene (S165). Lowered T_g of styrene phase of block copolymer is evident when compared with the Tg of pure polystyrene (PS13) of equal molecular weight.

Table 6.1 Tabulation of data from Figures 6.1-2

Sample	Process history	Scanning speed	T_g^B ^{0}C	T_g^S ^{0}C	T_g' ^{0}C	T_{peak} ^{0}C	T_{other} ^{0}C
SBS[z]	As received	5 dpm	-90.5	65.2	—	209.5	—
SBS	As received	10 dpm	-90.0	68.0	—	226.48	—
SBS	Dipentene	5 dpm	-88.6	65.4	-22.0	—	—
SBS	Dipentene	10 dpm	-84.6	70.0	13.2	—	—
PS[y]13	As received	5 ^{0}C/min	—	96.8	—	—	208.8
PS65	As received	5 ^{0}C/min	—	102.3	—	—	209.0
PB350	As received	10 ^{0}C/min	-91.1	—	—	—	—

[z]

[y] polystyrene

— not observed

6.3 DSC Scans (For Solution Blends with $M_S = M_{PS} = 13,000$)

There were six blends made in this series (4%, 8%, 18%, 37%, 44% and 60% homopolystyrene) and pure copolymer as a reference material.

6.3.1 Results of Three Heating Cycles

These blends were passed through three heating cycles at a scanning rate of 10^{0}C/min and all the scans were recorded.

The samples were cooled to -140^{0}C, held isothermal for two minutes at this temperature and heated at scanning rate of 10^{0}C/min up to 150^{0}C and then cooled down to -140^{0}C at same scanning rate. This process was repeated two more times giving a total of three heating cycles. In the last heating cycle, samples were heated up to 350^{0}C.

Figures 6.3-6.5 show the heating scans for first, second and third cycles respectively and the results are summarized in Table 6.2.

Considering the thermal behavior of these blends, they could be classified into three sets. The first set would include copolymer and blends with small addition of hPS (i.e., 4%, 8% and 18%hPS), whereas the second set would include blends with intermediate proportions of hPS (i.e. 37% and 44%hPS) and the last one consists of the blend with 60%hPS.

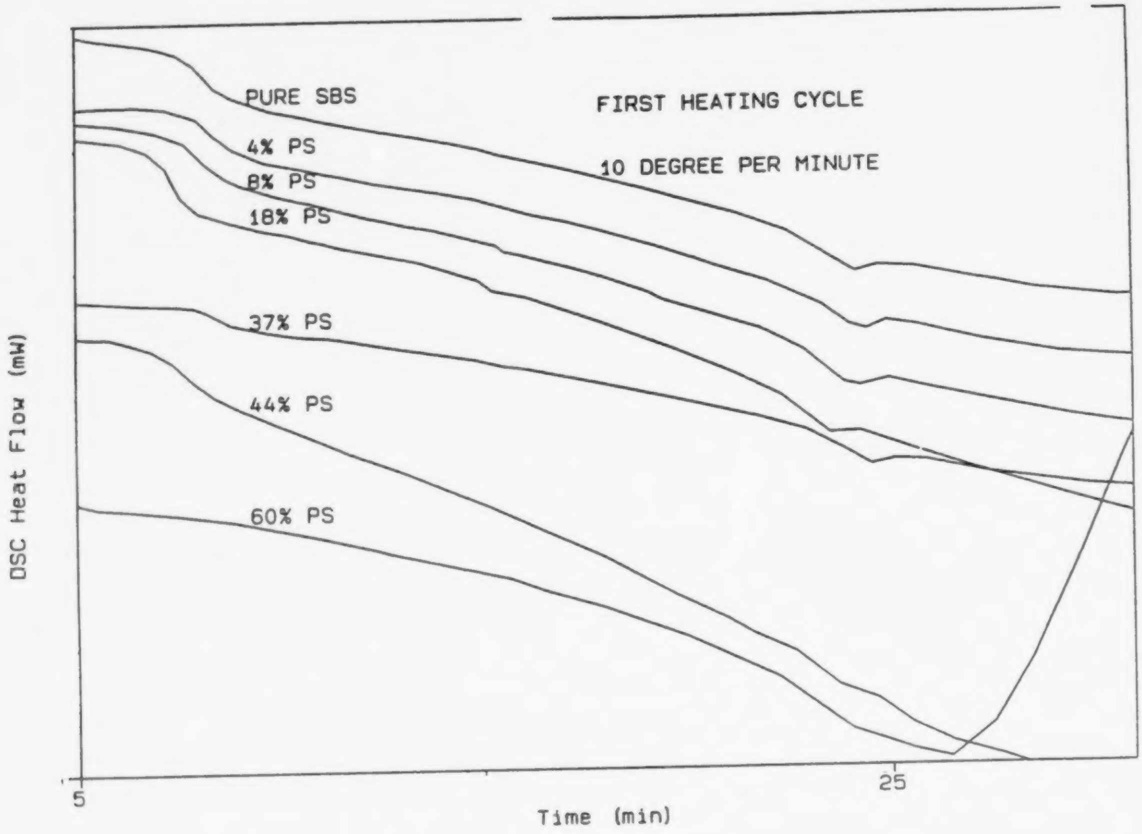

Figure 6.3 DSC scans for a series of blends where pure polystyrene (PS13) of equal molecular weigth to that of the styrene block of the copolymer was used in blending. Scanning rate was 10^0C/min. 1st heating cycle.

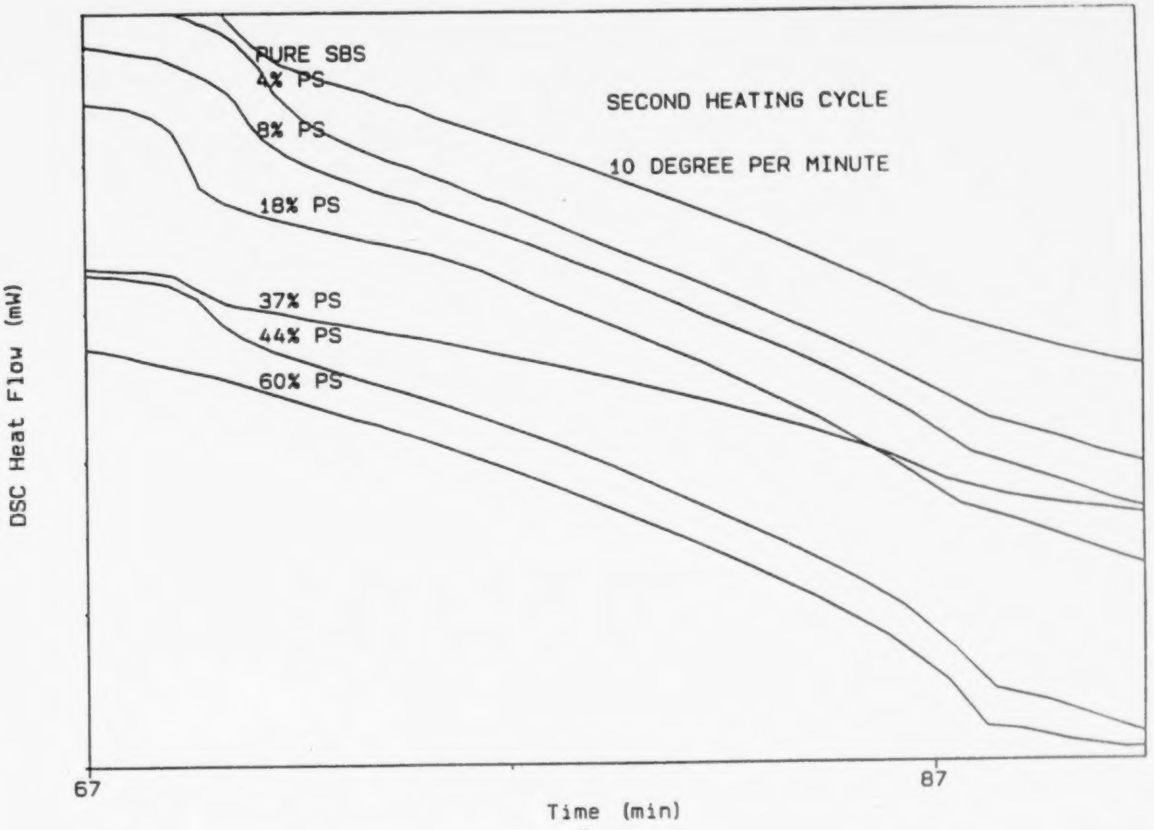

Figure 6.4 DSC scans of second heaing cyle for a blend series in Figure 6.3.

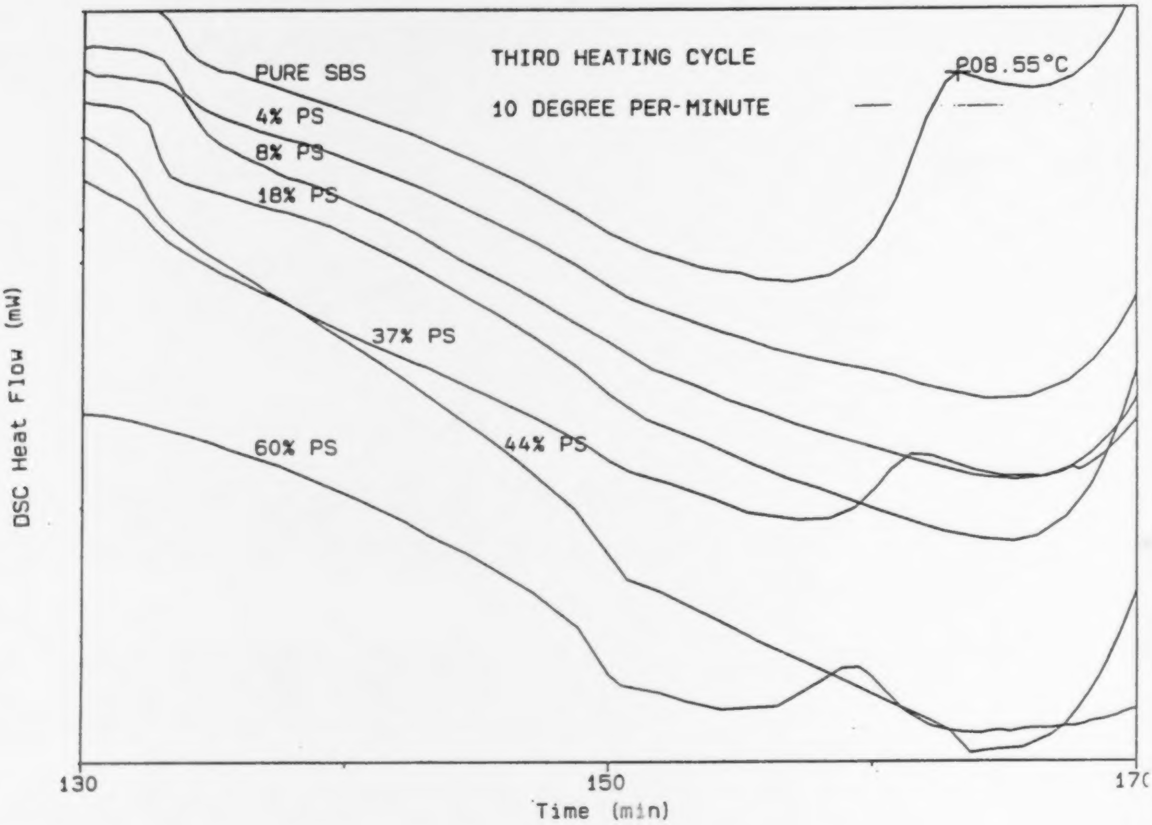

Figure 6.5 DSC scans of third and last heating cycle for the blend series in Figure 6.3.

Table 6.2 Tabulation of data from Figures 6.3-5

Sample	Run number	T_g^B °C	T_g^S °C	T_g^I °C	T_g' °C	T_{peak} °C	T_{other} °C
SBS[z]	1	-86.6	68.4	-20.9	—	—	—
	2	-85.9	70.0	—	—	—	—
	3	-87.3	70.4	—	—	210.5	—
4%PS[y]	1	-87.0	65.9	-14.18	31.5	—	—
	2	-86.3	75.0	—	29.0	—	—
	3	87.2	78.7	—	—	—	—
8%PS	1	-86.2	66.2	-12.5	24.52	—	—
	2	-85.0	73.9	—	—	—	—
	3	-87.1	78.5	—	—	—	—
18%PS	1	-88.2	66.7	-13.1	25.1	—	—
	3	-88.4	80.9	—	—	—	—
37%PS	1	-88.8	67.4	-18.1	—	—	—
		2	-89.6	86.8	—	—	—
	3	-85.8	83.0	—	—	—	204.8
44%PS	1	-83.7	91.3	—	34.4	—	52.8*
	2	-85.7	89.8	-26.8	—	—	—
	3	-84.5	90.3	—	—	—	—
60%PS	1	—	55.1	-14.2	—	—	—
	2	—	87.3	—	—	—	—
	3	—	86.7	—	—	179.8	—

---

[z]

[y] polystyrene

— not observed

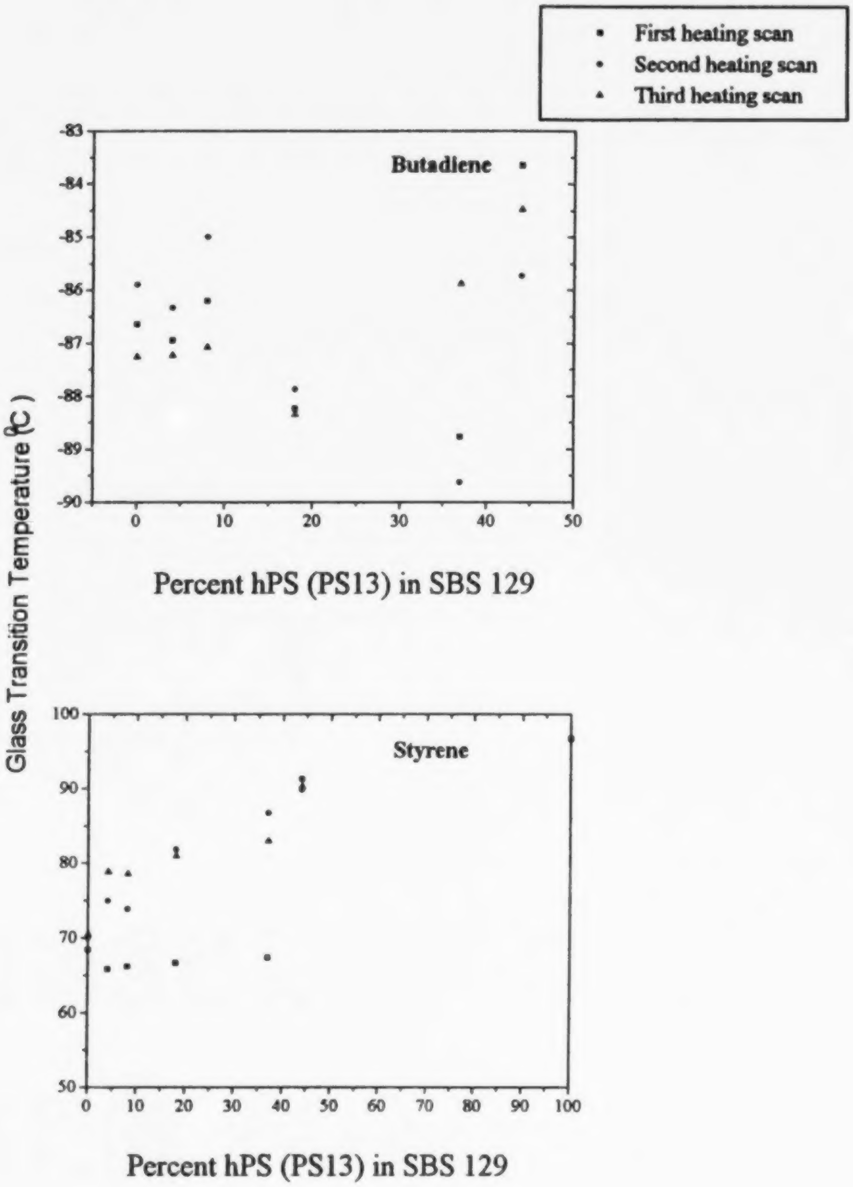

Figure 6.5-a,b Variation of Glass transition temperatures in cyclic thermal tests.

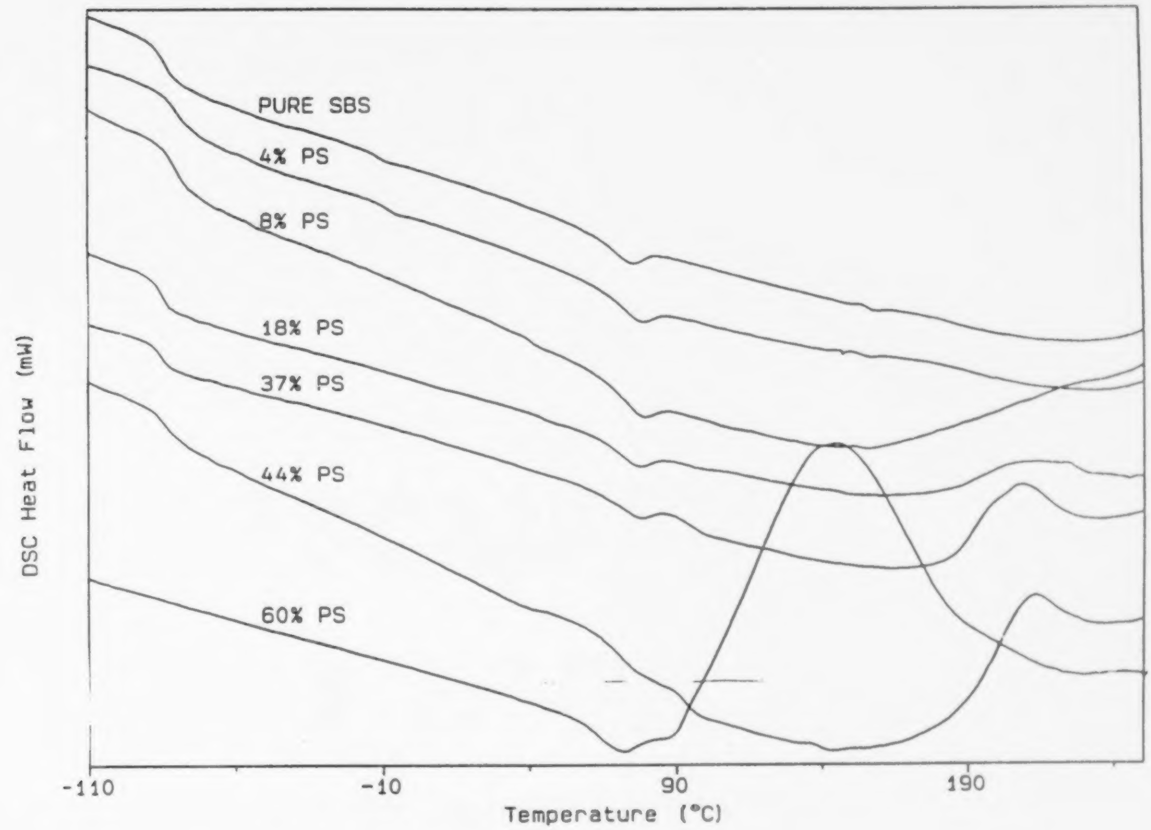

Figure 6.6 DSC scan of the blend series at 10^{0}C/min.

All blends and pure copolymer except 60%hPS blend showed glass transition corresponding to butadiene phase. Intermediate transitions were observed (in first heating cycle only) in pure copolymer and blends with 4%, 8%, 18% and 60% hPS.

In first set of blends (which included pure copolymer) value of T_g^B increased in the second heating cycle over the values obtained in the first heating cycle. However, T_g^B in the third heating cycle showed lowest values, implying purer butadiene phases had been produced by the thermal cycling through the third cycle. The glass transition corresponding to the styrene phase (T_g^S)obseved in these blends showed higher values with subsequent heating cycles. This is consistent with the simultaneous decrease of T_g^B (by the 3rd cycle), if phase purification is occuring. Also the intermediate transition was observed in all blends including pure copolymer in this set.

The second set includes blends with 37% and 44%hPS. No intermediate transition was observed in these blends. The glass transition corresponding to the butadiene phase showed lower values in the second heating cycle in comparison to those obtained with first heating cycle. The third heating cycle showed higher values (and thus less pure butadiene phases) than those of second heatng cycle. The butadiene glass transition obtained in the third heating cycle was the lowest for 37%hPS, whereas for 44%hPS blend, the lowest T_g^B came after the first cycle. The blend with 44%hPS showed more or less constant value of T_g^S in all three heating cycles. The blend with 44%hPS showed the lowest value for styrene phase glass transition in the first heating cycle and the highest value in the second heating cycle and the values of second and third heating cycles are comparable and distinctly higher than that of first heaing cycle.

The blend with 60%hPS showed an intermdiate transition around -14^{0}C and a much lower (55^{0}C) styrene transition in the first heating cycle. The second and the third heating cycles showed much higher and comparable values (87.31^{0}C and 86.73^{0}C) of styrene glass transition

An exothermic peak was observed for the blend with 60% hPS, beginning at ~ 125^{0}C and went all the way to 150^{0}C where the sample was held isothermal for two minutes followed by cooling to -140^{0}C. This exothermic peak would continue to develop at higher temperature (above 150^{0}C) if sample is heated above this temperature.

Figure 6.4 shows the second heating cycle. The intermediate transitions observed in the first scans for the blends with 8% and 18% hPS were not observed in the second scan (although a set of much weaker peaks can be discerned at a lower temperature range). Also, hysteresis observed in T_g^S in the cases of blends with 4%, 8%, 18%, 37% hPS as well as in the case of pure copolymer in the first heating cycle was not observed in this second heating cycle. On the other hand, styrene glass transitions for the cases of 44% and 60% hPS blends became sharper in comparison to those from the first heating cycle. Their slopes also came into alignment with each other and with those of 0-18% hPS; 37% remained the only one out of line.

Figure 6.5 shows the third and last heating cycle, in which sample was heated up to 350^{0}C, unlike in first and second heating cycles where sample was heated only up to 150^{0}C. Glass transition corresponding to the styrene phase was least strong in this third heating cycle for blends with 4%, 8%, 18% and 37% hPS and pure block copolymer as well. Blends with 44% and 60% hPS showed distinct glass transition regimes corresponding to styrene regions, as expected for systems heavily loaded with PS. Exothermic peaks were observed in the range of 170-210 ^{0}C for the blends with 37% and 60% hPS and pure copolymer. Exothermic peaks were also found in "as-received" pure copolymer samples (Figure 6.1) in the same temperature range. The trend suggests that the temperature of the highest point of exothermic peak decreased with increase in hPS composition of the blends. Figure 6.5 shows, for the first time, that the 37% sample (in most scans totally different from other compositons) can resemble any of the others (here, 60%).

6.3.2 Scanning to 270^{0}C at Rate of 10^{0}C/min.

The samples were cooled to -140^{0}C, held isothermal for two minutes at this temperature and then heated at a scanning rate of 10^{0}C/min up to 270^{0}C. The scanning procedure here was identical (up to 150^{0}C) to the first heating cycle of section 6.3.1 (Figure 6.3).

Although absolute values of glass transitions found in this series did not match with those obtained from first heating cycle of previous DSC experiment (6.3.1), the overall trend was in good agreement with the exception of the styrene glass transition for 44%hPS (70.75^{0}C and 91.32^{0}C respectively) and intermediate glass transition (-13.21^{0}C and -20.93^{0}C respectively) in pure block copolymer. DSC scans are shown in Figure 6.6 and the results are summarized in Table 6.3.

The high temperature exothermic peaks were observed for all samples except pure copolymer and the blend with 4% hPS. The temperature of the peak maximum (T_{peak}) decreased with increase in hPS composition of blends, giving the lowest value of ~ 144^{0}C for the blend with 60% hPS.

Table 6.3 Tabulation of data from Figure 6.6

Sample	T_g^B ^{0}C	T_g^S ^{0}C	T_g^I ^{0}C	T_g' ^{0}C	T_{peak} ^{0}C	T_{other} ^{0}C
SBS^z	-84.6	69.6	-13.2	—	—	154.6
4%PS^y	-84.2	68.2	-11.8	—	—	142.6
8%PS	-84.0	68.4	—	37.1	228.3	146.3
18%PS	-86.8	70.3	—	42.6	211.4	144.8
37%PS	-87.3	63.7	—	—	205.8	—
44%PS	-84.9	70.8	—	92.0	213.8	138.7
60%PS	—	62.3	—	—	144.2	—

[z]

[y] polystyrene

— not observed

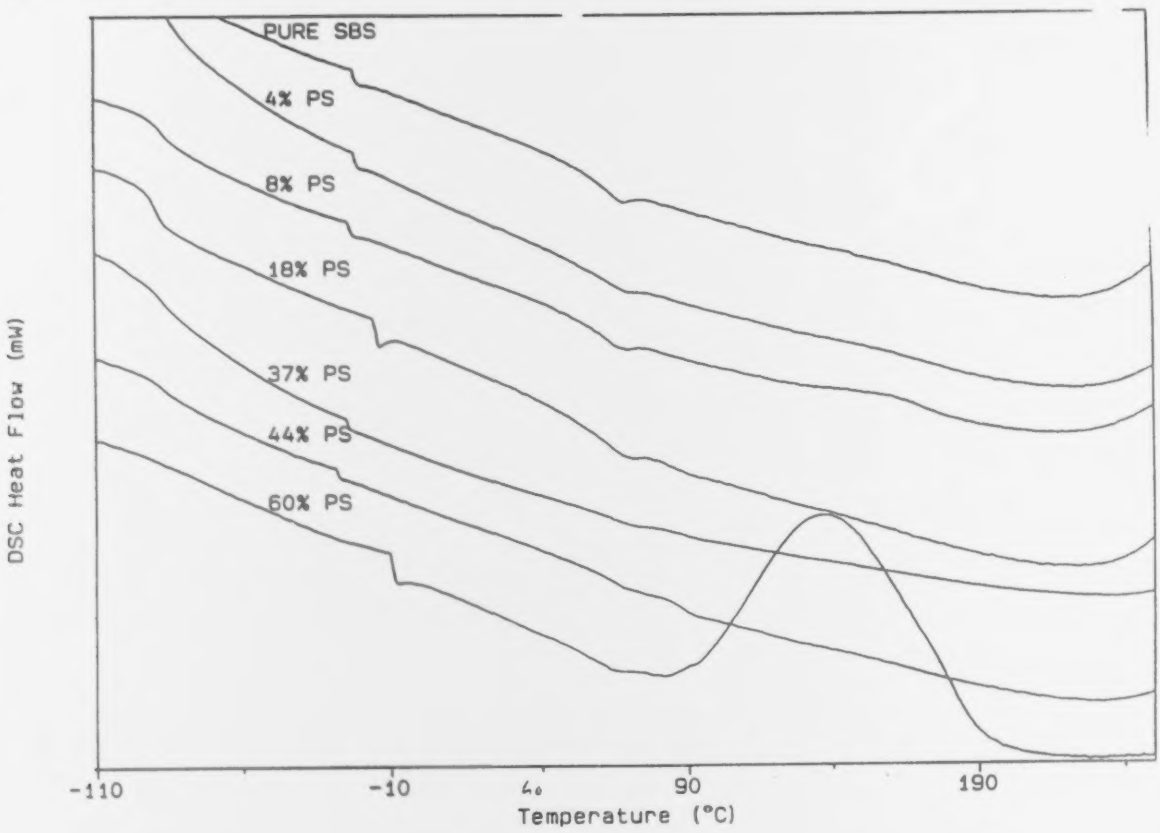

Figure 6.7 DSC scans for the blend series at scanning rate of 5°C/min.

6.3.3 Scanning to 270^0C at Rate of 5^0C/min.

The scanning procedure was the same as in section 6.3.2 except the scanning rate. DSC scans are shown in Figure 6.7 and the results are summarized in Table 6.4. General alignment and parallelism of the curves is far superior to the behavior exhibited in the 10^0C/min scans.

With the exception of the 60%hPS blend, butadiene glass transition was found in all blends as well as pure block copolymer. Styrene phase glass transition and intermediate glass transition were found in all blends and copolymer. The intermediate transitions were observed sharply for all samples between -30^0C to -10^0C. In the case of 60%hPS blend, styrene glass transition was at a much lower value (44.09^0C), and intermediate glass transition is at higher value (-10.19^0C) in comparison to those of other blends and copolymer. The exothermic peak was observed in two cases, the 60% hPS and the 8% hPS blend.

Scanning at 10^0C (Figure 6.6) failed to show intermediate transition for all the blends in this series, but showed exothermic peaks in most blends (except pure copolymer and 4%hPS blend). On the other hand scanning at 5^0C showed intermediate transitions in all blends but showed exothermic peaks in only two of them (8% and 60% hPS).

Table 6.4 Tabulation of data from Figure 6.7

Sample	T_g^B ^{0}C	T_g^S ^{0}C	T_g^I ^{0}C	T_g' ^{0}C	T_{peak} ^{0}C	T_{other} ^{0}C
SBS[z]	-88.6	65.4	-22.0	—	—	147.5*
4%PS[y]	-85.9	60.7	-23.5	—	—	—
8%PS	-87.1	62.7	-23.5	—	172.3	—
18%PS	-89.2	62.8	-14.9	—	—	—
37%PS	-88.2	62.0	-26.8	—	—	—
44%PS	-87.1	61.3	-28.0	87.5	—	—
60%PS	—	44.1	-10.2	—	136.7	—

[z]

[y] polystyrene

— not observed

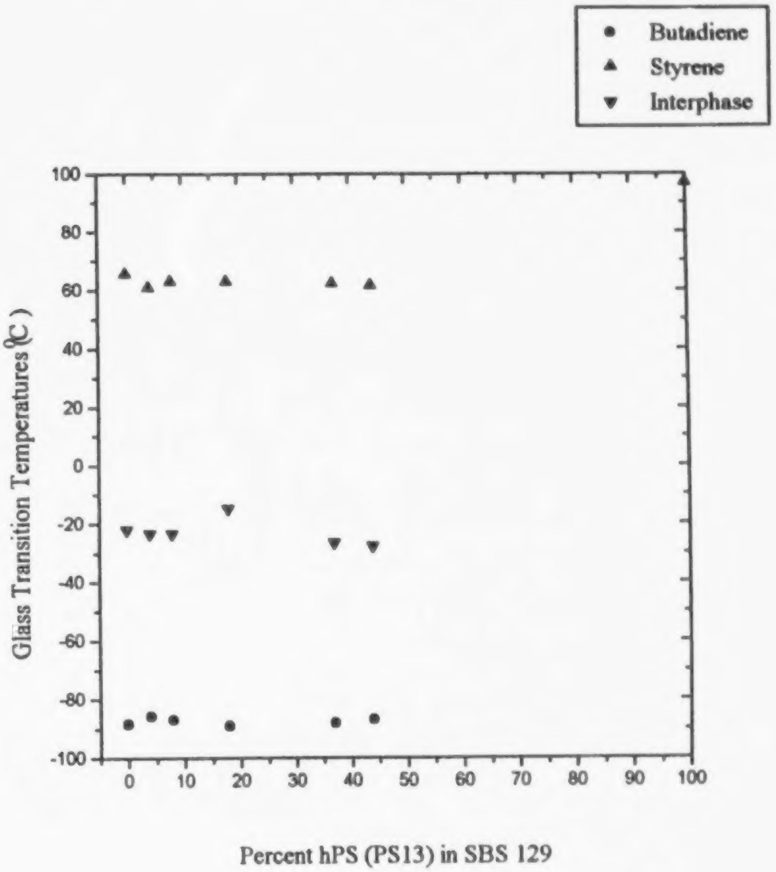

Figure 6.7-a Effect of PS addition on Glass transition temperatures in SBS-PS blends.

6.3.4 60% hPS Blend with Trace Amount of Solvent (Dipentene)

A sample of this blend was taken for investigation. The solvent (dipentene) was allowed to evaporate at 60^0C in vacuum for eight weeks and a sample was chosen for DSC analysis before the rest of the annealing and drying procedures were performed as in Table 4.2.

Sample was cooled to -140^0C, held isothermal at this temperature for two minutes and then heated up to 260^0C. It was held at this temperature for two minutes and then cooled down to ~-135^0C, and again heated up to 260^0C, and cooled down to 30^0C. Scanning rate was 10^0C/min throughout the experiment. DSC scan is shown in Figure 6.8 and results are summarized in Table 6.5.

In the first heating cycle, a weaker T_g^B was observed at -78.18^0C, a broad styrene glass transition at 95.84^0C, a strong intermediate transition at 4.67^0C as well as broad low peak over 170^0-210^0C were observed. In the second heating cycle, glass transitions for butadiene and styrene phases were observed at around -81.46^0C and 92.68^0C respectively and the higher peak was sharpened to the 180^0-200^0C range (and seen at a slightly lower temperature upon cooling). In the second cycle, a weaker transition was observed at 45.66^0C and the intermediate transition was not observed.

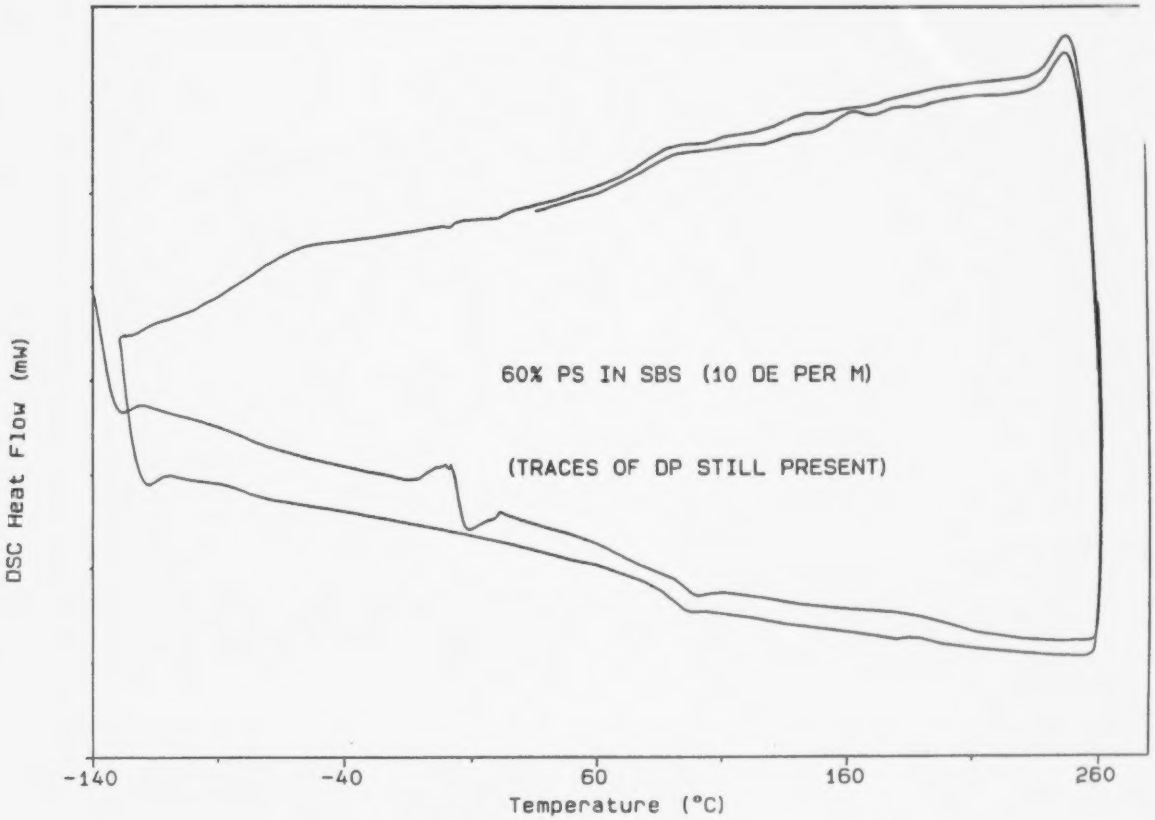

Figure 6.8 DSC scan for 60% hPS blend at scanning rate of 10^0C/min.

Table 6.5 Tabulation of data from Figure 6.8

Sample	Run Number	T_g^B ^{0}C	T_g^S ^{0}C	T_g^I ^{0}C	T_g' ^{0}C	T_{peak} ^{0}C
60%PS	1	-78.2	95.8	4.7	—	201.7
	2	-81.5	92.7	—	45.7	193.0

— not observed

6.4 DSC Scans (For Solution Blends With $M_{SBS} = M_{PS} \cong 62{,}000$)

The samples were cooled to -140^{0}C, held isothermal for two minutes at this temperature and heated up to 350^{0}C at the scanning rate of 10^{0}C/min. DSC scans are shown in Figure 6.9 and the results are summarized in Table 6.6.

Polymer material came out of the DSC sample pan at higher temperature in all blends studied in this series and as a result weird types of scans were observed above 240^{0}C. This peculiar phenomenon often occurs when material comes out of the sample pan, as observed by many other researchers in our laboratory.

The T_g^B was not observed in the blends of this series with the exception of 4%SBS blend. Except 4%SBS blend, all other blends showed two glass transitions corresponding to styrene region; 32%SBS blend showed the most distinct transitions and strength of glass transition corresponding to hPS decreased with decrease in copolymer composition showing only one transition with 4%SBS. The DSC scans for pure SBS and PS are for reference only.

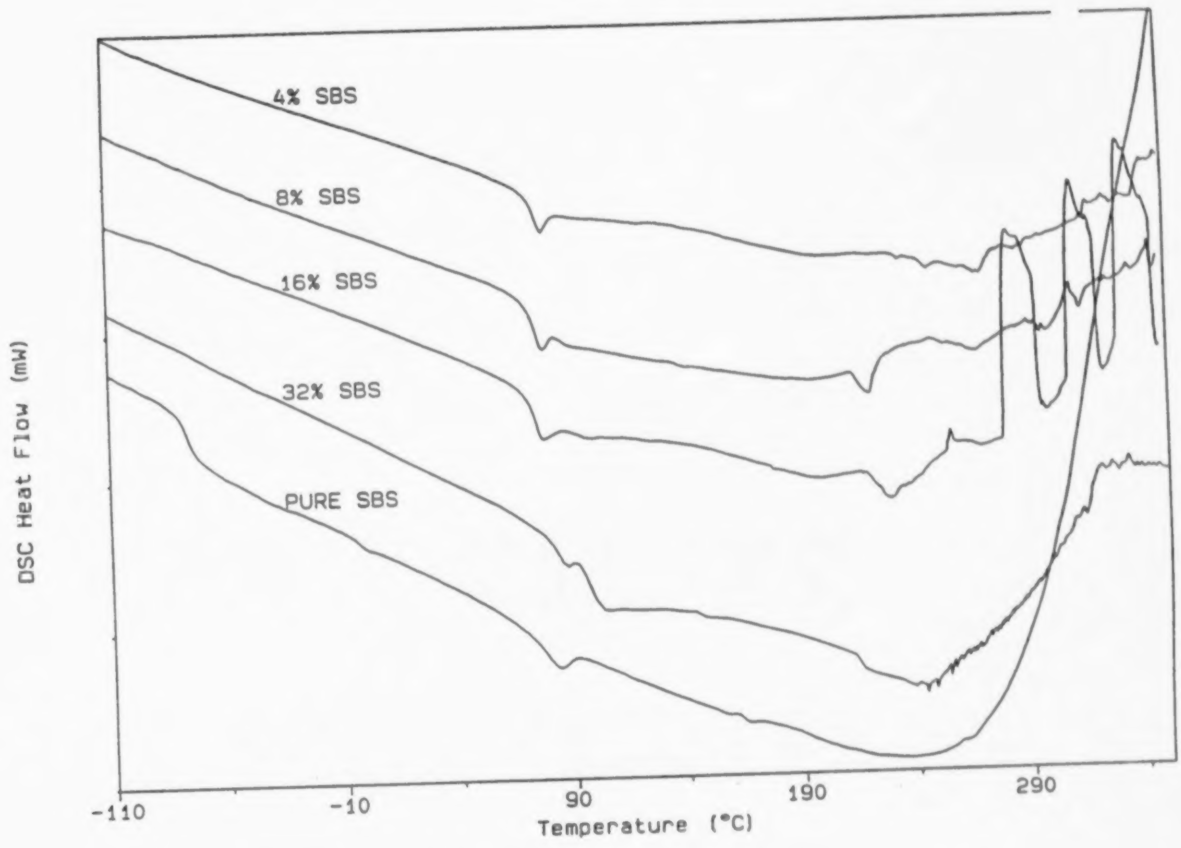

Figure 6.9 DSC scans of blends (second series) at scanning rate of 10^0C/min.

Table 6.6 Tabulation of data from Figure 6.9

Sample	T_g^B ^{0}C	T_g^S ^{0}C	T_g^I ^{0}C	$T_g^{'}$ ^{0}C	T_{other} ^{0}C
4%SBS	—	74.9	—	189.6	—
8%SBS	—	75.6	90.4	215.9	114.3
16%SBS	—	74.8	93.9	225.5	—
32%SBS	—	81.2	93.4	210.4	141

— Not observed

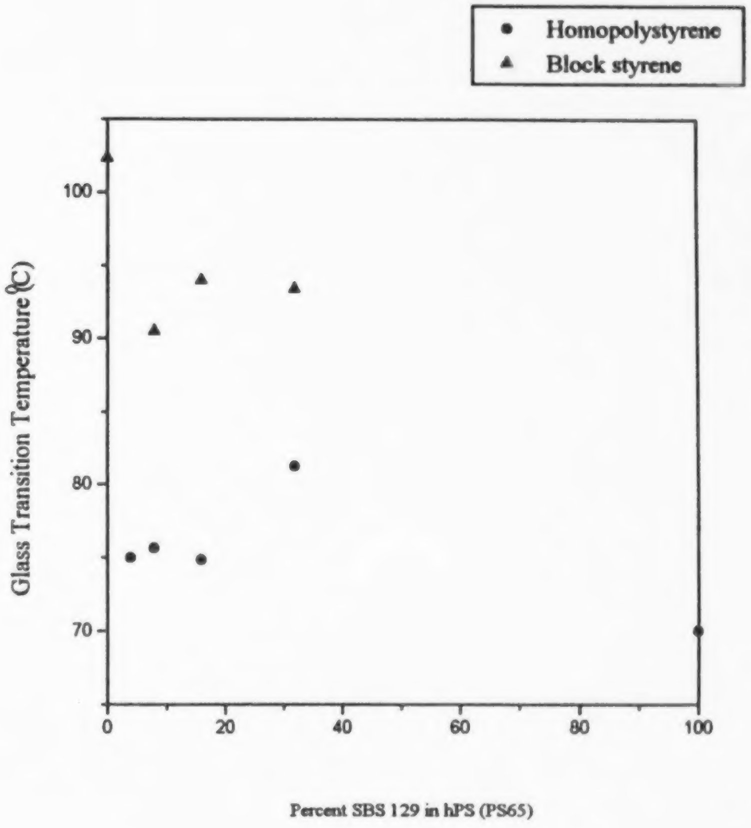

Figure 6.9-a Pertu~~r~~btions in Glass Transitions of homopolystyrene and block styrene upon SBS addition.

6.5 DSC Results: Effects of Scanning Rate and Solvent of Blending

Our DSC results indicated that scanning at different rates would give more information about the material. DSC scan of SBS copolymer (as-cast from solution using dipentene solvent) at scanning rate of 1^0C/min showed a broad butadiene glass transition and an expthermic peak at ~180^0C. Scanning at 5^0C/min and 10^0C/min showed three glass transitions corresponding to butadiene, styrene and an intermediate phases. Scanning at 10^0C/min showed additional transitions (e.g., exothermic peaks) which were not seen at lower scanning rates. DSC scans are shown in Figure 6.10.

SBS copolymer showed an intermediate glass transition when dipentene solvent was used in preparing as-cast films. No intermediate glass transition was observed for the same copolymer when, instead of dipentene, toluene was used as a solvent in preparation of as-cast films. DSC scans for SBS films prepared with both solvents are compared in Figure 6.11 and results are summarized in Table 6.7.

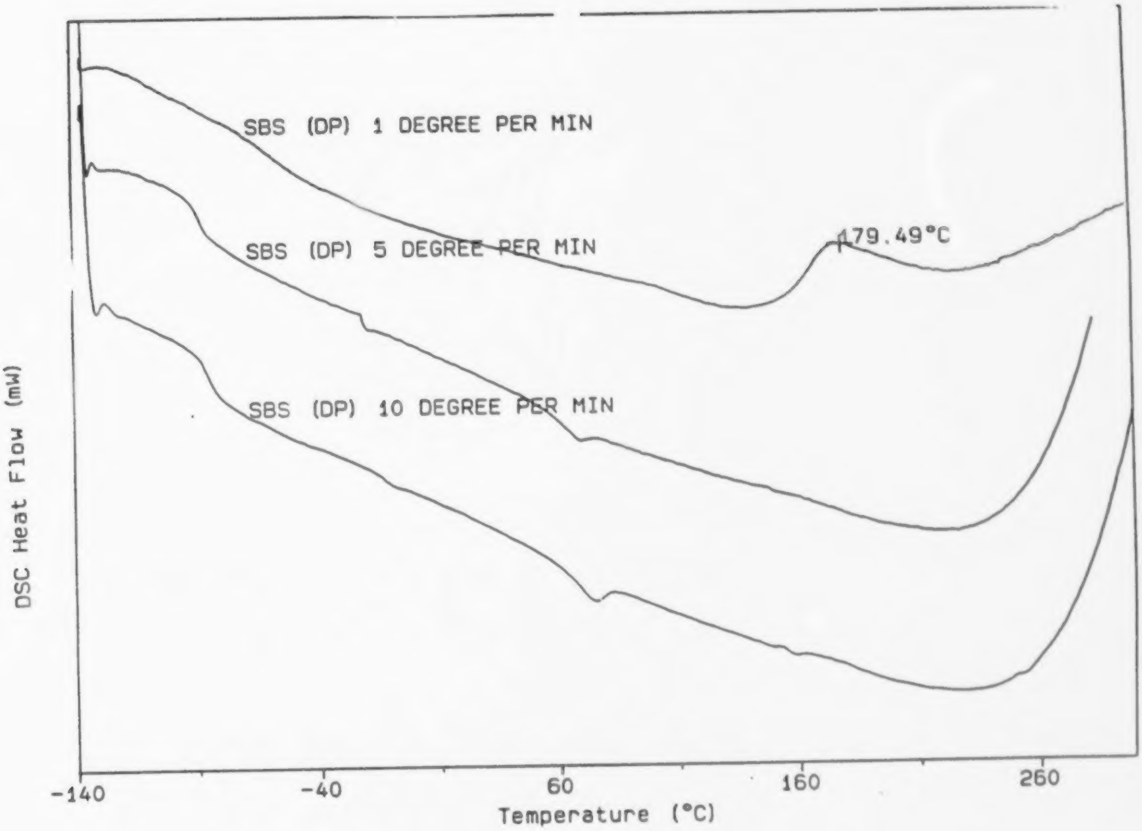

Figure 6.10 DSC scans of pure block copolymer (at scanning rates of 1, 5, 10 ^{0}C/min.).

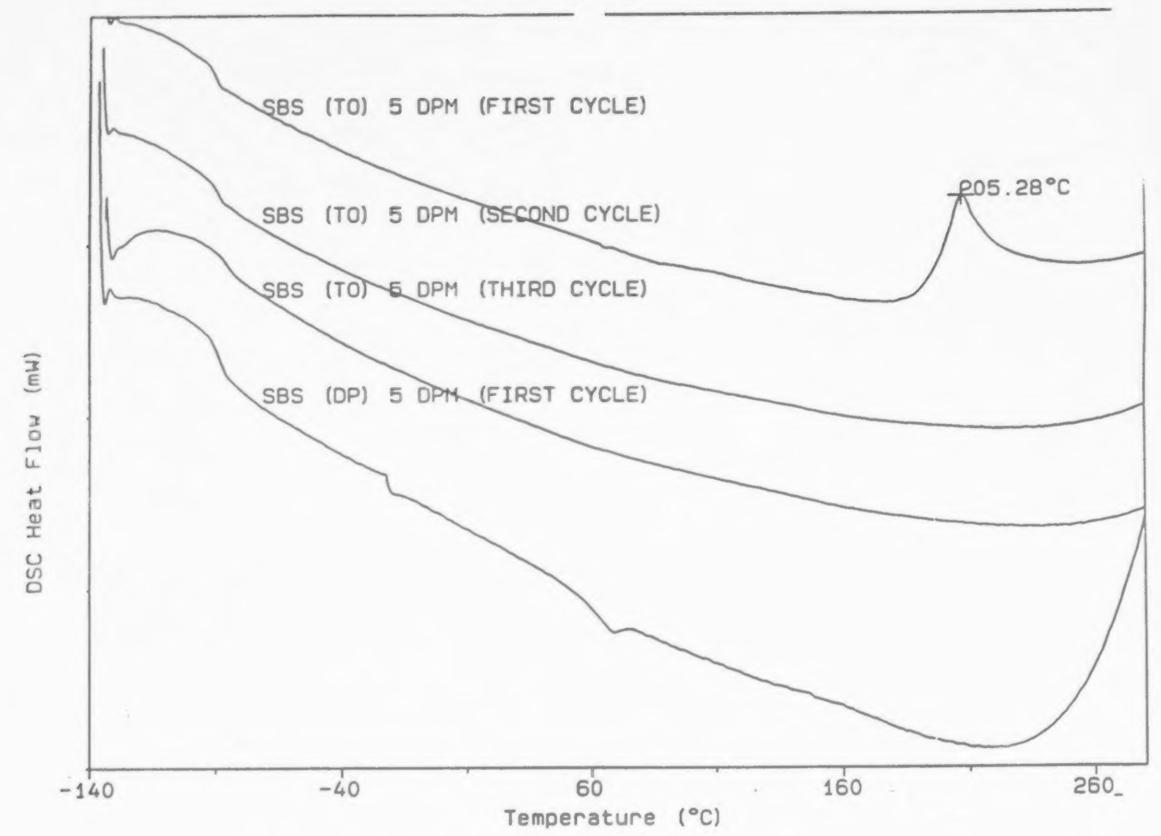

Figure 6.11 DSC scans of pure block copolymer as cast from dipentene and toluene (at scanning rate of 5^0C/min.).

Table 6.7 Tabulation of data from Figure 6.11

Sample	Process history	Run number	Scanning rate	T_g^B ⁰C	T_g^S ⁰C	T_g^I ⁰C	T_{peak} ⁰C
SBS	Dipentene	1	5^0C/min	-88.6	65.4	-22.0	—
SBS	Dipentene	1	10^0C/min	-84.6	70.0	-13.2	—
SBS	Toulene	1	5^0C/min	-91.5	73.1	—	205.8
SBS	Toulene	2	"	-89.4	—	—	—

— Not observed

CHAPTER 7

DISCUSSIONS

7.1 Is Dipentene a True Neutral Solvent?

Various tests such as solubility parameter consideration, turbidity analysis of solutions, and molecular structural similarities can be applied in defining and identifying a neutral solvent. However, the most convincing test would be the results obtained from actually using such a solvent with a block copolymer and its blends. That is, the liquid-state character of the solutions and the subsequent microstructure and properties of solids cast from these solutions would verify the neutral nature of the solvent.

7.1.1 Solubility Parameter Consideration

The process of dissolving a polymer in a solvent is governed by the familiar thermodynamic statement that describes a potential mixing (or demixing) process,

$$\Delta G_M = \Delta H_M - T\,\Delta S_M \qquad 7.1$$

where ΔG_M = the change in Gibbs free energy, ΔH_M = the heat of mixing, T = the absolute temperature and ΔS_M = the entropy of mixing. If $\Delta G_M < 0$, the mixing process will occur spontaneously.

Since the dissolution of a polymer is always connected with a small increase in entropy ($\Delta S_M > 0$), the magnitude of the heat term ΔH_M is the deciding factor in determining the sign of the free energy change. Hildebrand and Scott proposed in their regular solution theory for binary mixing,

$$\Delta H_M = V\left[\left(\Delta E_1/V_1\right)^{1/2} - \left(\Delta E_2/V_2\right)^{1/2}\right]^2 \Phi_1 \Phi_2 \qquad 7.2$$

where ΔH_M = overall heat of mixing; V = total volume of the mixture (assumed not to change upon mixing); ΔE_i = energy of vaporization of component i (i = 1 or 2); V_i = molar volume of component i; Φ_i = volume fraction of component i in the mixture. The expression ($\Delta E_i/V_i$) is the energy of vaporization per unit volume for component (i), often described as 'cohesive energy density'. Rearranging Equation 7.2

$$\frac{\Delta H_M}{V\,\Phi_1\,\Phi_2} = \left[\left(\frac{\Delta E_1}{V_1}\right)^{1/2} - \left(\frac{\Delta E_2}{V_2}\right)^{1/2}\right]^2 \qquad 7.3$$

It may be seen that the heat of mixing per unit volume at a given concentration is equal to the square of the difference between the square roots of the cohesive energy densities of the components. This latter quantity, $(\Delta E/V)_i^{1/2}$ is called the solubility parameter of component i and usually designated by symbol 'δ_i'. Its dimensions are $(\mathrm{cal/cm^3})^{1/2}$ (called the "Hildebrand" still used for historical and convenience reasons) and usually δ has numerical values in the range of 7-12 for organic polymers and their solvents.

Therefore the unit heat of mixing of two substances is dependent on $(\delta_1 - \delta_2)^2$, is always positive (in this theory) and serves to oppose the dissolution process. If ΔH_M is not to be so large as to prevent mixing, then $(\delta_1 - \delta_2)^2$ has to be relatively small. In fact, if $(\delta_1 - \delta_2)^2 = 0$, solution is assured by the entropy term. As $\delta_1 \rightarrow \delta_2$, the substances will be miscible. In the derivation of δ, only energies associated with Van der Waals intermolecular forces are taken into account; the possible roles of polar interactions and hydrogen bonding are ignored, as is crystallinity. Thus δ governs only the heat of mixing of the simplest hydrocarbon amorphous polymers.

The solubility parameter of a solvent is a readily calculable quantity, from data on energy of vaporization. The solubility parameter of a polymer can not be determined directly because most polymers can not be vaporized without decomposing. The solubility parameter of a polymer (δ_P) is therefore defined as the same as that of the solvent in which the polymer will mix (a) in all proportions, (b) without heat change, (c) without volume change, and (d) without reaction.

For polybutadiene, values of δ_B are in the range 7.2-8.6 with an average around 8.1; for polystyrene δ_S is in the range 8.5-9.4 with an average around 8.9 to 9.1; and δ_D = 8.5 for dipentene. Choosing the values $\delta_B = 8.1$ and $\delta_S = 8.9$ would make dipentene mathematically ideal as a neutral solvent, with $\delta_D = (\delta_B + \delta_S)/2$. Leary and Williams [60] found that measurements of T_S for SBS copolymers were best predicted by their theory if $\delta_S - \delta_B = 0.8$, which is also consistent with the values cited above.

Solubility parameter results vary depending on method of measurement, which results in much of the scatter of values reported. Therefore, this consideration (δ_D exactly halfway between δ_S and δ_B, for example) is not sufficient in determining a neutral solvent for systems of block copolymers.

7.1.2 Turbidity Analysis of Solution

Pico and Williams [77] found that predictions for solubility based on δ alone were not entirely correct. However, a certain consistency was found between this scheme and a compatibility rating derived from the turbidity of SBS/solvent solutions. Subjective turbidity ratings among solutions of Sbs in several solvents, on a scale of 0 to 5, were made by three individuals observing these solutions; results were identical among the three, suggesting dipentene as the only true neutral solvent (no turbidity) among toluene, benzene and several other solvents.

7.1.3 Molecular Structural Similarities

Figure 4.1 (Chapter 4) gives chemical structures of polybutadiene, polystyrene and dipentene. The benzene ring (cyclic structure) of dipentene is the part compatible with the benzene rings of polystyrene, whereas the portion of dipentene outside the cyclic structure is more compatible with polybutadiene, especially the double bond.

7.1.4 Microstructures

If a solvent is truly neutral, there should be no thermodynamic incentive for a block copolymer solute to form micelles at any concentration. (To the best of our knowledge, no micelle structures have been observed in dipentene solutions.) Instead, the solvent should solubilize all blocks equally and have no solvent "bias" whatsoever. The implication is that solvent molecules permeate all portions of the solution equally, with the same local solvent volume fraction ϕ_S. Thus, when the solvent is evaporated, the condensed polymer solid should have a microstructure identical to (or very similar to) that of a bulk polymer sample prepared without solvent -- but without vestiges of a bulk processing history (e.g., shearing and orientation in melt flow).

Evidence in support of this concept was produced in terms of the successful predictions of T_S (ϕ) by the theory of Pico and Williams [79]. The systems studied were a series of SBS polymers dissolved in dipentene, and predictions were made using $\Delta\delta_P = \delta_S - \delta_B = 0.8$ (the Leary-Williams recommended value, based on T_S measured in bulk copolymers). In this theory, the solvent -- if truly neutral -- is basically a simple diluent, separating the polymer chains from each other and therby weakening their chemical interaction. This depresses T_S (ϕ) and affects all other thermodynamic properties of the solution in a predictable fashion. Among other things, the same morphologies are predicted to form when $T < T_S$ as those formed from cooling bulk copolymers. To our knowledge, this has always been the case for microstructures formed from dipentene, with even greater order and regularity. This is possible because of greater mobility of the polymer chains in solution.

This behavior was employed by Hugenberger and Williams [42] who found dipentene to be also a very good solvent for S-EB-S copolymers (δ_{EB} supposedly being close to δ_B). Their solutions were adjusted in concentration to produce T_S (ϕ) $\approx 30^0$C, a convenience for experimental work because a very slight cooling to room temperature produced the transition to form a microphase-separated solid (gel, with about 68% solvent) with structural similarities to what the S-EB-S melts would have produced (except for the fact that their bulk T_S exceeded their decomposition temperatures).

There are other advantages to using a neutral solvent in block copolymer studies, beyond the production of liquid-state systems that morphologically mimic bulk block copolymer melts in phase-separated states and yielding lower viscosity fluids at convenient temperatures. The use of a neutral solvent can be carried to the completely dry state of total solvent removal. Presumably, the remaining pure polymer solid-state microstructures should also resemble those formed from bulk polymer directly (and even more closely represent thermodynamic equilibrium). One test of this is to examine microstructures by TEM, and the results (section 7.2, below) have generally confirmed the expectation stated here.

Another type of test of these contentions is to analyze DSC evidence, to determine whether solvent-prepared solid copolymers exhibit the same thermal properties as their bulk counterparts. Our work here has found that, in one respect, there are differences and that these are associated with the inerphase. This will be discussed shortly, in section 8.3 (Differential Scanning Calorimetry).

7.2 TEM Micrographs

The top and bottom portions of the polymer films were scraped before cryo-ultramicrotomy in order to avoid the polymer areas dominated by surface effects. As a result, the microstructures observed are believed to be characteristic of the bulk SBS copolymer.

7.2.1 Microphase and Macrophase Separation in Homopolymer/Copolymer Blends

Intuition leads us to believe that as higher amounts of hPS are added to the block copolymer (SBS) of lamellar morphology, swelling of styrene domains will be observed until it reaches a saturation limit above which macrophase separation will take place, separating the system into two macrophases (e.g., a pure hPS phase and an hPS-saturated phase of swollen SBS). Instead, Winey et.al [112] and Quan et.al. [83] reported a reduction in the lamellar spacing of diblock /homopolymer blends and triblock /homopolymer blends when a small fraction of low-M homopolymer was blended with copolymer.

In the present study, 4% PS blend did not show a reduction in the lamellar spacing in the blend which is consistent with $M_{hPS}/M_S \sim 1.0$, as very low molecular weight homopolymer ($M_{hPS}/M_S < 1.0$) is necessary to reduce the lamellar spacing [38, 78] relative to the neat block copolymer. However, a very different morphology did appear. The simple near-parallel lamellar arrangement observed in the pure block copolymer (S129) was no longer seen in the 4%hPS blend. Wavy-rod morphology (Figure 5.5 and 5.7) and a regular network pattern of alternating globules of styrene and butadiene (Figure 5.6) suggest the trend in accommodating moderate molecular weight homopolymer (M_{hPS}/M_S ~ 1.0) in triblock copolymer. It appears that a catenoid type of morphology is prevalent in the regular network of Figure 5.6. This was the type of morphology found in some areas of this blend, and the driving force for such a morphology at 4% average hPS composition is not clear. We speculate this could to be due to microphase separation occurring in regions where local composition (%hPS) was significantly different (higher) than the overall composition of the blend, but such patterns were not seen again at higher (average) hPS contents.

The 8%hPS blend showed short range lamellar morphology with many areas disrupted by hPS-rich regions (Figure 5.10) and styene-swollen copolymer domains (Figure 5.9). The 18%hPS blend showed lobular structures with internal lamellar morphology (Figure 5.11) and the precursor for these structures could be seen in the 8%hPS blend (top right-hand corner in Figure 5.10). Instability in the system was observed beginning at very small addition of hPS (4%hPS blend), however, onset of macrophase separation was clearly indicated for the first time in the 18%hPS blend (Figure 5.12), where styrene domains experienced excessive swelling in accommodating hPS and butadiene domain thickness remained unchanged. If the swelling is this large, it seems reasonable to identify those regions as macrophase separated.

With increasing hPS concentration, the lamellar repeat period expanded linearly, but the thickness of the butadiene layer remained constant. This means that the added hPS was unable to expand the lamellae laterally and to force the average interfacial area occupied by a copolymer junction point to increase. A similar phenomenon was observed when $M_{hPS}/M_S > 1.0$ [112]. On the other hand, change in butadiene thickness was noted when $M_{hPS}/M_S < 1.0$ [112]. These results suggest that the crossover point is near M_{hPS}/M_S ~1.0 as in our case. The 37%hPS blend underwent macrophase separation but no pure copolymer or homopolymer phases were observed. Instead, a new ‘soda-straw’ morphology emerged and is discussed separately in this chapter.

Blends with 44%hPS (Figure 5.17) and 60%hPS (Figure 5.18) underwent macrophase separation forming copolymer-rich and homopolymer-rich phases. Lamellar morphology was retained in the copolymer-rich phase in the 44%hPS blend, whereas, irregular lattice structure with trapped hPS was observed for 60%hPS blend in the same (copolymer-rich) region. Macrophase separated hPS was more or less free from trapped copolymer in 44%hPS, but an appreciable amount of copolymer was trapped in hPS macrophases in 60%hPS blend (note the edge view of dark PB lamellar from the regions of trapped SBS which is also microphase-separated).

Quan et al. [83] observed that the microdomain spacings reverted to the value for the pure triblock copolymer when high molecular weight hPB was blended with SBS (49% styrene) (M_{hPB}/M_{SBS} ~1.13) using dichloromethane as a solvent. This result is similar to our blend (32%SBS) where M_{hPS}/M_{SBS} ratio is ~1.06, although the molecular topology differs (since PB was the mid-block in the Quan work).

Although theories that specifically treat the case of microphase separated homopolymer/triblock copolymer are not yet available, some qualitative explanation of the morphological behavior of these materials may be proposed from theories developed for diblock copolymers. Microdomain expansion and the onset of macrophase separation, observed in this work, are predicted for phase-separated diblock copolymer blended with homopolymer [15, 41]. The homopolymer molecules become less mobile with higher molecular weight and can no longer distribute themselves preferentially within the microdomain as a result of their own size constraint. They can not mingle with the lamellar styrene microphases by a lateral extension, as considerable entropic force imposes a near-spherical symmetry on the homopolymer chain; more obvious constraints exist in cylindrical and spherical morphologies.

Thus, the presence of homopolymer forces the host PS microphase apart, causing extension of the copolymer sequences. The increased volume fraction of the hPS segments (volume fraction also increases with increasing homopolymer composition at constant molecular weight) causes the microdomain to swell. When the size of the homopolymer chain approaches or exceeds that of the styrene block sequence, the entropic constraints involved in locating the homopolymer in the microdomain becomes restrictive, and macrophase separation of the homopolymer is favored. Under these conditions, the dimensions of the microdomains return to those of the pure block copolymer, consistent with our experimental results (Figure 5.23). This homopolymer macrophase separation should be very sudden as M_{hPS} exceeds M_S, so the phenomenon may have applications to molecular weight fractionation processes for homopolymers.

Blends with 44%hPS and 60%hPS underwent macrophase separation, however, copolymer-rich regions did not revert to microdomain dimensions of pure copolymer; a substantial amount of hPS remained trapped within PS lamella of the copolymer-rich phase. This could be explained in part by the fact that $M_{hPS} = M_S$ in these experiments; as a result, the copolymer would show more compatibility with this hPS in comparison to high molecular weight hPS and a more complete macrophase separation into pure phases would not take place. Jeon and Roe [47] examined a blend system of SB copolymer ($M_{SB} = 48,000$; 51% styrene and lamellar morphology) with homopolystyrene ($M_{hPS} = 24,500$). Here, with a diblock, we have $M_S = M_{hPS}$ and again this condition led to good solubility. TEM results showed evidence for solubility over the full range of blend compositons that were studied (18% to 85%hPS). In our study with a triblock, solubility of hPS (examined over smaller range of hPS concentration) is consistent with results of Jiang et al. [46], where solubility of hPS was found to decrease with increase in complexity of block copolymer architecture. Maximum solubility was found for the case of diblock (simplest architecture), minimum for the case of four-arm star copolymer (most complex architecture of the three block copolymers studied) and moderate for the case of triblock copolymer. Combination of the results of Jeon and Roe [47] and Jiang et al. [46] explains finite solubility as well as finite compatibility of hPS (PS13) in SBS (S129). Inoue et al. [45] found that for a system of diblock (SI) copolymer and homopolymer (hPS) having $M_{hPS}/M_S \sim 1.0$, very good solubilization of hPS in styrene domains took place; up to

80%hPS was solubilized, resulting in thickening of PS lamellar but not gross macrophase separation.

7.2.2 A Priori Predictions of Miscibility and Comparison with Results

In *a priori* predictions, intuition, as well as thermodynamic factors (δ_i, M_S, M_B) can be invoked to predict where the added hPS should be located in the blend microstructure. The added hPS had a molecular weight of 13,000, identical to M_S in the copolymer. These styrene copolymer domains would have a minimum dimension roughly twice that of the S-block random coil [19]. Homopolystyrene of substantially smaller molecular weight ($M_{hPS}/M_S < 1.0$) would be capable of fitting entirely within a styrene domain, if only a small amounts of hPS were added. In our case, M_{hPS}/M_S is 1.0, and we are on the border of microphase solubilization and macrophase separation. We would expect some miscibility for small amounts of hPS, but at higher volume fractions of hPS the system would be unstable. Unlike a styrene block, which is connected on one end to the butadiene block, the added hPS has two ends free and can rearrange itself in the S-domain to keep the free energy of the system at a minimum. Considering thermodynamic incompatibility between B-block and hPS and freedom available to hPS, it is unlikely that hPS would reside at the interphase region. However, the presence of hPS in an S-domain is not totally without thermodynamic "penalty" as it would cause the copolymer S-blocks to become strained and acquire some orientation.

The 4%hPS blend showed no difference in the ratio T_S/T_B ($T_S/T_B \sim 1.0$) relative to pure copolymer, indicating initial acceptance of hPS in styrene domains. We should point out that alternating globules of styrene and butadiene were observed in this same blend, which we attribute to difficulty of hPS in accommodating itself in styrene domains in some regions of the blend. However, an overall view of morphology would support the inclusion of hPS in S-domains, albeit with an increase of strain energy in the microstructure.

The 8%hPS blend showed a higher value of this ratio ($T_S/T_B \sim 1.2$), with T_B remaining constant, indicating swelling of S-domains. At 18%hPS, saturation of hPS in S-domains was reached and was inferred by comparing T_S/T_B ratios of the 18%hPS blend

(~2.55) with those of the 37%hPS blend (~2.55). Saturation solubility was also supported by two more observations. First, micrographs of 18%hPS blends showed large variations in styrene lamella thickness (variation observed in the micrographs was as high $\{T_S\} \pm 40\%\{T_S\}$). The second clue came from the morphology of .37%hPS blend. Above a saturation limit, we would expect macrophases of styrene due to additional hPS as well as the occurrence of structural alterations. We observed both of these in the 37%hPS blend. Styrene-rich and copolymer-rich macrophases were seen, as well as structurally altered soda-straw morphology, which could be a response to reduce molecular strain. If the latter is true, it would explain why such morphologies have not been seen in diblock/homopolymer systems.

7.2.3 Compositions of Phases in Homopolymer/Copolymer Blends

Electron microscopy is a powerful technique for obtaining information on the structures of materials, but a deficiency is its inability to provide detailed information on the chemical composition of microphases. This is not so true for the cases of pure block copolymers or their blends with small amounts of homopolymer. Measurements of lamellar thickness (assisted by staining to provide phase contrast) confirmed the compositions in cases of pure copolymer (Figure 5.4) and 4% PS blend (Figure 5.5), where dark regions were identified as pure PB and light regions as pure PS. Difficulties began when higher amounts of hPS addition induced nonuniform swelling in the styrene domains. At this stage, cursory assessment of compositions, by comparison of light and dark areas in the micrographs, did not always reflect the composition of the blend. This was especially true at higher concentrations of hPS in blends where macrophase separation led to formation of copolymer-rich and homopolymer-rich phases followed by local microphase separation in these phases.

More detailed examination of micrographs provided additional evidence that the postulated differences in compositions (i.e., phases not pure PS or PB) were real, and discussions in terms of copolymer-rich and homopolymer-rich phases are justified. For example, 37%PS blend micrographs showed asymmetric swelling of the styrene domains when viewed in a slice cut normal to the surface of the polymer film (Figure 5.15). A careful scrutiny of these regions and comparison of light and dark areas did not agree with the known overall composition of the blend. The same was found for a micrograph taken from a slice cut parallel to the surface of the polymer film (Figure 5.16a). However, a lower-magnification micrograph (Figure 5.16b) coupled with all other micrographs (Figures 5.13-5.16) would justify both the existence of copolymer-rich and homopolymer-rich phases as well as the overall composition.

7.2.4 Observations of New Morphologies

The saturation solubility limit of this hPS in this SBS copolymer was suggested by achievement of a limiting value of T_S/T_B (~2.55), and the strategy should be applicable to other homopolymer/block copolymer systems even when different levels of T_S/T_B are obtained. Here, the limit was reached around 18%hPS addition for the system with $M_{hPS}/M_S \sim 1.0$. Above this limit, added hPS might have been expected to form its own phase as the system undergoes macrophase separation. Indeed, we found a transition, but not to a macrophase system with one pure component. Instead, the transition led from lamellar to soda-straw morphology (Figures 13-16). The origin of this structure is unknown. Structural features observed provided some hints. In Figure 5.16b, light circles appear in dark cores, suggesting a cylindrical core of styrene surrounded by a butadiene annulus and then a styrene sheath. This feature has some resemblance to the alternating concentric-shell morphology of spherical domains found in dispersed copolymer-rich phases in immiscible copolymer/homopolymer blends [21, 40]. Jiang et al. [48] invoked ‘minimization of interfacial energy ‘ as the driving force for this transition (with diblocks) from lamellar structure to concentric shell structure. Spherical morphology gives minimum interfacial area, and the interfacial energy will depend on the chemical composition in the interfacial region. Apparently, the dispersed phase of the copolymer AB will present the minimum interfacial energy with homopolymer matrix A if the outermost shell of the phase is totally composed of A blocks. When block A forms the outermost shell, block B is expected to form the adjacent inner shell. Continuation of this process leads to the formation of alternating concentric layer morphology, until the interior remains as the core of either A or B.

Figure 5.16b shows irregular-shaped regions of copolymer-rich (dark) and hPS-rich regions (light). Concentric morphology is seen in the transition region between these two (copolymer-rich and hPS-rich) phases. However, the morphology is not spherical but rather long cylinders as in Figures 5.14-15. At 37%hPS addition, a substantial amount of copolymer is present in the system and we speculate that in minimizing the interfacial area, one possible choice is a transition from planar lamellar morphology to a morphology of long annular cylinders. We could see only three alternating layers of copolymer components, unlike multiple layers observed by others in spherical domains of diblock systems [21, 40]. This may be due to kinetic as well as compositional limitations of the system. In the copolymer-rich and hPS-rich areas, morphology can be described as a butadiene core surrounded by a styrene annulus.

What is initially surprising and remains to be explained is the fact that core of the concentric layers found in some regions (shown by arrows in Figure 5.16b) is made up of styrene. One might expect butadiene to form the core, as it would be less compatible with the large amount of external hPS than the PS block. Thus, of the two components of copolymer, the styrene block should be on the outside of the cylinder, to give minimum interfacial energy at copolymer-hPS interface.

We also note that this soda-straw morphology falls into 'a composition range' where Winey et al. [114] and Spontak et al. [97] observed the OBDD morphology in the blends of diblock copolymer and homopolymer. This region is characterized by 62-66% total polystyrene composition of the blend system. The OBDD morphology was generally observed when $M_{hPS}/M_S \sim 0.5$ and homopolymer was in disperse region. In addition to OBDD, the lamellar catenoid, cylindrical and disordered morphologies were observed for the above set of conditions along the upper and lower limits of this styrene composition range.

Disko et al. [18] reported catenoid-lamellar morphology for the case of SB diblock copolymer and hPS blend in the same composition range (66% total PS). Here, M_{SB} =

49,800 with 51.1% styrene, making M_S = 25,500 and M_B = 24,400. For the hPS, M_{hPS} = 26,000 and thus $M_{hPS}/M_S \sim 1.0$. Another similarity to our work was that their blend had a copolymer/homopolymer composition of 65/35, a composition that almost matches with our 37% hPS blend.

7.3 Differential Scanning Calorimetry

Microphase-separated SBS block copolymer would show at least two glass transition temperatures, one corresponding to the butadiene phase and another corresponding to the styrene phase. Thermal analysis using DSC is therefore the most convenient and inexpensive method to determine the phase behavior of polymer blends. A third transition, which occurs only for block copolymer, is T_s (separation temperature described in Section 1.4), which may be observed in DSC if the copolymer does not undergo decomposition before it reaches T_s. Block copolymer also has a third phase, known as 'interphase', which is a mixed phase formed near the junction of A-blocks and B-blocks. Interphase thickness is broad at low molecular weight of the copolymer but decreases as molecular weight increases. It is possible to detect this interphase glass transition using DSC, although not as readily as transitions in the A and B phases.

7.3.1 Pure Copolymer and Homopolymers

Glassy samples are never at true equilibrium, and an infinitely slow scanning rate is needed to get idealized values of T_g in these materials. At finite heating speed, transition is observed as a delayed transition and this is the reason of getting higher values at 10^0C/min (higher scanning speed) in comparison to 5^0C/min (lower scanning speed) (Table 6.1). Thermal equilibrium is approximated better at lowere speeds than at higher speed and this is why the intermediate transition in SBS in a 5^0C/min scan is more evident than that at 10^0C/min. (Figure 6.1). This was the case for styrene transitions in both (as-received and as-cast) samples, and for butadiene in as-cast samples. This intermediate transition was observed as a delayed transition at 10^0C/min (-13.2^0C) in comparison to that observed at 5^0C/min (-22.0^0C). No comment can be made on the nature of the high-temperature 'exothermic peak' found in as-received samples with our present knowledge of this copolymer. In general, an 'exothermic peak' in a heating scan would represent a bond formation (e.g. cross-linking), and the peak was never seen in a second heating cycle..

Variation in T_{gA} and T_{gB} values for the copolymer relative to those of pure homopolymers is a common phenomenon observed in block copolymers. The T_{gB} in block copolymer varied in the range of -84 to -88^{0}C (pure polybutadiene glass transition is ~-91^{0}C), whereas, variation of T_{gS} is in the range 65-70^{0}C (pure polystyrene glass transition of molecular weight equal to that of M_S of copolymer was ~96.77 (5^{0}C/min). Polybutadiene, being a rubber (and thus having larger free volume than PS), could form purer microphases in an SBS block copolymer, giving a relatively sharper glass transition without significant deviation from the pure polybutadiene glass transition. On the other hand, glassy polystyrene would always have trapped some butadiene in its microphase, giving more free volume in the styrene phase and resulting in lower T_g's than for a pure styrene phase. This is also the reason we observe a broad styrene glass transition in block copolymers.

7.3.2 Thermal Cyclic Tests on Blends of Block Copolymer and Homopolymer

Values of T_g^B and T_g^S showed significant changes when registered on the first, second and third DSC heating scans. The T_g^B in the second scan apeared higher than in the first scan, but showed its lowest value in the third DSC heating scan for the cases of pure copolymer and blends with 4%,8% and 18%hPS. The reasons behind higher values of T_g^B in the second scan are not clear, since a higher T_g^B would normally mean that the PB phase was contaminated by a higher-T_g substance (i.e., PS) during the annealing experience of the first cycle. However, the subsequent decrease of T_g^B seen on the third cycle can be explained by the reverse argument. Annealing (during the second cycle) would permit diffusional processes to occur that lead to a more complete microphase separation, creating lower T_g^B and higher T_g^S. This 3rd-cycle reduction of T_g^B (and increase of T_g^S) was also more pronounced as more hPS was added to the SBS host. Thus, the greater change was seen for 18%hPS in which T_g^B dropped to -88.35^{0}C and T_g^S

increased to 80.94^{0}C. This trend can be explained by arguing that increasing the volume fraction of hPS in SBS induces additional incompatibility between the S and B blocks of the copolymer, and as a result purer microphases are formed.

Blends with 37%hPS and 44%hPS showed an entirely the opposite trend change in T_g^B upon repeated heating. In the second scan, T_g^B dropped to an all time low (^{0}C and ^{0}C respectively) and the third scan showed higher values: . ^{0}C for 37%hPS and ^{0}C for 44%hPS. We do not have an explanation for these trends in T_{gB} with cyclic heating.

The styrene glass transitions observed in all three heating cycles did not show appreciable differences for pure copolymer. In the blends, however, the T_{gS} observed in the second and third heating scans were at considerably higher values than those of the first scan and higher values were obtained with increasing fraction of hPS. We attribute this phenomenon to the demixing between the S-block chains and hPS chains by Brownian motion, the driving force being incompatibility between S-block and hPS. This observation reveals the importance of the chemical linkage between the styrene and butadiene blocks of a block copolymer. Because the hPS is not "anchored" to the surface of PB domains, it is free to migrate as far from that surface as it can get during the high temperature ($T > T_{gS}$) portion of the DSC heating cycle.

At lower concentrations of hPS (4%,8%hPS), demixing between S-block chains and hPS would take place without macrophase separation. It is very difficult to make predictions of morphological changes occurring at higher hPS concentrations with successive heating cycles. The T_g^S in 18% and 37%hPS suggests the presence of separate regions of hPS in S-block domains, since the styrene glass transition is a perturbed event that resembles a mixture of two different S-block and hPS T_g's.

In the case of the 60%hPS blend, two transitions (at -10^{0}C and 55^{0}C) were observed in the first heating scan which probably represent two non-pure phases of different composition. We speculate these were due, respectively, to a copolymer-rich phase (with irregular lattice morphology) and to a PS-rich phase (with trapped copolymer in the form of butadiene ribbons); see Figure 5.2 Successive heating produced a purer hPS phase and T_g^S increased to 87^{0}C, then, 86^{0}C, still lower than that of pure hPS transition due to the presence of rubbery butadiene in the blend. The heating also caused the lower transition (-10^0C) to vanish, probably because the annealing permitted a near-equilibrium order of the SBS domain structure to be established thus, the chaotic/mixed SBS microstructure which had behaved essentially like a randomized solution with $T_g = (W_B T_g^B + W_S T_g^S)$.

7.3.3 Equilibrium or Non-equilibrium Morphologies?

It is almost inevitable that only non-equilibrium morphologies are observed in practical systems. Microphase separation in a copolymer-rich phase to give a butadiene matrix would trap excess hPS in that phase. Once homopolymer has been dissolved in a domain system, there is no realistic way for it to escape or adjust composition to a new equilibrium condition, unless complete disruption is achieved (e.g. by solution or melt). Using dipentene for solvent-blending such systems has the potential to form near-equilibrium morphology. The neutral nature of dipentene ensures uniform concentration of solvent in both phases, and its low vapour pressure (note its high boiling point) leads to slow evaporation, avoiding gradient formation in the system. In my opinion this is the best that can be done in achieving near-equilibrium morphology.

DSC results of thermal cyclic tests suggest that although the preferred regions within a microphase-separated SBS host for added hPS are the S-block domains, hPS would prefer to be in a demixed state. This demixed state, corresponding to a minimum ΔG_M for the whole system, would have the S-block chains restored to a non-strained condition of hPS-free equilibrium and the hPS in its own separate phase. Evidence for these tendencies is strongest in the 60%hPS blend, which exhibited two midrange T_g's which both evolved in the direction expected of complete phase separation. Higher glass transition temperatures corresponding to the hPS-rich phase were seen with successive cyclic heating, which suggests exclusion of hPS chains from S-block chains upon annealing.

7.3.4 Intermediate Glass Transition in Blends of SBS and hPS

Dipentene-cast samples of SBS and its blends with hPS often produced DSC evidence of an intermediate glass transition (at T_g^I). It is instructive to attempt an 'a priori' prediction of T_g^I, based upon various assumptions about the microstructure. First, one can naively assume that the intermediate T_g^I is due to an interphase whose (uniform) composition equals that of overall polymer system. A linear mixing rule,

$$T_g^I = (W_S F_{SBS} + F_{hPS})\, T_g^S + W_B F_{SBS}\, T_g^B \qquad 7.4$$

where F_i = fraction of component i (= SBS or hPS) and W_j = weight fraction of component j in the block copolymer (j = S or B) was used for convenience. Excellent agreement was seen in the case of pure copolymer, whereas values higher than observed were predicted for blends. This is not surprising, as added hPS would not contribute significantly to the interphase due to its incompatibility with butadiene. These predicted T_g^I are compared in Table 7.1 with those measured at different scanning rates.

Table 7.1 Comparison of predicted† T_g^I with those of observed by DSC (W_S =0.44, W_B =0.56, T_g^S and T_g^B were obtained from the DSC scans)

Sample (F_{hPS})	Process history	Scanning speed	T_g^I °C (observed)	T_g^I °C (predicted-linear rule)
SBS 0%hPS	Dipentene	10 °C/min	-20.93	-18.42
4%hPS	"	"	-14.18	-16.20
8%hPS	"	"	-12.50	-11.82
18%hPS	"	"	-13.20	-4.13
37%hPS	"	"	-18.06	12.25
SBS 0%hPS	"	5 °C/min	-22.02	-20.83
4%hPS	"	"	-23.51	-18.50
8%hPS	"	"	-23.48	-14.14
18%hPS	"	"	-14.88	-6.66
37%hPS	"	"	-26.75	8.96
44% hPS	"	"	-28.00	14.70

† Interphase composition was assumed to be equal to the composition of blend.

The strong intermediate glass transitions were observed in all blends at DSC scanning rate of 5°C/min. At 100C/min scanning rate, some of the blends showed intermediate transition and at 10C/min no glass transition was observed.

At the slower heating rate, polymer would be closer to thermal equilibrium with the scan temperature, and thus values of T_g's obtained at 5°C/min were chosen for predictions of intermediate glass transition in second set of calculations shown below. These results indicate that scanning rate would have to be optimized to get intermediate transitions, and that varying scanning rates would supply more information on nature of blends.

In a second set of calculations, TEM information was used to guide the procedure. We assumed no change (in relation to pure SBS) in interphase composition in 4% and 8%hPS blends, which is consistent with T_S/T_B ratios remaining constant as observed by TEM. Predictions using the linear mixing rule (with $W_S = 0.44$ and $W_B = 0.56$) were in very good agreement with the observed values (Table 8.2). At saturation solubility of 18%hPS (predicted by T_S/T_B ratio obtained from TEM micrograph), S-block chain would be less constrained in its domain and could pull back to give higher styrene content at the interphase. We used the measured T_g^I to infer the amount of styrene in interphase for this blend and obtained $W_S = 0.462$. The blends with 37% and 44%hPS showed good agreement with observed values when the interphase composition was assumed to be the same as that of pure copolymer (44% styrene). The results are summarized in Table 7.2.

Table 7.2 Comparison of predicted[§] T_g^I with those of observed by DSC ($W_S = 0.44$, $W_B = 0.56$, T_g^S and T_g^B were obtained from the DSC scans)

Sample	T_g^I °C (observed)	T_g^I °C (predicted-linear rule)
SBS	-22.02	-20.83
4%hPS	-23.51	-21.42
8%hPS	-23.48	-21.19
18%hPS	-14.88	†
37%hPS	-26.75	-22.12
44%hPS	-28.0	-21.81

[§] Interphase composition was assumed to be equal to pure block copolymer composition.

[†] Observed T_g^I was used to calculate interphase styrene composition. Assuming this composition, the predicted glass transition (-12.61°C) of 18%hPS at a different scanning rate (10 °C/min) was in excellent agreement with the observed value (-13.12°C).

7.3.5 Interphase Glass Transition: Comparison with Other Data

Djermouni and Ache [20] studied the phase behavior of SBS block copolymer (M_w =140,000 and M_w/M_n = 1.16) using a positron annihilation technique over a wide range of temperatures. Samples were prepared from solution by casting them on glass plates and removing the solvent under vacuum at 80^{0}C. The solvents used were toluene, carbon tetrachloride, ethyl acetate and methyl ethyl ketone, having solubility parameters of 8.9, 8.6, 9.1 and 9.3 respectively. Samples cast from all solvents showed peaks at -70^{0}C, -14^{0}C and +85^{0}C. Samples cast from ethyl acetate and methyl ethyl ketone showed a fourth peak around 10^{0}C. Peaks at -70^{0}C and 85^{0}C were interpreted as T_g^B and T_g^S respectively. The peaks at -14^{0}C and +10^{0}C were both interpreted as due to interphase glass transition, the former peak corresponding to a phase with polybutadiene as the major component and the latter corresponding to a phase with polystyrene as the major component.

In another study Miyamoto et al. [74] reported the existence of a third peak in their mechanical loss curves and DSC thermograms in cases of SBS films cast from ethyl acetate and methyl ethyl ketone. However, the two techniques produced different numerical values for T_g of the third peak. Rheo-Vibron techniques demonstrated the existence of a third peak at +10^{0}C and DSC methods gave a peak at -14^{0}C. These authors interpreted these peaks as originating from the same phenomenon. The temperature difference probably due to the different sensitivity and thermal characteristics of the techniques used.

We disagree with their interpretation and feel that detection of two peaks at -14^{0}C and +10^{0}C by positron annihilation represent an independent confirmation of the Djermouni and Ache result, interpreted as T_g's arising from two different regions of the material and thus two different phenomena are occurring in the same copolymer in the intermediate temperature region.

Not all studies have found these two intermediate transitions. Beecher et al. [10] reported the presence of a single broad intermediate transition (-26 to 4^{0}C) in SIS triblock copolymer using a vibrating reed apparatus. On the other hand, Wilkes et al. [118] did not observe any transition in the intermediate temperature range in SBS triblock copolymer using the Rheo-Vibron technique.

Meyer and Widmaier [68] studied two SIS copolymers (30% styrene) with DSC and found intermediate glass transitions in both, at slightly different temperatures: 39.5^{0}C and 36^{0}C, for samples with molecular weights of 31,000 and 24,500 respectively. Compression-molded films were used. Specimens were annealed at 147^{0}C for 10 minutes and then cooled at a scanning rate of 4^{0}C/min. Other SIS copolymers with 30% styrene but lower molecular weights showed only one intermediate transition, whereas similar copolymers having higher molecular weights showed the normal two transitions corresponding to isoprene (T_g^I) and styrene (T_g^S). Thus, T_g^I seems to depend on MW as well as on casting solvent, possibly because both can influence the interphase composition profile.

In the present work, SBS (S129) cast from dipentene solution produced an intermediate glass transition as observed by DSC. This was not observed when toluene was used as a solvent, but then a broad styrene glass transition was observed.

Table 7.3 Comparisons of data on intermediate glass transitions

Sample	Molecular weight	% Styrene	Process history	Scanning rate	T_g^I (observed)	T_g^I (predicted) linear rule	References
SBS	140,000	30	Toulene, Carbon tetrachloride Ethyl acetate, Ethyl methyl ketone	Positron annihilation technique	-14^{0}C	-24.00^{0}C	131
SBS	140,000	30	Ethyl acetate , Ethyl methyl ketone	Rheovibron DSC	10^{0}C -14^{0}C		133
SIS					-26 to 4^{0}C		134
SIS	31,000	70.1	Compression-molded film	4^{0}C/min	39.5^{0}C	33.40^{0}C	62
SIS	24,500	69.9	Compression-molded film	4^{0}C/min	36^{0}C	23.85^{0}C	62
SBS	61,000	44	Dipentene	5^{0}C/min	-22.02^{0}C	-20.83^{0}C	our data
SBS	61,000	44	Dipentene	10^{0}C/min	-13.21^{0}C	-16.6^{0}C	our data
SBS	61,000	44	Dipentene	10^{0}C/min	-20.93^{0}C	-18.42^{0}C	our data

7.3.6 Effect of Solvent on Interphase Composition

Polymer (SBS129) cast from toluene solution showed a transition corresponding to a butadiene phase (-91.45^{0}C) and a weaker transition corresponding to a styrene phase (73.09^{0}C) but did not show an intermediate glass transition corresponding to interphase. On the other hand, when the same polymer was cast from dipentene solution, three transitions corresponding to butadiene, styrene and intermediate phases were observed (Figure 6.11).

A true neutral solvent in the last stages of evaporation from an SBS film would eventually concentrate in the interphase. In solubilizing the interphase chains, it would promote uniformity of composition through the interphase and produce a step function composition profile from the PS regions to the PB regions. If toluene (a good PS solvent) is used, it would concentrate in the PS domains and the PS-rich regions of the interphase, not producing a homogeneous interphase. A uniform interphase will produce its own distinct T_g^I, while a graduated interphase will not.

7.3.7 Glass Transitions in Copolymer/Homopolymer Blends with $M_{SBS} = M_{hPS} \cong 62{,}000$

When added hPS is solubilized into the corresponding microphase in a block copolymer ($M_{hPS} < M_S$), one should expect the mixture to exhibit a styrene glass transition temperature, T_g^S, between that of the homopolymer and that of the styrene microphase. On the other hand, when the homopolymer forms a separate phase in the mixture, one should expect the mixture to exhibit the T_g of the homopolymer (perhaps somewhat perturbed by the large surface-to-volume ratio of the homopolymer domains) as well as a separate Tg of the corresponding microphase. In the present work, with the larger hPS ($M_{hPS} \approx M_{SBS} \approx 5M_S$), two Tg's were observed in the styrene glass transition region for all blends except 4%SBS.

The lower styrene glass transition (74-81^{0}C), corresponding to the S-block microphase was observed in these hPS-rich blends to be higher than the S-block glass transition in pure copolymer (68-69^{0}C). The higher glass transition (90-93^{0}C), corresponding to the hPS macrophase, was at a lower value than the pure hPS glass transition (102.25^{0}C). Both observations can be explained in terms of a co-mingling (solubilizing)of the two styrene chains (of different length), each dilute in the others domain. Even if this represented an entrapment situation during sample preparation rather than an equilibrium result, the consequences cited above would follow. For the 4%SBS, it is likely that micelles of SBS formed in the hPS matrix and caused extensive intermingling of PS chains with no formation of an aggregated SBS macrophase.

7.4 TEM and DSC Results: A Comparison

A careful analysis of the composite nature of microphase-separated block copolymers reveals an additional influence on the T_g of the soft phase, namely the presence of a thermal stress field in the samples at temperatures below the T_g of the hard phase and especially below the T_g of the soft phase [58]. This thermal stress field is caused by the unequal coefficients of thermal expansion of the two phases and will be quite different depending on whether the hard phase is an inclusion in a matrix of the soft phase, or the soft phase is an inclusion in a matrix of the hard phase or the hard and soft phases have a lamellar morphology. Rubber-modified glassy plastics such as high impact polystyrene have soft inclusions in a hard matrix. The dilatational stresses around the rubber particles should and do lead to a small decrease in T_g of these particles, and an increase of T_g of the soft microphase should be expected when this phase comprises the matrix rather than the inclusions [58].

Blends with 4%, 8%, 18% and 37%hPS showed slight decrease in the styrene glass transition which might be attributed to these dilational stresses around the rubber sheets (lamellae of butadiene) and is consistent with the co-continuous lamellar morphology of these blends (confirmed by TEM). On the other hand, in the case of 60%hPS blend, the decrease in styrene glass transition is significant and could be understood in terms of inclusions of butadiene ribbons in macrophase-separated hPS (Figure 5.20). Higher values of styrene glass transition in 44%hPS is supported by its macrophase-separated hPS domains (Figure 5.??) which are virtually free from butadiene inclusions. Addition of hPS in SBS above the saturation limit results in purification of butadiene domains [116] as shown by lower T_g of butadiene for 18% and 37%hPS blends. Both these blends had hPS equal to and above saturation limit respectively (Figure 5.??). Increase of T_g of butadiene in 44%hPS blends corresponds to copolymer-rich butadiene matrix phase (Figure 5.??) and this result is consistent with the predictions and observations of Paterno [58]. Paterno's [58] conclusions were drawn for HIPS, and it is significant to see their validity for a system similar to but not the same as HIPS.

The increase in intermediate glass transition of 18%hPS blend was understood in terms of rearrangement of S-block chain near interphase at solubility limit of hPS (and was identified by TEM, Figure 5.??). The higher intermediate glass transition of 60%hPS may be understood to be either due to altered interphase composition (as a result of destruction of lamellar morphology) or due to a copolymer-rich butadiene matrix phase with substantial amount of styrene inclusions, the facts confirmed by TEM (Figure 5.??).

DSC scans of pure copolymer and 4%, 8% and 18%hPS blends showed no significant difference in the slopes of the scan line. Change in DSC slope was observed for 37%hPS blend relative to the slope for the 18%hPS blend (Figure 6.3). Change of slope was also observed between DSC scans of 37% and 44%hPS blends as well as between 44% and 60%hPS blends. There exists some similarity of these observations with TEM observed morphologies for these blends. The lamellar morphology is retained without macrophase separation for 0-18%hPS addition. Change from lamellar to soda-straw transition in morphology was seen over the range 18% to 37%hPS.

REFERENCES

1. Agar, A.W., et. al., Principles and Practice of Electron Microscope operation, North- Holland Publishing Company, Amsterdam, 1985.

2. Bates, F.S., Dicker, S.B., and Wignall, G.D., "Phase behavior of amorphous binary mixtures of perdeuterated and normal 1,4-polybutadienes", Macromolecules, 19, 1938 (1986).

3. Berney, C.V., Cheng, Pao-Luo, and Cohen, R.E., " Distribution of Matrix Homopolymer in Block Copolymers of Spherical Morphology", Macromolecules, 21, 2235-2240 (1988).

4. Bradford, E.B., "The effect of Environment on the Morphology of Styrene-Butadiene Block Copolymers", Colloidal and morphological behavior of block copolymers (G. Molar, Ed.) Plenum press, NY (1971)

5. Baek, D.M., Han, C.D., and Kim, J.K., "Phase equilibra in mixtures of block copolymer and homopolymer", Polymer, 33(22), 4821-4831 (1992).

6. Bates, F.S., Berney, C.V., and Cohen, R.E., "Microphase Structure of Solvent-Cast Diblock Copolymers and Copolymer-Homopolymer Blends Containing Spherical Microdomains", Macromolecules, 16, 1101-1108 (1983).

7. Berglund, C.A. and McKay, K.W., "Viscoelastic properties of a styrene-isoprene-styrene triblock copolymer and its blends with polyisoprene homopolymer and styrene-isoprene diblock copolymer", Polymer Engineering and Science, 33, 1195-1203 (1993).

8. Berney, C.V., Cheng, P. and Cohen, R.E., "Distribution of matrix homopolymer in block copolymers of spherical morphology", Macromolecules, 21, 2235-2240 (1988).

9. Bates, F.S.; Cohen, R.E. and Argon, A.S., 'Dynamic mechanical properties of Polystyrene containing microspherical inclusions of polybutadiene: Influence of domain boundaries and rubber molecular weight', Macromolecules, 16, 1108-1114 (1983).

10. Beecher, L., Marker, L., Bradford, R.D. and Aggarwal, S.L., Journal of Polymer Science, Polymer symposium, 26, 117-123 (1969).

11. Chescoe, D. and Goodhew, P.J., The Operation of the Transmission Electron Microscope, Oxford University Press, New York, 1984.

12. Cheng, P.L., Berney, C. and Cohen, K., Macromolecular chemie, 190, 589-596 (1990).

13. , R.E., and Torradas, J.M., "Homopolymer-Induced Microphase Separation of a Homogeneous Diblock Copolymer", Macromolecules, 17, 1101-1102 (1984).

14. Chu, H., Guo, S., Chiu, W. and Tseng, H., "Viscosity-morphology-compatibility relationship of polymer blends", Journal of Applied Polymer Science, 49, 1791-1797 (1993).

15. Diamant, J. and Williams, M.C., "Microstructural diagnosis of block copolymer nonlinear mechanical properties ii. free recovery from a large tensile deformations", Polymer Engineering and Science, 29 (4), 227-234 (1989).

16. Diamant, J., Soong, D.S., and Williams, M.C., in Contemporary Topics in Polymer Science (W.J. Bailey, Ed.), Vol. 4, Plenum Press, New York, 1984.

17. Diamant, J., Soong, D., and Williams, M.C., " The Mechanical Properties of Styrene-Butadiene-Styrene (SBS) Triblock Copolymer Blends with Polystyrene (PS) and Styrene-Butadiene Copolymer (SBR)", Polymer Engineering and Science, 22 (11), 673-683 (1982).

18. Disko, M.M., Liang, K.S., Behal, S.K., Roe, R.J., and Jeon, K.J., "Catenoid-Lamellar Phase in Blends of Styrene-Butadiene Diblock Copolymer and Homopolymer", Macromolecules, 26, 2983-2986 (1993).

19. Diamant J., Soong, D., and Williams, M.C., "The Mechanical Properties of Styrene-Butadiene-Styrene (SBS) Triblock Copolymer Blends with Polystyrene (PS) and Styrene-Butadiene Copolymer (SBR)", Polymer Engineering and Science, 22(11), 673-683 (1982).

20. Djermouni, B. and Ache, H., "Effect of casting solvents on the properties of styrene-butadiene-styrene block copolymers studied by positron annihilation techniques", Macromolecules, 13, 168-170 (1980).

21. Eastmond, G.C., and Phillips, D.G., "Macroscopic phase separation in multicomponent polymer homopolymer blends: general consideration based on studies of AB-crosslinked polylmers", Polymer, 20, 1501-1511 (1979).

22. Fredrickson, G.H., and Leibler, L., "Theory of Block Copolymer Solutions: Nonselective Good Solvents", Macromolecules, 22, 1238-1250 (1989).

23. Flosenzier, L.S., Rohlfing, J.H., Schwark, A.., and Torkelson, J.M., "The Effects of Blending Small Amounts of Homopolystyrene on the Mechanical Properties of a Low Styrene Content Styrene-Butadiene-Styrene Block Copolymer", Polymer Engineering and Science, 30(1), 49-58 (1990).

24. Folkes, M.J., and Reip, P.W., "S-B-S block copolylmer-polystyrene blends: 1. Morphology and swelling properties", Polymer, 27, 377-383 (1986).

25. Flosenzier, L.S., Rohlfing, J.H., Schwark, A.., and Torkelson, J.M., "The Effects of Blending Small Amounts of Homopolystyrene on the Mechanical Properties of a Low Styrene Content Styrene-Butadiene-Styrene Block Copolymer-Corrections", Polymer Engineering and Science, 30(1), 1180-1181 (1990).

26. Fernandez-Moran, H., "A Diamond Knife for Ultrathin Sectioning", Expl. Cell Research, 5, 255-267 (1953).

27. Goldstein, J.I. and Yakowitz, H., Practical Scanning Electron Microscopy, Plenum Press, New York, 1975.

28. Gabriel, B.L., SEM: A User's Manual for Materials Science, American Society for Metals, Metals Park, Ohio, 1985.

29. Goldstein, J.I., Scanning Electron Microscopy and X-ray Analysis: A text for biologists, materials scientists, and geologists, Plenum Press, New York, 1992.

30. Gabizlioglu, O., Argon, A. and Cohen, R., Polymer, 26, 529-534 (1985).

31. Holden. G., and Bishop. E.T., and Legge, N.R., J.Polym. Sci., Part C, 26, 37 (1969).

32. Henderson, C.P. and Williams, M.C., J. Polym. Sci., Polym. Lett. Ed., 17, 257 (1979).

33. Han, C.D. and Kim, J., J. Polym. Sci., Polym. Phys. Ed., 25, 1741 (1987).

34. Henderson, C.P. and Williams, M.C., Polymer, 26, 2021 (1985).

35. Hadziioannou, G. and Skoulios, A., "Structural study of mixtures of styrene/isoprene two and three block copolymers", Macromolecules, 15, 267 (1982).

36. Hashimoto, T., Shibayama, M., and Kawai, H., "Domain-boundary structure of styrene-isoprene block copolymer films cast from solution. 4 Molecular weight dependance of lamellar microdomains", Macromolecules, 13, 1237 (1980).

37. Hashimoto, T., Fujimura, M., and Kawai, H., "Domain-boundary structure of styrene-isoprene block copolymer films cast from solution. 5 Molecular weight dependence of spherical microdomains", Macromolecules, 13, 1660 (1980).

38. Hadziioannou, G., Picot, C., Skoulios, A. Ionescu, M., Mathis, A. Duplessix. R., Gallot, Y., and Lingelser, J., "Low-angle neutron scattering study of the lateral extension of chains in lamellar styrene/isoprene block copolymers", Macromolecules, 15, 263 (1982).

39. Han, C.D., Kim, J., Kim, J.K., and Chu, S.G., " Viscoelastic Behavior of Mixtures of a Block Copolymer and a Homopolymer", Macromolecules, 22, 3443-3451 (1989).

40. Hashimoto, T., Koizumi, S., Hasegawa, H., Izumitani, T., and Hyde, S.T., "Observation of "Mesh" and "strut" Structures in Block Copolymer/Homopolymer Mixtures", Macromolecules, 25, 1433-1439 (1992).

41. Hong, K.M., and Noolandi, J., "Theory of Phase Equilibria in Systems Containing Block Copolymers", Macromolecules, 16, 1083-1093 (1983).

42. Hugenberger, G.S., and Williams, M.C., "Complex viscosity of Block Copolymer Solutions with Models of Microstructural Degradation", Macromolecules, 21, 1773-1783 (1988).

43. Hasegawa, H., Tanaka, H., Hashimoto, T. and Han, C.C., "SANS and SAXS study of block copolymer/homopolymer mixtures", Journal of Applied Crystallography, 24, 672-678 (1991).

44. Henderson, C.P. and Williams, M.C., "Asymmetric composition profiles inblock copolymer interphase: 1. Experimental evidence", Polymer, 26, 2021-2025 (1985).

45. Inoue, T.; Soen, T.; Hashimoto, T. and kawai, H., 'Studies on domain formation of the AB type block copolymer from its solutions. Ternary polymer blends fo the styrene-isoprene block copolymer with polystyrene and polyisoprene', Macromolecules, 3, 87-92 (1970).

46. Jiang,M., Cao, X., and Yu, T., "Phase separation in polymer blends comprising copolymers: 6. Effects of molecular architecture of block copolymers", Polymer, 27, 1923-1927 (1986).

47. Jeon, K. and Roe, R., "Solubilization of a homopolymer in a block copolymer", Macromolecules, 27, 2439-2447 (1994).

48. Jiang, M., "Miscibility in copolymer/homopolymer blends", Chinese Journal of Polymer Science, 6, 193-198 (1988).

49. Kraus, G. and Railsback, H.E., in Recent Advances in Polymer Blends, Grafts, and Blocks (L.H. Sperling, Ed.), Plenum Press, New York, 1974.

50. Kraus, G. and Rollmann, K.W., J. Polym. Sci., Polym. Phys. Ed., 14, 1133 (1976).

51. Kinning, D.J., Winey, K.I., and Thomas, E.L., "Structural Transitions from Spherical to Nonspherical Micelles in Blends of Poly (styrene-butadiene) Diblock Copolymer and Polystyrene Homopolymers", Macromolecules, 21, 3502-3506 (1988).

52. Kummerlowe, C. and Kammer, H.W., "Pecularities in morphologies of poly (2,2-dimethyltrimethylene carbonate-b-epsilon-caprolactone) blended with poly (2,2-dimethyltrimethylene carbonate)", Polymer Networks and Blends, 4, 101-103 (1994).

53. Koizumi, S., Hasegawa, H. and Hashimoto, T., "Mutual diffusion of block copolymer and homopolymer. Visualization using microdomain as a probe", Macromolecules, 23, 2955-2962 (1990).

54. Krause, S. and Wang, B., "Miscibility of high molecular weight polystyrene with the styrene block in styrene-dimethylsiloxane diblock copolymers and thermal stresses in their mixtures", Journal of Polymer Science; Polymer letters edition, 24, 35-39 (1986).

55. Kinning, D.J.; Thomas, E.L. and Fetters, L.J., 'Morphological studies of micelle formation in block copolymer/homopolymer blends.

56. Kinning, D.J. and Thomas, E.L., 'Hard sphere interactions between spherical domains in diblock copolymers', Macromolecules, 17, 1712-1718 (1984).

57. Kotaka, T., Miki, T. and Arai, K., "Morphology-mechanical property relationship of a polystyrene-polybutadiene-polystyrene block copolymer and its blends with homopolymer", Journal of Macromolecular Science; Physics, B17(2), 303-336 (1980).

58. Krause, S., Iskandar, M. and Iqbal, M., "Properties of low molecular weight block copolymers. 1. Diffenential scanning calorimetry of styrene-dimethylsiloxane diblock copolymers", Macromolecules, 15, 105-111 (1982).

59. Leary, D.F. and Williams, M.C., "Statistical thermodynamics of a-b-a block copolymers: I.", J. Polym.Sci., Polym. Lett. Ed. 8, 335-340 (1970).

60. Leary D.F. and Williams, M.C., "Statistical thermodynamics of aba block copolymers. ii", J. Polym. Sci., Polym. Phys. Ed., 11, 345-358 (1973).

61. Latta, H. and Hartmann, J.F., "Use of a Glass Edge in Thin-sectioning for Electron Microscopy", Proc. Soc. exp. Biol. Med., 74, 436-441 (19500.

62. Lu, Z., Krause, S., and Iskandar, M., "Properties of Low Molecular Weight Block Copolymers. 3. Mixtures of Styrene-Dimethylsiloxane Diblock Copolymers with Polystyrene", Macromolecules, 15, 367-370 (1982).

63. Lowenhaupt, B., Steurer, A., Hellmann, G.P. and Gallot, Y., "Microphase and macrophases in polymer blends with a diblock copolylmers", Macromolecules, 27, 908-916 (1994).

64. Leibler, L., Orland, H. and Wheeler, J.C., 'Theory of critical micelle concentration for solutions fo block copolymers', Journal of Chemical Physics. 79, 3550-3559 (1983).

65. Meek, G.A., Practical Electron Microscopy for Biologists, John and Wiley and Sons, New York, 1976.

66. Matsuo, M., and Sagaye, S., "Micromorphology-Property Relationships in Graft and Block Copolymers", Polymer preprints, 11, 384-389 (1970).

67. Mayes, A.M., and Olvera de la Cruz, M., "Cylindrical versus Spherical Micelle Formation in Block Copolymer/Homopolymer Blends", Macromolecules, 21, 2543-2547 (1988).

68. Meyer, G.C. and Widmaier, J.M., "Glass transition temperatures of ABA (styrene-isoprene-styrene) block copolymers by differential scanning calorimetry", Journal of Polymer Science, Polymer physics edition., 20, 389-398 (1982).

69. Ming, J., Xianyi, C., and Tongyin, Y., "Some Aspects of Morphologies and Interfaces in Copolymer/Homopolymer Blends", Chinese Journal of Polymer Science, 6(4), 345-352 (1988).

70. Molau, G.E., in Block Copolymers (S.L. Aggarawal, Ed.), Plenum Press, New York, 1970.

71. Meier, D.J., "The soulbilization of homopolymers by block copolymers", Polymer preprints, 19, 340-345 (1977).

72. Meier, D.J., "Theory of block copolymers. I. domain formation in a-b block copolymers", Journal of Polymer Science: Part C, 26, 81-98 (1969).

73. Matsushita, Y., Torikai, N., Mogi, Y., Noda, I. and Han, C.C., "Chain conformations of homopolymers dissolved in a microdomain of diblock copolymer", Macromolecules, 27, 4566-4569 (1994).

74. Miyamoto, T., Kodama, K. and Shibayama, K., Journal of Polymer Science. Physics Edition, 8, 2095-2097 (1970).

75. Nojima, S., Wang, D. and Ashida, T., "Ringed spherulite in binary blends of poly (epsilon-caprolactone) and epsilon-caprolactone-butadiene diblock copolymer", Polymer Journal, 23, 1473-1482 (1991).

76. Nojima, S., Roe, R., Rigby D. and Han, C.C., "Combined SANS-SAXS study fo blends of styrene-butadiene block copolymer with deuteriated polybutadiene", Macromolecules, 23, 4305-4312 (1990).

77. Pico, E.R., and Williams, M.C., "Solvation and Phase Separation in ABA Block Copolylmers", Journal of Applied Polyemer Science, 22, 445-457 (1978).

78. Paul. D. Polymer Blends (Paul, D. and Newman, S., Eds.) Vol. 2, chapter 12. Academic press, NY (1978).

79. Pico, E.R., and Williams,M.C., "Thermodynamics of Plasticized Triblock Copolymers. I. Theory", Journal of Polymer Science: Polymer Physics Edition, 15, 1585-1600 (1977).

80. Parker, M.A., and Vesely, D., "Contrast Enhancement and Polymer Indetification in the Electron Microscope by the Formation and Stainingof Unsaturated Double Bonds", Microscopy Research and Technique, 24, 333-339 (1993).

81. Park, I., Keskkula, H., and Paul, D.R., "Toughening of Polystyrene and Poly (phenylene oxide) Matrices with Elstomeic Styrene-Based Block Copolymers: Role of Molecular Architecture", Journal of Applied Polymer Science, 45, 1313-1328 (1992).

82. Quan, X., Gancarz, I., Koberstein, J.T., and Wignall, G.D., " Observaiton of Single-Chain Scattering from Homopolymer Blended with a Triblock Copolymer" , Journal of Polymer Science: Part B: Polymer Physics, 25, 641-650 (1987)

83. Quan,X., Gancarz, I., Koberstein, J.T., and Wignall, G.D., "Effect of Homopolymer Molecular weight on the Morphology of Block Copolymer/Homopolymer Blends", Macromolecules, 20, 1431-1434 (1987).

84. Reimer, L., Transmission electron microscopy: Physics of Image Formation and Microanalysis, Springer-Verlag, New York, 1984.

85. Rodriguez, F., Principles of Polymer Systems, Hemisphere Publishing Corp., New York, 1982.

86. Richards, R.W. and Thomason, J.L., Polymer, 24, 1089 (1983).

87. Rigby, D., and Roe, Ryong-Joon, " Small-Angle X-ray Scattering Study of Micelle Formation in Mixtures of Butadiene Homopolymer and Styrene-Butadiene Block Copolymer. 2. Effects of Block Lengths", Macromolecules, 19, 721-728 (1986).

88. Roe, R., "Small-Angle X-ray Scattering Study of Micelle Formation in Mixtures of Butadiene Homopolymer and Styrene-Butadiene Block Copolymer. 3. Comparison with Theory", Macromolecules, 19, 728-731 (1986).

89. Rigby, D., and Roe, R., "Small-Angle X-ray Scattering Study of Micelle Formation in Mixtures of Butadiene Homopolymer and Styrene-Butadiene Block Copolymer", Macromolecules, 17, 1778-1785 (1984).

90. Roe, R., "Phase Diagram of Polymer Blends Containing Block Copolymers", Polymer Engineering and Science, 25(17), 1103-1109 (1985).

91. Reid, N. Ultramicrotomy, North-Holland publishing company, Amsterdam (1974).

92. Roe, R., and Zin, W., "Phase Equilibria and Transition in Mixtures of a Homopolymer and a Block Copolymer. 2. Phase Diagram", Macromolecules, 17, 189-194 (1984).

93. Riess, G. "Thermoplastic elastomers (N.Legge, Holden, G. and Schroeder, H. Eds) Chapter 12, Section 2, Hanser Publishers (1987).

94. Riess, G. and Jolivet, Y., in 'Copolymers, Polyblends and Composites (N. Platzer, Ed.), Advance Chemistry series, 142, 243-250 (1975).

95. Sawyer, L.C. and Grubb, D.T., Polymer Microscopy, Chapman and Hall, New York, 1987.

96. Selb, J., Marie, P., Ramuau, A., Duplessix, R., and Gallot, Y., "Study of the structure of block copolymer-homopolymer blends using small angle neutron scattering", Polymer Bulletin, 10, 444-451 (1983).

97. Spontak, R.J., Smith, S.D., and Ashraf, A., "Dependence of the OBDD Morphology on Diblock Copolymer Molecular Weight in Copolymer/Homopolymer Blends", Macromolecules, 26, 956-962 (1993).

98. Spontak, R.J., Williams, M.C., and Schooley, C.N., "Morphology of bulk SBS block copolymers prepared by wet cryo-ultramicrotomy", Journal of Materials Sciences, 21, 3173-3178 (1986).

99. Smith, D.R., and Meier, D.J., "New techniques for determining domain morphologies in block copolymers", Polymer, 33(18), 3777-3782 (1992).

100. Spanns, R.D., M.Sc. Thesis, "Nonlinear Visco-elasticity and Microstructural Recovery of Block Copolymers under Shear deformation", University of Alberta, 1993.

101. Spontak, R.J., Smith, S.D. and Ashraf, A., "Linear multiblock copolymer/homopolymer blends fo constant composition. 1. low-moleculr-weight homopolymers", Macromolecules, 26, 5118-5124 (1993).

102. Sakurai, K., Macknight, W., Lohse, D., Schulz, D. and Sissano, J.A., "Amorphous-crystalline block copolymer and amorphous homopolymer blends. 1. A preliminary report", Macromolecules, 26, 3236-3238 (1993).

103. Spontak, R.J., Smith, S.D. and Ashraf, A., "Dependence of the OBDD morphology on diblock copolymer molecular weight in copolymer/homopolymer blends", Macromolecules, 26, 956-962 (1993).

104. Sardelis, K.; Michels, H.J. and Allen, G., 'Toughened polystyrene containing block, graded block, and randomized copolymers of butadiene-styrene', Polymer, 28, 244-250 (1987).

105. Tucker, P.S., and Paul, D.R.,"Simple Model for Enthalpic Effects in Homopolymer/Block Copolymer Blends", Macromolecules, 21, 2801-2807 (1988).

106. Tanaka, H. and Hashimoto, T., "Thermal concentration fluctuations of block copolymer/homopolymer mixtures", Macromolecules, 24, 5398-5407 (1991).

107. Takishima, S., Konno, M., Arai, K. and Saito, S., "Phase-separation structure of polymer blend of polystyrene and polyisoprene in the presence of styrene-isoprene diblock copolymer", Journal of Chemical Engineering of Japan, 19, 554-560 (1986).

108. Toy, L., Ninomi, M. and Shen, M., "Dynamic mechanical and morphological studies of homopolymer/block copolymer blends", Journal of Macromolecular Science; Physics, B11(3), 281-299 (1975).

109. Vaughan, D., Energy-dispersive X-ray Microanalysis: An Introduction, Kevex Corporation, Foster City, California, 1983.

110. Veith, C.A., Cohen, R.E. and Argon, A.S., "Morphologies of poly (dimethlysiloxane)-nylon-6 diblock copolymers and blends", Polymer, 32, 1545-1554 (1991).

111. Williams D.B., Practical Analytical Electron Mecroscopy in Materials Science, Philips Electronic Instruments Inc., Mahwah, New Jersey, 1984.

112. Winey, K.I., Thomas, E.L., and Fetters, L.J., " Swelling a Lamellar Diblock Copolymer with Homopolymer: Influence of Homopolymer Concentration and Molecular Weight", Macromolecules, 24, 6182-6188 (1991).

113. Winey, K.I., Thomas, E.L., and Fetters, L.J., "Isothermal Morphology Diagrams for Binary Blends of Diblock Copolymer and Homopolymer", Macromolecules, 25, 2645-2650 (1992).

114. Winey, K.I., Thomas, E.L., and Fetters, L.J., "The Ordered Bicontinuous Double-Diamond Morphology in Diblock Copolymer/Homopolymer Blends", Macromolecules, 25, 422-428 (1992).

115. Whitmore, M.D., and Noolandi, J., "Theory of Micelle Formation in Block Copolymer-Homopolymer Blends", Macromolecules, 18, 657-665 (1985).

116. Wang, Y.Z., Hsieh, K.H., Chen, L.W. and Tseng, H.C., "Effect of compatibility on Heat Capacity of Molten Polyblends", Journal of Applied Polymer Science, 49, 1047-1054 (1993).

117. Winey, K.I., Thomas, E.L. and Fetter L.J., "Swelling a lamellar diblock copolymer with homopolymer. Influences of homopolymer concentration and molecular weight", Macromolecules, 24, 6182-6188 (1991).

118. Wilkes, G., Bagrodia, S., Ophir, Z. and Emerson, J.A., Journal of Applied Physics, 49, 5060-5064 (1978).

119. Xie, H., Liu, Y., Jiang, M., and Yu, T., "Phase separation in polymer blends comprising copolymers: 7. Statistcal theory of block copolymer-homopolymer systems", Polymer, 27, 1928-1934 (1986).

120. Zin, W., and Roe, R., "Phase Equlibria and Transition in Mixtures of a Homopolymer and a Block Copolymer. 1. Small-Angle X-ray Scattering Study", Macromolecules, 17, 183-188 (1984).

Appendix A

This section presents some of the results on binary blends of SBS triblock copolymer (S145) and homopolystyrene (S189) and ternary blends of SBS (S145), homopolystyrene (S189) and homopolybutadiene (S). This is a small part of the bigger project undergoing in 'Polymers and Rheology research group" of chemical engineering department. As a result data presented here does not form a complete set which would warrant a separate discussion.

Table A-1 lists all the blends prepared with the Brabender Docorder.

TABLE A-1

Melt Blends of Homopolystyrene (S189) and SBS (S145)

@ Temperature = 160 ^{0}C, Speed = 30 rpm, Time = 55 min

Serial #	1	2	3	4	5	6
wt% SBS	10	20	30	40	50	70*

* Time of blending for this blend was 33.5 min

@ Temperature = 160^{0}C, wt%SBS = 30,

Serial #	7	8
Speed (rpm)	60	90
Time of blending (min)	55	42

@ wt%SBS = 30, Speed = 30 rpm,

Serial #	9	10
Temperature (^{0}C)	170	180
Time of blending (min)	82	55

Morphology using SEM:

Figures A-1 and A-2 show scanning electron micrographs of freeze-fractured surfaces of some of the blends. In principle, transmission electron microscopy (TEM) would give more definitive morphological information provided optimized staining conditions were used. Selective etching of the sample surface followed by surface analysis using SEM can give an adequate idea (only if the domains are large enough to see using SEM) of dispersed particle size and shape [79].

Torque measurements:

Since the Brabender torque is sensitive to the mass and the volume of material in the mixing bowl, torque measurements were carried out with great care to keep mass same in all runs. The nominal volume of the mixing bowl is 60 cm^3. We elected to use 40 g of material in all blends, which (because of differences in component densities) resulted in increase in volume of the material with the increased amount of block copolymer in the blend. Assuming density of polybutadiene (0.92 g/cm3) and polystyrene(1.05 g/cm3), the volume of the blending mixture varied from 38 to 42 cm^3, close enough to constancy for purposes of this study well within the volumetric capacity of the bowl.

Results:

Freeze-fractured surfaces analyzed by SEM showed variation in surface texture with respect to composition variation in blends. Figure A-1 shows variation in surface morphology with addition of SBS. Figure A-2 demonstrates role of block copolymer in compatibilizing blends of immiscible homopolymers.

Figure A-3 shows typical torque traces of some of the blends, during first 10-15 minutes of blending. Generally, at the end of this phase of blending, steady torque is realized and blending process can be terminated. The steady torque value showed increase with increasing amount of SBS as in Figure A-4. Figure A-5 shows Band-width measurements taken at various time intervals (10, 20, 30 min) during blending. These measurements showed interesting pattern over the range of composition. Band width values measured at t=10 min, were lowest up to 30%SBS addition, and were highest for 40-70%SBS addition. The 50%SBS blend showed the lowest value for band width. Figure A-5 shows Brabender torque measurements taken at various time intervals (10, 20, 30 min). The pattern observed in these measurements was rather straightforward, increasing torque with increasing SBS addition. Torque reading measured at 20 and 30 min for 40%SBS blend showed slight decrease over corresponding values of 30%SBS blend.

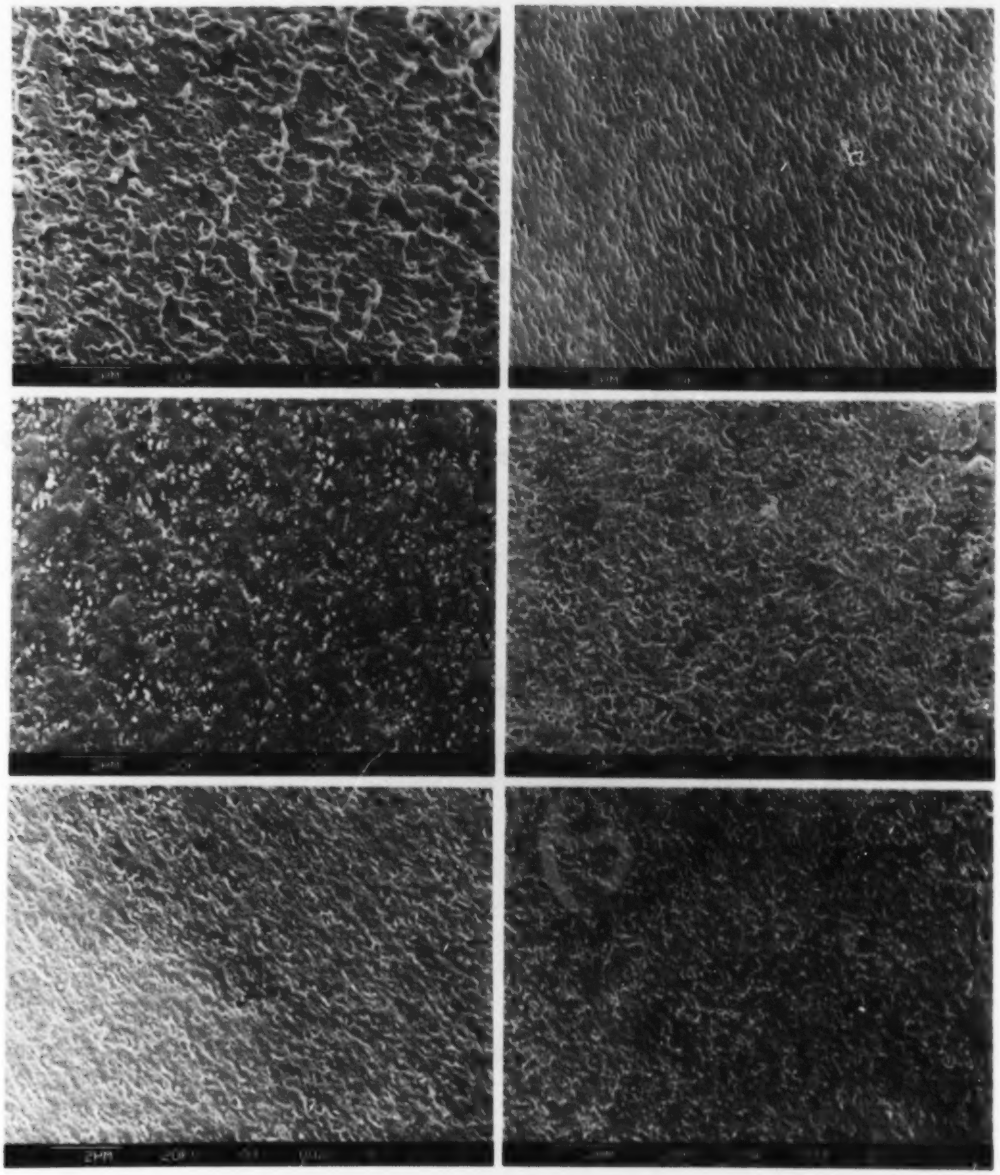

Figure A-1. Scanning electron micrographs of freeze-fractured surfaces of SBS (S145) and PS (S189) blends. Blends were prepared using Brabender Do-Corder with roller blades at temperature of 160 °C and 30 rpm. Blending time was 55 minutes. The composition of blends was varied from 10% to 70% SBS. Clockwise from the top left: 10% SBS, 20% SBS, 30% SBS, 40% SBS, 50% SBS and 70% SBS.

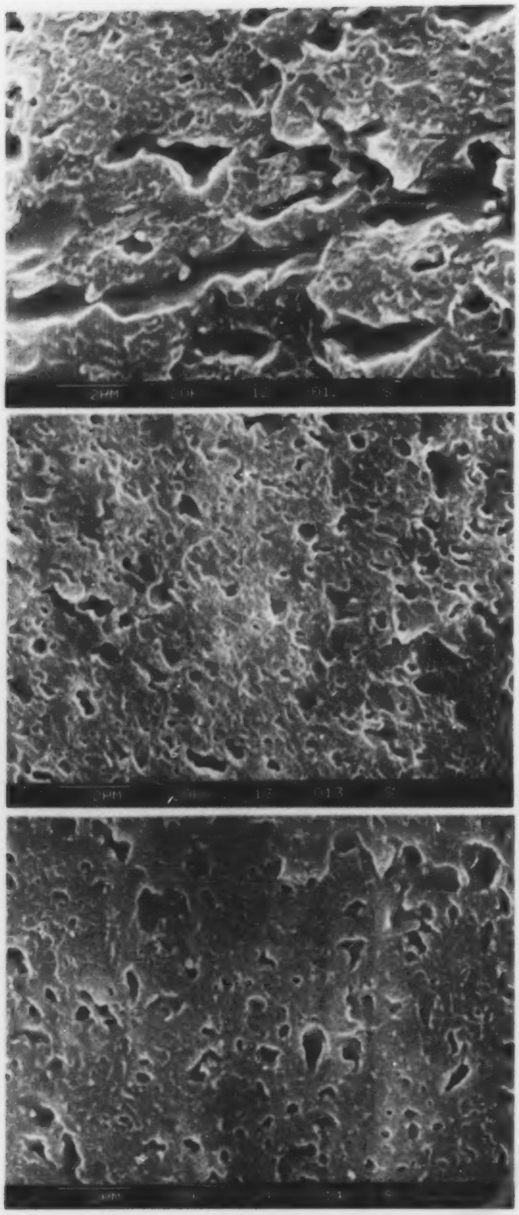

Figure A-2. Scanning electron micrographs of freeze-fractured surfaces of binary (Polystyrene and Polybutadiene) and ternary (Polystyrene, Polybutadiene and SBS) blends. Blends were prepared using Brabender Do-corder with roller blades at temperature of 160 ^{0}C and 60 rpm. Blending time was 55 minutes. Binary blend of 75% PS (S189) and 25% PB (S165) [top], Ternary blend of 75% PS (S189) with 20% PB (S165) and 5% SBS (S145) [middle] and Ternary blend of 70% PS (S189) with 20% PB (S165) and 10% SBS (S145) [bottom].

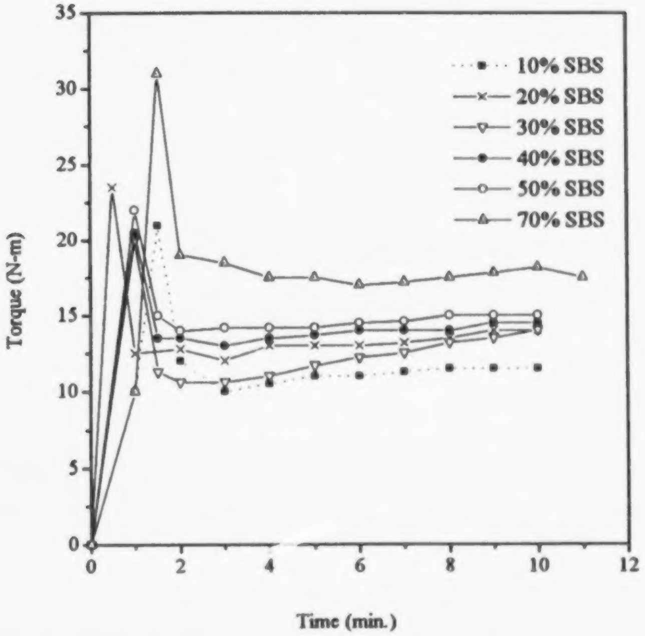

Figure A-3. Torque traces for SBS-PS blends (Brabender Docorder)

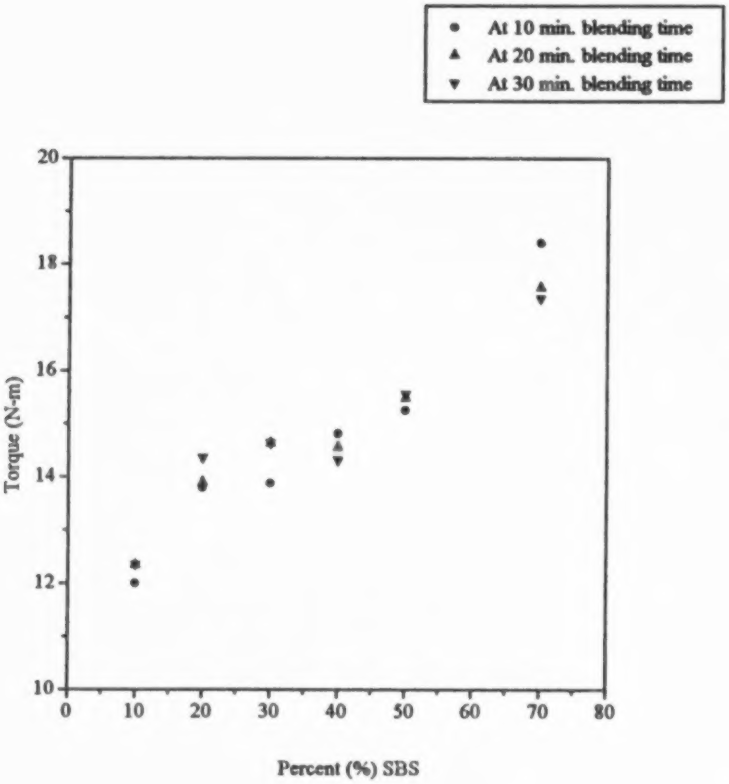

Figure A-4. Variation in Brabender Torque with change in composition of SBS in SBS-PS blends.

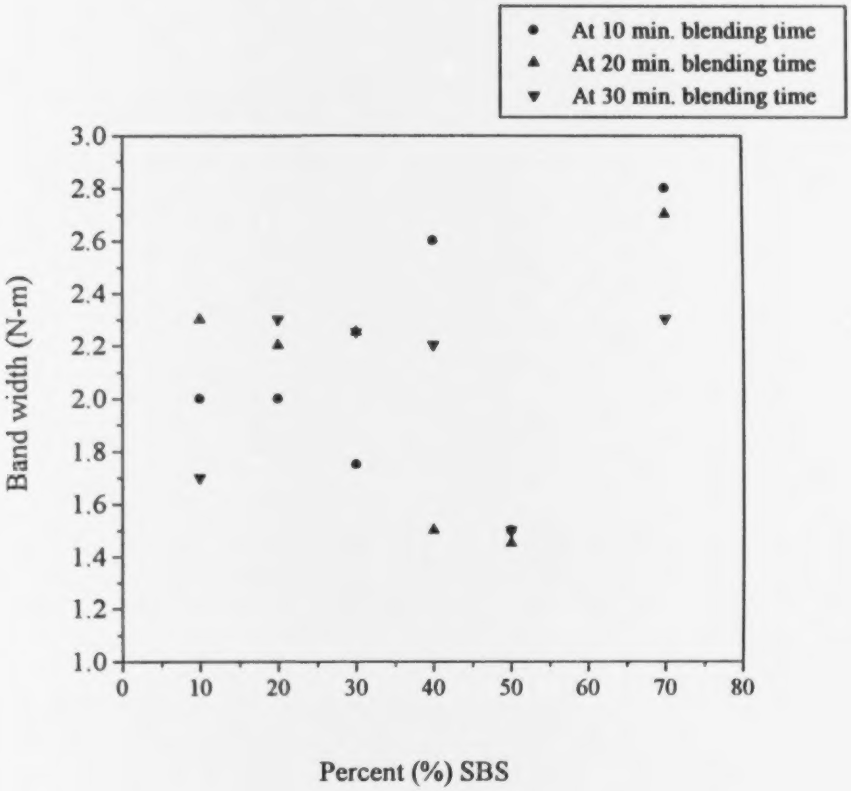

Figure A-5. Variation in band width of Brabender Torque trace with change in composition of SBS-PS blends.

Triblock Copolymers Blends with Polystyrene

Styrene-Butadiene-Styrene, SBS (M_{SBS} = 61300, W_S = 44% Styrene),

$M_S/M_B/M_S$ = 13,500/34,300/13,500

Polydispersity = $M_w/M_n \leq 1.06$ for all polymers

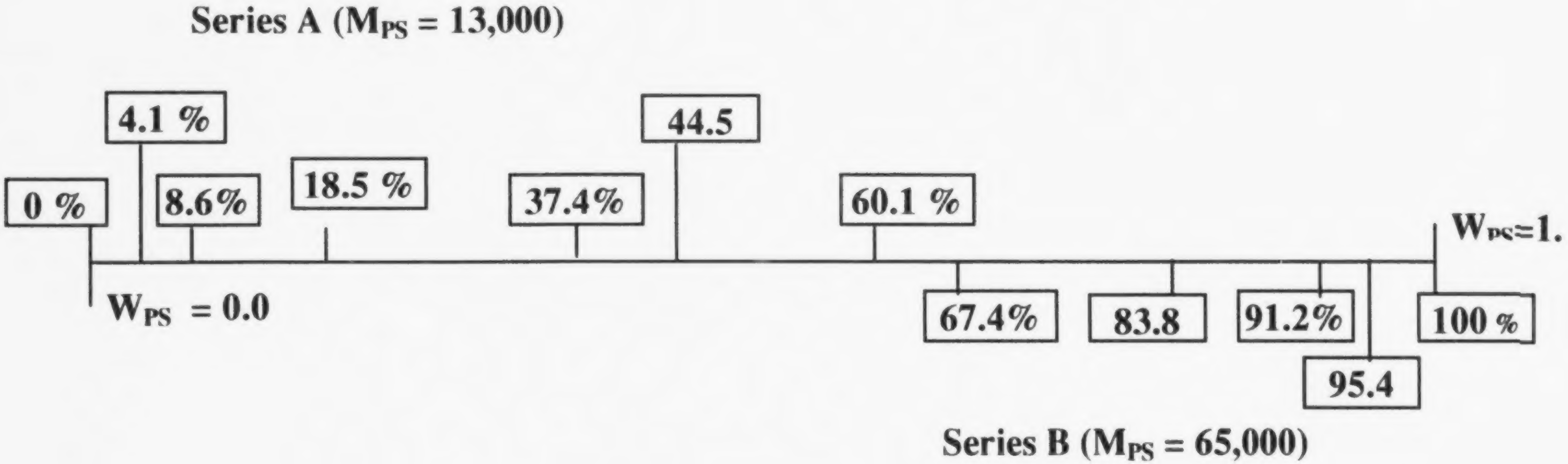

Series A (M_{PS} = 13,000)

0 %
4.1 %
8.6%
18.5 %
37.4%
44.5
60.1 %
W_{PS} = 0.0
W_{PS}=1.
67.4%
83.8
91.2%
95.4
100 %

Series B (M_{PS} = 65,000)